Integrated Ocean Drilling Program
Expedition 341 Scientific Prospectus

Southern Alaska Margin

Interactions of tectonics, climate, and sedimentation

John Jaeger
Co-Chief Scientist
Department of Geological Sciences
University of Florida
241 Williamson Hall
Gainesville FL 32611-2120
USA

Sean Gulick
Co-Chief Scientist
Institute for Geophysics
Jackson School of Geosciences
University of Texas at Austin
10100 Burnet Road, 196-ROC
Austin TX 78758-4445
USA

Alan Mix
APL-786 Proponent
College of Oceanic and Atmospheric Sciences
Oregon State University
COAS Administration Building 104
Corvallis OR 97331-5503
USA

Katerina Petronotis
Expedition Project Manager/Staff Scientist
Integrated Ocean Drilling Program
Texas A&M University
1000 Discovery Drive
College Station TX 77845-9547
USA

Published by
Integrated Ocean Drilling Program Management International, Inc.,
for the Integrated Ocean Drilling Program

Publisher's notes

Citation:
Jaeger, J., Gulick, S., Mix, A., and Petronotis, K., 2011. Southern Alaska margin: interactions of tectonics, climate, and sedimentation. *IODP Sci. Prosp.,* 341. doi:10.2204/iodp.sp.341.2011

Distribution:
Electronic copies of this series may be obtained from the Integrated Ocean Drilling Program (IODP) Scientific Publications homepage on the World Wide Web at **www.iodp.org/scientific-publications/.**

This publication was prepared by the Integrated Ocean Drilling Program U.S. Implementing Organization (IODP-USIO): Consortium for Ocean Leadership, Lamont-Doherty Earth Observatory of Columbia University, and Texas A&M University, as an account of work performed under the international Integrated Ocean Drilling Program, which is managed by IODP Management International (IODP-MI), Inc. Funding for the program is provided by the following agencies:

National Science Foundation (NSF), United States

Ministry of Education, Culture, Sports, Science and Technology (MEXT), Japan

European Consortium for Ocean Research Drilling (ECORD)

Ministry of Science and Technology (MOST), People's Republic of China

Korea Institute of Geoscience and Mineral Resources (KIGAM)

Australian Research Council (ARC) and GNS Science (New Zealand), Australian/New Zealand Consortium

Ministry of Earth Sciences (MoES), India

Disclaimer

This IODP *Scientific Prospectus* is based on precruise Science Advisory Structure panel discussions and scientific input from the designated Co-Chief Scientists on behalf of the drilling proponents. During the course of the cruise, actual site operations may indicate to the Co-Chief Scientists, the Staff Scientist/Expedition Project Manager, and the Operations Superintendent that it would be scientifically or operationally advantageous to amend the plan detailed in this prospectus. It should be understood that any proposed changes to the science deliverables outlined in the plan presented here are contingent upon the approval of the IODP-USIO Science Services, TAMU, Director in consultation with IODP-MI.

August 2011

Abstract

Global climate during the Neogene to Quaternary is distinguished by the transition into a colder, more variable world dominated by the onset and intensification of major Northern Hemisphere glaciations and is associated with an increase in erosion rates and sediment delivery to basins. The effects of this increased erosion may be profound, as worldwide analyses of orogenic belts have shown that earth systems cannot be considered to be the product of a series of distinct, decoupled tectonic and climatic processes. Rather, there is complex interplay between deformation, exhumation, and climate systems. Exhumation plays a key role in controlling the regional distribution of metamorphic rocks, local climate change, and development of structures throughout an orogen. As tectonic processes influence regional climate by raising mountains that enhance orographic precipitation patterns and intensity, the Neogene–Quaternary climate transition likely affected tectonic processes through changes in erosion rates, which redistributed mass and subsequently altered stresses in orogenic wedges. Analytical models examining the coupling between glacial erosion and orogenic processes reveal that glacial erosion can significantly modify the patterns and rates of erosion in an orogenic wedge. A critical question is, at what stage of the deteriorating Neogene climate is an orogen ultimately driven into subcriticality? Does this lead to increased exhumation in the glaciated core of a mountain belt, enhanced topographic relief, and migration of the locus of sediment accumulation to the toes of an orogen that impacts deformation patterns?

Addressing the linkages between global climate change, modification of the dynamics of surficial processes, and subsequent tectonic responses requires integrated studies of orogenic systems in areas that exemplify specific end-members of the problem. The Gulf of Alaska borders the St. Elias orogen of Alaska and Canada, the highest coastal mountain range on Earth and the highest range in North America. This orogen is <30 Ma in age, and mountain building occurred during a period of significant global climate change, allowing this expedition to examine the response of an orogenic system to the establishment of a highly erosive glacial system. Additionally, the implications of the Neogene glacial growth in the circum-North Pacific are far-reaching, beyond a tectonic response to increased glacial erosion and exhumation. As climate determines the timing and patterns of precipitation, it controls glacial dynamics, erosion, and sediment/meltwater and chemical fluxes to the ocean. Establishing the timing of northwestern Cordilleran ice sheet (NCIS) advance–retreat cycles in southern Alaska will address a major challenge in Quaternary paleoclimatology, which is to know the extent to which glacial-age climate change was a synchronous worldwide event and

what the driving mechanisms were for potentially propagating millennial-scale warming–cooling cycles around the globe. Evidence of substantial changes in surface productivity in the Gulf of Alaska since the Last Glacial Maximum indicates that millennial-scale climate change and eustasy in the northeast Pacific Ocean has a first-order effect on primary productivity. Thick Pleistocene glacimarine deposits of the Gulf of Alaska continental margin contain a rich history of climate change recorded in both proxy climate data and sediment accumulation rates that can help decipher the architecture of massive late Tertiary and Quaternary high-latitude Northern Hemisphere continental margin sedimentary sequences. Exceptionally high rates of glacigenic sediment accumulation in this region also allow for development of a paleomagnetic record of geomagnetic field variability on submillennial scales to assess geomagnetic persistence, a signature of the mantle's influence on the geodynamo and the paleomagnetic record.

Integrated Ocean Drilling Program (IODP) Expedition 341, which combines IODP Proposal 686-Full and ancillary proposal letter (APL)-786 will drill a cross-margin transect to investigate the northeast Pacific continental margin sedimentary record formed during orogenesis during a time of significant global climatic deterioration in the Pliocene–Pleistocene, which led to the development of the most aggressive erosion agent on the planet, a temperate glacial system. Sedimentary provenance and paleoclimatic, glacimarine, and structural sedimentary indicators tied to a multicomponent chronology will be used to generate detailed records of changes in the locus and magnitude of glacial erosion, degree of tectonic shortening, and sediment and freshwater delivery to the coastal ocean and their impact on oceanographic conditions in the Gulf of Alaska, and the resulting continental margin stratigraphic record on the interaction of these processes. Because the oceanographic processes in the Gulf of Alaska directly impact the Bering Sea, Expedition 341 will strongly complement IODP Expedition 323 by addressing the late Neogene evolution of continental glaciation and freshwater and nutrient inputs, but in a more proximal source to glacial drivers of many of these processes.

Major objectives of planned drilling in the Gulf of Alaska are as follows:

1. Document the tectonic response of an active orogenic system to late Miocene to recent climate change.
2. Establish the timing of advance and retreat phases of the NCIS to test its relation to dynamics of other global ice sheets.

3. Implement an expanded source-to-sink study of the complex interactions between glacial, tectonic, and oceanographic processes responsible for creation of one of the thickest Neogene–Quaternary high-latitude continental margin sequences.
4. Understand the dynamics of productivity, nutrients, freshwater input to the ocean, and surface and subsurface circulation in the Northeast Pacific and their role in the global carbon cycle.
5. Document the spatial and temporal behavior during the Neogene of the geomagnetic field at extremely high temporal resolution in an undersampled region of the globe.

Schedule for Expedition 341

Integrated Ocean Drilling Program (IODP) Expedition 341 is based on drilling Proposals 686-Add and 786-APL (available at **iodp.tamu.edu/scienceops/expeditions/alaska_tectonics_climate.html**). Following ranking by the IODP Scientific Advisory Structure, the expedition was scheduled for the research vessel R/V *JOIDES Resolution,* operating under contract with the U.S. Implementing Organization (USIO). At the time of publication of this *Scientific Prospectus,* the expedition is scheduled to take place in summer 2013. A total of 61 days will be available for the coring and downhole measurements described in this report (for the current detailed schedule, see **iodp.tamu.edu/scienceops/**). Further details about the facilities aboard the *JOIDES Resolution* and the USIO can be found at **www.iodp-usio.org/.**

Introduction

Global climate during the Neogene to Quaternary is distinguished by the transition into a colder, more variable world dominated by the onset and intensification of major Northern Hemisphere glaciations (Zachos et al., 2001). Corresponding to this alteration is a generally acknowledged global increase in sediment accumulation in both continental and marine sedimentary basins (Donnelly, 1982; Molnar and England, 1990; Zhang et al., 2001; Hay et al., 2002; Molnar, 2004; Willett, 2010), which is attributed to increased erosion in orogenic belts related to larger-amplitude climate fluctuations (Zhang et al., 2001; Willett, 2010). For many orogenic settings, this increased erosion may be driven by the expansion of alpine ice, but the direct correlation between increased erosion and specific climate drivers is lacking. Yet, the

consequences of this increased erosion are potentially far-reaching. Worldwide analyses of orogenic belts (Koons, 1995; Pinter and Brandon, 1997; Pavlis et al., 1997; Zeitler et al., 2001; Hoth et al., 2006; Roe et al., 2006; Stolar et al., 2006; Whipple, 2009) have shown that earth systems cannot be considered to be the product of a series of distinct, decoupled tectonic and climatic processes. Rather, there is a complex interplay between deformation, exhumation, and climate systems.

Exhumation plays a key role in controlling the regional distribution of metamorphic rocks, local climate change, and development of structures throughout an orogen (Fig. **F1**). As tectonic processes influence regional climate by raising mountains that enhance orographic precipitation patterns and intensity, the Neogene–Quaternary climate transition likely affected tectonic processes through changes in erosion rates that redistributed mass and subsequently altered stresses in orogenic wedges (Willet, 1999; Roe et al., 2006; Whipple, 2009). Analytical models examining the coupling between glacial erosion and orogenic processes reveal that glacial erosion can significantly modify the patterns and rates of erosion in an orogenic wedge (Roe et al., 2006; Tomkin, 2007; Tomkin and Roe, 2007). Glacial climate interacts with mountain building through erosion and sediment transport, dispersal, and accumulation. At a critically tapered wedge, erosion in the inner part of an orogen results in increased thrusting in order to attempt to maintain critical taper (e.g., Berger et al., 2008a; Whipple, 2009). Deposition of the eroded sediments in the outer part of an orogen can in turn suppress deformation due to loading (e.g., Simpson, 2010; Worthington et al., 2010). A critical question is, at what stage of the deteriorating Neogene climate is an orogen ultimately driven into subcriticality? Does this lead to increased exhumation in the glaciated core of a mountain belt, enhanced topographic relief, and migration of the locus of sediment accumulation to the toes of an orogen that impacts deformation patterns?

Addressing the linkages between global climate change, modification of the dynamics of surficial processes, and subsequent tectonic responses requires integrated studies of orogenic systems in areas that exemplify specific end-members of the problem. The Gulf of Alaska borders the St. Elias orogen of Alaska and Canada, the highest coastal mountain range on Earth and the highest range in North America (Fig. **F2**). This orogen is <30 Ma in age, and mountain building occurred during a period of significant global climate change (Fig. **F3**), allowing this expedition to examine the response of an orogenic system to the establishment of a highly erosive glacial system (Hallet et al., 1996; Jaeger et al., 1998; Sheaf et al., 2003; Berger et al., 2008b; Enkelmann et al., 2010; Spotila and Berger, 2010; Finzel et al., 2011). The sediments emanating from the

orogen are deposited in a relatively geographically confined area offshore, providing a rare opportunity to use the stratigraphic record to quantify spatial and temporal variations in the erosional flux from land to sea. The geological processes in southern Alaska are comparable to those observed in the Himalayan orogeny and include extremely high erosion rates, active faulting beneath mountains and alpine glaciers, and orogenesis coincident with extensive glacial cover. Important advantages of Alaska over the Himalaya include the proximity of a high coastal mountain range next to an energetic ocean with essentially no intervening basins to trap sediment. Therefore, tectonic and climatic signals have the potential to be quickly recorded in offshore areas with little modification resulting from long transport in rivers or temporary storage in intervening sedimentary basins.

Additionally, the implications of the Neogene glacial growth in the circum-North Pacific are far reaching beyond a tectonic response to increased glacial erosion and exhumation. As climate determines the timing and patterns of precipitation, it controls glacial dynamics, erosion, and sediment/meltwater fluxes to the ocean. Establishing the timing of northwestern Cordilleran ice sheet (NCIS) advance–retreat cycles will address a major challenge in Quaternary paleoclimatology, which is to know the extent to which glacial-age climate change was a synchronous worldwide event and what the driving mechanisms were for potentially propagating millennial-scale warming–cooling cycles around the globe (oceanic, atmospheric, or both) (Clapperton, 2000; Mix et al., 2001; Hill et al., 2006). Although many paleoclimate and glaciologic records provide strong evidence for millennial-scale climate change along the Gulf of Alaska margin (i.e., Last Glacial Maximum [LGM], Younger-Dryas, early Holocene Hypsithermal, late Holocene Neoglacial) (Peteet and Mann, 1994; Mann et al., 1998; Calkin et al., 2001; Davies et al., 2011), the timing and character of these variations in relation to North Atlantic or Southern Ocean records over the Pliocene–Pleistocene are largely still unknown. NCIS glaciation is fueled by low rates of evapotranspiration, extensive North Pacific moisture delivery, and extreme rates of precipitation due to the predominant storm track coupled with orographic lift along the high coastal mountain range (Royer, 1982; Emile-Geay et al., 2003; Neal et al., 2010). Melting of this ice and return of the freshwater to the modern coastal ocean results in high specific discharge, presently two- to sixfold higher than the Amazon and Congo (Neal et al., 2010). This discharge creates nearly estuarine-like salinity conditions in the coastal ocean and is a substantial contributor to the freshwater budget of the Bering Sea and the Arctic Ocean (Weingartner et al., 2005), which in turn may impact the thermohaline stability of the North Atlantic during interglacials (Keigwin and Cook, 2007). North Pacific Intermediate Water episodically forms in the Gulf of

Alaska (You et al., 2000) but may have been much more significant during the last deglacial (Heinrich Event 1), potentially linked to global adjustment of thermohaline circulation and teleconnections that impact atmospheric moisture delivery to the North Pacific (Okazaki et al., 2010; Menviel et al., in press). The Gulf of Alaska/North Pacific Ocean is the largest high-nutrient–low-chlorophyll (HNLC) area in the Northern Hemisphere, and productivity in this area is largely iron-limited (Harrison et al., 1999), with shelf oceanographic processes and surface water discharge appearing to play a role in regulating surface-ocean iron concentrations (Stabeno et al., 2004; Schroth et al., 2009; Wu et al., 2009). Evidence of substantial changes in surface productivity in the Gulf of Alaska since the LGM (Davies et al., 2011; Addisson et al., submitted) indicates that millennial-scale climate change and eustasy in the northeast Pacific Ocean has a first-order effect on primary productivity. Furthermore, the modes of transfer of glacigenic sediments and the spatio-temporal variation in transfer rates are critical to deciphering the architecture of the massive (as thick as 5 km), high-latitude late Tertiary and Quaternary Northern Hemisphere continental margin sedimentary sequences (Riis, 1992; Vagnes et al., 1992; Eidvin et al., 1993; Lagoe et al., 1993; Elverhøi et al., 1995; Powell and Cooper, 2002; Dahlgren et al., 2005). These thick deposits contain a rich history of climate change recorded in both proxy climate data (e.g., iceberg-rafted debris and microfossils) and sediment accumulation rates that, in part, reflect climate-driven glacial sediment yields. Exceptionally high rates of glacigenic sediment accumulation in the undersampled northeast Pacific also allow development of a paleomagnetic record of geomagnetic field variability on submillennial scales to assess geomagnetic persistence, a signature of the mantle's influence on the geodynamo and the paleomagnetic record (Gubbins et al., 2007; Stoner, 2009; Amit et al., 2010).

Integrated Ocean Drilling Program (IODP) Expedition 341, which combines IODP Proposal 686-Full and ancillary proposal letter (APL)-786, will investigate the northeast Pacific continental margin sedimentary record formed during orogenesis during a time of significant global climatic deterioration in the late Miocene to recent, which has led to development of the most aggressive erosion agent on the planet, a temperate glacial system. Sedimentary provenance and paleoclimatic, glacimarine, and structural sedimentary indicators tied to a multicomponent chronology will be used to generate detailed records of changes in the locus and magnitude of glacial erosion and sediment and freshwater delivery to the coastal ocean and their impact on oceanographic conditions in the Gulf of Alaska and the resulting continental margin stratigraphic record on the interaction of these processes. Additionally, drilling on the Surveyor Fan, which undergoes a mixture of subduction and accretion at the Aleutian

Trench (Fig. F4), will recover a detailed Pleistocene tephra record of Aleutian arc volcanism and will aid in understanding how sediment inputs influence subduction zone processes. Because the oceanographic processes in the Gulf of Alaska directly impact the Bering Sea, Expedition 341 will strongly complement IODP Expedition 323 by addressing the late Neogene evolution of continental glaciation and freshwater and nutrient inputs, but in a more proximal source to the glacial drivers of many of these processes.

Background

Geological setting

Continental margin strata in southern Alaska are created from sediment derived from the Yakutat terrane and several antecedent Mesozoic-to-modern accreted terranes that compose much of the northern North American Cordillera (Fig. F5) (Plafker, 1987; Plafker et al., 1994). The Yakutat terrane was likely excised from western Canada and translated to the northwest along the dextral Queen Charlotte-Fairweather Fault system (Plafker, 1987; Plafker et al., 1994; Landis, 2007; Perry et al., 2009) (Fig. F5). The age of initial Yakutat-North America subduction, when the leading edge of the microplate encountered the Aleutian Trench, and thus initiation of flat-slab subduction, is poorly constrained but may have occurred as early as ~40 Ma. Increased uplift has occurred in the past 10 m.y. associated with the convergence of increasingly thick crust and the formation of a syntaxial bend in the Pacific/North American plate boundary (Plafker et al., 1994; Rea and Snoeckx, 1995; White et al., 1997; Enkelmann et al., 2010; Finzel et al., 2011). Ongoing collision and flat-slab subduction of a thick (up to 35 km) oceanic plateau and cover strata (Christeson et al., 2010; Worthington et al., submitted) is constructing the present high topography of the Chugach-St. Elais Ranges (Pavlis et al., 2004; Eberhart-Phillips et al., 2006; Gulick et al., 2007), with active tectonic deformation spread throughout southern Alaska and northwestern Canada (Fig. F4) (Plafker et al., 1994; Mazzotti and Hyndman, 2002; Pavlis et al., 2004; Spotila et al., 2004; Eberhart-Phillips et al., 2006; Meigs et al., 2008; Spotila and Berger, 2010; Enkelmenn et al., 2010; Worthington et al., 2010; Finzel et al., 2011). Focused deformation occurs in two indentor corners (Fig. F4), one in the west that is experiencing thin-skinned young deformation (Bruhn et al., 2004) and the other in the east (Seward corner) (Spotilla and Berger, 2010; Enkelmann et al., 2010) where there is intense strain and high exhumation rates (“tectonic aneurysm”) associated with the change from strike-slip to collision (Enkelmann et al., 2008, 2010; Elliot et

al., 2010). The active deformation front for this convergence cuts diagonally from the eastern syntaxis near Mt. St. Elias along the Malaspina Fault, reaching Icy Bay and then across the shelf as the Pamplona zone, and down the slope to the Aleutian Trench, thereby linking Yakutat-North America deformation structures with the Pacific-North America Faults (Bruns, 1983; Worthington et al., 2010). The northward boundary, or backstop, of deformation within the St. Elias orogen is debatable because of extensive ice cover and may include the Chugach-St. Elias Fault or the Contact fault (Fig. **F6**) (Spotila and Berger, 2010; Enkelmann et al., 2010); however there are suggested far-field effects more than 1000 km away (Mazzotti and Hyndman, 2002; Redfield et al., 2007).

The Yakutat terrane consists of Eocene to modern sedimentary rocks of the Kulthieth, Poul Creek, and Yakataga Formations that are primarily siliciclastic marine and glacimarine strata interbedded with volcanics and coal beds (Fig. **F6**) (Plafker et al., 1994). The Kulthieth Formation sediments are the oldest, deposited at ~60–35 Ma, and are composed of nonmarine to shallow-marine deltaic feldspathic and micaceous sandstones and siltstones formed during a general relative sea level regression (Risley et al., 1992; Plafker et al., 1994; Perry et al., 2009). The Poul Creek Formation appears to conformably overlie the Kulthieth, ranging in age from late Eocene to Oligocene (Risley et al., 1992; Plafker et al., 1994). This formation is characterized by a high abundance of argillaceous sediment that is in part glauconitic and organic rich, representing deposition during a general marine transgression in outer shelf/slope environments. It also contains waterlain basaltic tuff, andesitic breccia, pillow lava, and related deposits of the intertonguing Cenotaph volcanics (Plafker, 1987; Risley et al., 1992; Plafker et al., 1994). The Yakataga Formation represents glacimarine siliciclastic shelf/slope deposits dating from the onset of St. Elias glaciation in the late Miocene (~5.5 Ma) to the present (Plafker et al., 1994; Lagoe et al., 1993; Risley et al., 1992; Plafker, 1987; Eyles et al., 1991). It is composed of oldest diamict, possibly debris flows, transitioning upward into turbidites, diamictites, mudstones, and shallow-water sandstones with occasional coquinas and boulder pavements. The uppermost Yakataga mostly comprises facies that indicate significant lateral translation of the ice margin (paraglacial mudstones to boulder pavements). It is exposed onshore along the leading edge of the fold and thrust belt and is >5 km thick on the continental shelf.

Volumetrically, the major potential contributors of sediment to the Yakutat terrane during the Cenozoic are the Wrangellia, Alexander, Chugach, and Yukon-Tanana terranes (Fig. **F5**). The Kulthieth and Poul Creek Formations are likely derived from a par-

ent source in British Columbia (Cowan, 1982; Plafker, 1987; Plafker et al., 1994; Landis, 2007; Perry et al., 2009). At the time of Kulthieth and Poul Creek Formation deposition, sediment transport pathways likely originated from the east, deriving material from the Intermontaine Belt (Cache Creek, Nisling, and the Stikine terranes), Coast Belt (Coast Plutonic Complex, Central Gneiss Complex), and Insular Belt (Wrangellia, Alexander, Chugach, and Yakutat terranes) in British Columbia during the latter stages of uplift (Fig. **F5**) (Gehrels and Berg, 1994; Plafker et al., 1994). The Wrangellia terrane consists of a lower section of Permian to Middle Triassic limestone, chert, and pelitic strata. These units are overlain by 4–5 km of mid-Triassic mafic lava flows and associated mafic and ultramafic rocks, providing a diagnostic isotopic and compositional marker of sediment derived from the Wrangellia terrane (Jones et al., 1977; Nokleberg et al., 2001; Trop et al., 2002). The Alexander terrane consists of Precambrian(?) through Middle(?) Jurassic sedimentary, metamorphic, and plutonic rocks (Gehrels and Berg, 1994) with a distinctive magnetic mineralogy (Cowan et al., 2006). The Chugach terrane consists mainly of highly deformed, weakly metamorphosed Upper Cretaceous graywacke and slate. These accretionary prism strata are interpreted to have been mainly derived from plutonic and volcanic rocks of the Coast Plutonic Complex in British Columbia (Dumoulin, 1987). The final major terrane that may have contributed sediment to the Yakutat terrane is the Yukon-Tanana terrane (Fig. **F5**). Polydeformed metamorphic rocks of this terrane consist mainly of quartz-mica schist, quartzite, metarhyolite, and gneissic plutonic rocks (Foster et al., 1994). Protolith ages are only partly known but include middle Paleozoic radiometric ages for some of the igneous rocks and Devonian paleontologic ages for some of the carbonate strata (Gehrels and Saleeby, 1987; Plafker, 1987; Haeussler et al., 2006).

Yakataga Formation and Surveyor Fan provenance is likely a combination of material supplied mostly from the exhuming fold and thrust belt (Kultieth, Poul Creek, and recycled Yakataga terranes) and the potential backstop of accretion provided by the Chugach and Prince William terranes, with minor contributions from more inboard terranes (Fig. **F6**). The Chugach-Prince William terranes are a subduction complex welded onto the continent when the Kula-Farallon Ridge subducted beneath the margin, resulting in high-temperature, low-pressure metamorphism (Plafker et al., 1994; Pavlis et al., 2004). The Chugach and Prince William terranes are lithologically similar and have been considered one composite terrane (Kusky et al., 1997). Age distributions of detrital zircons suggest metasedimentary flyschoidal rocks of the Chugach terrane are derived from inboard accreted terranes of British Columbia (Haeussler et al., 2006; Perry et al., 2009). The lithologies of the Chugach terrane are dominated by graywacke flysch and mélange units with substantial basaltic constituents. These

mafic units have undergone very low grade metamorphism in the westernmost terrane, increasing in metamorphic grade to amphibolite-facies and phyllitic units of the Orca and Valdez groups in the Prince William terrane in the St. Elias region (Fig. F6) (Plafker et al., 1994; Haeussler et al., 2006). The Valdez group of the Prince William terrane north of the St. Elias Range is part of a mélange that is characterized by metavolcanic rocks and weakly foliated, green, glassy tuff, together with volcaniclastic graywacke and argillite (Plafker et al., 1994). Volcanic rocks of the southern margin of the Valdez group are dominantly tholeiitic pillow basalts with island-arc to mid-ocean-ridge basalt (MORB) compositions (Plafker et al., 1994). The Orca group dominates the Prince William terrane within the St. Elias Range. As with the Valdez group, this group is a deep-sea flysch complex with abundant oceanic basaltic rocks, sheeted dikes, and gabbroic intrusions of an ophiolite complex and underlies the Bagley Icefield along the contact fault system, from which the Bering Glacier sources (Plafker et al., 1994; Richter et al., 2006). Yakataga Formation strata accumulated in the later stages of the accretionary history of the Yakutat terrane. Sedimentary petrography of Yakataga lithic fragments reveals sedimentary, metasedimentary, and volcanic rock fragments. Zircon fission track, U-Th/He, and U/Pb analysis of the Yakataga Formation indicates intermixing of sediment derived from two or more sources, likely the Chugach-Prince William composite terrane and recycling of Poul Creek and Kulthieth rocks (Plafker et al., 1994; Enkelmann et al., 2008; Perry et al., 2009; Witmer et al., 2009).

Physical and oceanographic setting

The morphology of the Gulf of Alaska shelf seabed has been strongly influenced by active tectonics and glacial strata formation overprinted by glacial erosion (Carlson et al., 1982). The local bathymetry has been shaped by glacial and tectonic forces that produced five distinct across-shelf valleys in the study area: the Alsek Sea Valley, the Yakutat Sea Valley, the Bering Trough, the Kayak Trough, and the Hinchinbrook Sea Valley (Figs. F2, F7). These valleys are U-shaped, contain poorly sorted, glacially derived diamict along their flanks, and presumably formed during the advance of major ice streams and glaciers (Carlson et al., 1982). The extent of grounded ice cover on the shelf during the last sea level lowstand is poorly constrained, but it may have ranged from only the across-shelf valleys to the entire shelf (Fig. F8) (Molnia, 1986; Manley and Kaufmann, 2002). The glaciers that reached the sea were probably grounded tidewater, not floating ice sheets (Powell and Molnia, 1989). Little sampling has occurred on the continental slope or on Surveyor Fan. Grab samples recovered diamicton from

the continental slope, which likely date to the LGM (Molnia and Sangery, 1979). The recently acquired jumbo piston Core EW0408-85JC on the continental slope at Site KB-2A reveals slowly accumulating (<1 mm/y) Holocene-age silty clay in the vicinity of the Alaska Coastal Current (ACC) (Davies et al., 2011). Piston Core EW0408-87JC on the proximal Surveyor Fan (Site GOAL-16B) also contains slowly accumulating (<1 mm/y), likely Holocene-age silty clay that may be derived from intermediate nepheloid layers supplied with sediment from the Alaska Coastal Current (Jaeger et al., 2008).

The modern oceanographic environment in the Gulf of Alaska is characterized by strong wintertime wave and wind energy, pronounced coastal currents, and deepwater gyres (Stabeno et al., 2004). The regional meteorology of the Gulf of Alaska is chiefly affected by energetic storms associated with the Aleutian Low Pressure System (ALPS). The Gulf of Alaska experiences mean wind speeds and frequency of gale-force winds similar to those of the western and central North Pacific (Stabeno et al., 2004). Cyclonic motion of the subarctic gyre drives circulation in the outer Gulf of Alaska with the inner Gulf dominated by the Alaska Coastal Current, a wind- and buoyancy-forced coastal jet (Fig. **F7**) (Stabeno et al., 2004). The southern boundary of this subarctic gyre, the North Pacific drift, diverges as it impinges on North America, with the northward branch becoming the Alaska Current (Fig. **F7**). The Alaska Current dominates flow along the southwestern and southern Alaska continental slope, eventually transitioning into the Alaskan Stream farther to the west. Several large semipermanent to seasonal eddies form within the Alaska Current, leading to important mixing of water masses across the continental margin (Stabeno et al., 2004).

Water and sediment are dispersed on the continental shelf by the Alaska Coastal Current (Feely et al., 1979; Stabeno et al., 2004; Weingartner et al., 2005). The current is generally confined to within 40 km of the coast and has flow velocities occasionally in excess of 50 cm/s and mean annual transport of ~10^6 m^3/s (Royer, 1982; Stabeno et al., 1995). Although primarily wind driven, the Alaska Coastal Current is enhanced by a baroclinic response to coastal freshwater discharge to the Gulf of Alaska (Royer 1981, 1982). This freshwater flux is delivered via a series of small mountainous drainages that experience high precipitation rates (2–6 m/y) due to adiabatic cooling of warm, moist air associated with the cyclonic storm systems of the ALPS (Weingartner et al., 2005). Freshwater and sediment discharges are lowest in winter when much precipitation is stored as snow and peak in late summer/fall when meltwater and precipitation rates are greatest (Stabeno et al., 2004; Neal et al., 2010). Runoff creates a sharp shallow (<50 m) halocline of salinity contrast >3 over the shelf in the fall but

during the winter is mixed (>100 m) and much more subdued (contrast of ~1) as a result of strong storms (Stabeno et al., 2004). Strong cyclonic winds dominate from fall through spring, peaking in December and January at 9 m/s, and intense (>14 m/s) easterly coastal jets forced by mountain topography can occur (Stabeno et al., 2004). These winds lead to downwelling conditions and near-bed (3 m above bed) nontidal maximum currents of 0.15 m/s in the summer and >0.3 m/s in the winter (Hayes and Schumacher, 1976; Hayes, 1979). Wave energy is highest in the winter months, decreasing in the summer. Monthly mean significant wave heights at National Oceanic and Atmospheric Administration (NOAA) Buoy 46001 (Fig. **F7**) averaged over 25 y are 3.5 ± 2 m (1σ), and maximum significant wave heights are 14 m in November and December (Gilhousen et al., 1983). Summer significant wave heights average 1.5 m at Buoy 46001, but maxima of 6–10 m can occur.

Regional productivity in the Gulf of Alaska is strongly influenced by the interaction of high freshwater runoff and regional meteorology dictated by the ALPS. During fall through spring, strong cyclonic winds associated with the ALPS support onshore surface Ekman transport and downwelling on the shelf, along with storm-induced vertical mixing (Stabeno et al., 2004; Childers et al., 2005). During summer the onshore winds and subsequent downwelling conditions relax, allowing occasional brief periods of coastal upwelling in this dominantly downwelling system (Stabeno et al., 2004). Primary productivity in the Gulf of Alaska in the winter is inhibited by low insolation and enhanced vertical mixing that limits the near-surface residence time of algae. Algal blooms occur over the shelf in the early spring due to the increased solar irradiance, wintertime replenished nutrient supply, and the onset of water column stratification leading to enhanced cell residence time in surface waters. Productivity remains relatively high through early summer but is followed by a reduction in summer due to nutrient limitation created by the strong halocline (Childers et al., 2005; Stabeno et al., 2004). Key nutrients (nitrate, silicic acid, and phosphate) are derived mostly from the subsurface ocean, via open-ocean upwelling, onshore Ekman transport, tidal pumping, and storm or eddy mixing (Childers et al., 2005). Nutrients delivered by the fluvial system include iron and silicic acid (Stabeno et al., 2004). Relatively few data are available on the cycling of iron in this system, although it appears shelf processes and surface water discharge may play a role in regulating surface-ocean iron concentrations (Stabeno et al., 2004; Schroth et al., 2009; Wu et al., 2009; Davies et al., 2011; Addison et al., submitted). In contrast to the productive coast, the central Gulf of Alaska is a high-nitrate low-chlorophyll (HNLC) region (Stabeno et al., 2004), and primary productivity is likely limited by micronutrients such as iron (Boyd et al., 2004; Tsuda et al., 2005). Sources of iron to the central basin include curl-driven

upwelling, aeolian dust (Mahowald et al., 2005), advection of dissolved iron from the continental shelf and slope (Chase et al., 2007; Lam and Bishop, 2008), and terrestrial runoff (Stabeno et al., 2004; Royer, 2005). The Expedition 341 drill sites span from the productive nitrate-limited shelf system to the iron-limited open-ocean system.

Northwestern Cordilleran ice sheet dynamics

The glacial history of the Gulf of Alaska margin has been constructed through a combination of surface outcrop sampling (e.g., Lagoe et al., 1993; Lagoe and Zellers, 1996; White et al., 1997), scientific drilling (Rea, Basov, Janecek, Palmer-Julson, et al., 1993; Rea and Snoeckx, 1995; Prueher and Rea, 1998), and industry well cuttings (Lagoe et al., 1993; Zellers, 1995; Lagoe and Zellers, 1996). The chronology of these events has been established through paleomagnetic and diatom/radiolarian biostratigraphic control at Ocean Drilling Program (ODP) Site 887 (Barron et al., 1995), more limited tephrochronology, paleomagnetic, and biostratigraphic control at Deep Sea Drilling Project (DSDP) Site 178 (Von Huene et al., 1973; Lagoe et al., 1993), and foraminiferal biostratigraphy in industry wells on the shelf (Zellers, 1995) and in the Yakataga Formation outcrops (Lagoe et al., 1993). A summary of glacial history and the associated sediment record is shown in Figure **F3.** Alpine glaciation along the margin may have initiated as early as ~7 Ma (Lagoe et al., 1993) and was well under way by 5.5 Ma (Lagoe et al., 1993; Rea and Snoeckx, 1995; White et al., 1997), when elevation of the Chugach-St. Elias mountain belt was sufficient to trap precipitation from storms generated in the Gulf of Alaska. Initial onset of tidewater glaciation, Lagoe et al.'s (1993) "Glacial Interval A," is linked to the appearance of ice-rafted debris (IRD) in the Yakataga Formation at the Yakataga Reef outcrop at 5.5 Ma and at Site 887 from ~5 Ma (Krissek, 1995) to 4.3 Ma (Rea and Snoeckx, 1995) (Fig. **F3**). A reduction in glacimarine sedimentation correlating with the ~4.5–2.8 Ma mid-Pliocene warm period (MPW) (Shackleton et al., 1995) is observed in marine and nonmarine records, though timing varies between different locales in the Gulf of Alaska region. In outcrop and continental shelf samples, the MPW lasts from 4.2 Ma to 3.5–3.0 Ma (Lagoe and Zellers, 1996). At Site 887, the MPW lasts from 3.6 to 2.8 Ma (Rea, Basov, Janecek, Palmer-Julson, et al., 1993; Rea and Snoeckx, 1995). Renewed onset of intense glaciation after ~3 Ma, "Glacial Interval B" (Lagoe et al., 1993), is characterized by an increase in IRD accumulation at 2.6 Ma within deep-sea records (Lagoe et al., 1993; Prueher and Rea, 1998) and by thick successions of diamictite in outcrop (Lagoe et al., 1993).

At ~1 Ma, the rate of terrigenous sedimentation doubles, likely due to widespread glacial advance associated with the mid-Pleistocene transition (MPT) that carved a series of U-shaped sea valleys to the shelf edge (Carlson, 1989; Lagoe et al., 1993; Rea and Snoeckx, 1995). This glacial intensification is referred to as "Glacial Interval C" (Berger et al., 2008a). Since the onset of Glacial Interval C, a series of 100 k.y. glacial–interglacial cycles characterize the late Pleistocene climate signal. Recent high-resolution seismic reflection profiles in the Bering Trough image glacial erosion surfaces that extend to the shelf edge, likely correlating with widespread Pleistocene glacial advances potentially associated with the onset of Glacial Interval C (Berger et al., 2008a). The northwestern lobe of the Cordilleran ice sheet was present on the shelf during the LGM (Fig. **F8**) (Davies et al., 2011), although the full extent of ice cover is poorly known (Molnia, 1986; Manley and Kaufman, 2002). Terrestrial records suggest that the regional LGM expression lasted from 23,000 to 14,700 cal y BP (calendar years before present), with evidence for millennial-scale cooling and transient glacial re-advances during deglaciation (Engstrom et al., 1990; Mann and Peteet; 1994, Briner et al., 2002; Hu et al., 2006; Davies et al., 2011). Retreat of the Bering Glacier off the continental shelf following the LGM likely occurred after 16,000 cal y BP, as indicated by peat accumulation in parts of the Bering foreland, and had apparently retreated well onshore by 14,700 cal y BP (Peteet, 2007; Davies et al., 2011).

Continental margin and Surveyor Fan stratigraphy

Varying degrees of glacial erosion, tectonic deformation, and rock exhumation in the St. Elias Range in southern Alaska and northwestern British Columbia since the Miocene (Lagoe et al., 1993; Rea and Snoeckx, 1995; Enkelmann et al., 2010; Spotila and Berger, 2010) supplied sediment into the Gulf of Alaska, leading to periodic significant increases in growth of the continental margin and Surveyor Fan (Stevenson and Embley, 1987; Lagoe et al., 1993; Rea and Snoeckx, 1995; Zellers, 1995; Worthington et al., 2010; Reece et al., in press).

The seismic stratigraphy of the Bering Trough between the Kayak Island zone (KIZ) and Pamplona zone (PZ; Fig. **F4**) has been imaged at several scales. Regional seismic surfaces, deformation structures, and seismic sequences are observed (Table **T1;** Figs. **F9, F10**), but age control is coarse and limited to cuttings from industry wells (Zellers, 1995). In high-resolution seismic Line GOA2505 and coincident crustal scale Line STEEP09, a series of erosive surfaces is imaged between the seafloor and Horizon 1; these surfaces are the signature of glacial advance–retreat cycles as outlined in Berger et al. (2008a), Willems (2009), and Worthington et al. (2008), with Horizon 1 being

hypothesized as the first glacial advance to the edge of the modern continental shelf (Figs. **F9, F11**) at the start of the MPT. Proposed Site GOAL-15B will sample across Horizon 1 to test this hypothesized timing.

These seismic profiles also cross active faults on the slope (BT1, BT2) and abandoned faults beneath the current shelf (BT3, BT4, BT5; Fig. **F10**). Structures BT3, BT4, and BT5 are currently buried by more than ~1500 ms two-way traveltime of undeformed sediments and have gradually been rendered inactive since before the early Pleistocene deposition of Horizon 2 (Zellers, 1995; Berger et al., 2008a; Worthington et al., 2008). Site GOAL-15B is located adjacent to BT4 with the goal of determining the age of cessation of deformation as indicated by the absence of growth strata above Horizon 2 (Worthington et al., 2010). Lack of significant deformation in the sequences above Horizon 2 indicates that the underlying faults were abandoned prior to the MPT, possibly due to loading by sediments. On the forelimb of fold BT5, shelf-break seismic facies are present between 1.0 and 1.5 s two-way traveltime (TWTT), suggesting a previous depositional shelf break at this location subsequent to the MPT. Truncations of seismic strata, the presence of growth stratal packages on the backlimb, and overall geometry of BT5 provide evidence that this structure accommodated Yakutat-North America convergence as a growth fold in addition to acting as the former shelf edge. The overall architecture of the continental margin is thus the product of coupled depositional and tectonic processes.

At the southeastern end of the STEEP09 seismic profile (Fig. **F10**), two currently active faults (BT1 and BT2) are present on the continental slope exhibiting less burial than the structures on the shelf. Scarps ~750 m and ~300 m high associated with the active slope structures are visible on high-resolution bathymetry of the continental slope (Worthington et al., 2008). Site GOAL-17B is located just landward of BT2, which initiated after the Pliocene–Pleistocene transition, given the lack of growth strata observed below Horizon 3 (Fig. **F10**). The presence of two distinct sedimentary packages on BT2 is indicative of either a decrease in slope sedimentation during the early Pleistocene or an increase in deformation rate across BT2. Between Horizons 1 and 2, the angle of the observed growth strata becomes less pronounced, indicating a gradual decrease in fault growth rate during the early–mid-Pleistocene. Above Horizon 1, sediments are truncated by the anticline and are very slightly tilted toward the shelf, indicating minimal deformation on BT2 from ~1 Ma to the present. Taken together, the overall geometries of the upper and lower sedimentary packages within the Bering Trough suggest a fundamental shift in margin architecture from primarily tectonically influenced to primary depositionally influenced (Fig. **F12**).

Depositional basins on Khitrov Ridge along the continental slope west of the Bering Trough contain a sedimentary record of glacial–interglacial sedimentation overprinted by active tectonic deformation (Fig. **F13**). The seismic facies at this site are interpreted to represent contrasting hemipelagic (interglacial) and glacimarine (glacial maximum) cyclicity in sediment lithofacies. Processed CHIRP images, coincident with multichannel seismic (MCS) profiles, reveal that an upper postglacial transparent layer on the CHIRP profile that corresponds to the upper ~8 m of the sediment in Core EW0408-85JC dates to younger than 14.7 ka (Davies et al., 2011). The strong reflections in the CHIRP line and near the sediment/water interface to ~0.03 s (~8–25 m) in MCS Line GOA3201 likely represent the glacimarine sediments associated with the local LGM (likely 15–30 ka at an average accumulation of ~1.2 m/k.y., although with extremely high rates for brief intervals; Davies et al., 2011). It is hypothesized that the less reflective layered sediments in the MCS profile represent interglacials or interstadials, when the Bering Glacier terminus was in a greatly retreated position relative to the shelf break and ice-rafting of sediment was much reduced to absent. In contrast, the highly reflective intervals indicate times when ice rafting was active and there were higher accumulation rates of coarser glacigenic sediment. Active faulting is imaged in high-resolution seismic Profile GOA3101, showing surface deformation indicative of significant amounts of extension (Fig. **F13**). The faults in this extensional array, however, merge toward a common position, suggesting an underlying transtensional flower structure and a possible structural link between active structures within the offshore Yakutat block and the Aleutian Trench (Worthington et al., 2008) (Fig. **F4**).

The Neogene record of sedimentation on the Surveyor Fan, a terrigenous depocenter that comprises the majority of the Alaska Abyssal Plain (Fig. **F7**), comes from DSDP Leg 18 and ODP Leg 145 drilling. Leg 18 consisted of five sites drilled and interval-cored across the southwestern corner of the Surveyor Fan, the Aleutian Trench, and up the slope of the accretionary prism (Fig. **F2**) (Kulm, Von Huene, et al., 1973). In 1992, ODP Leg 145 occupied an additional site (887) in the far southwestern Gulf of Alaska on the Patton-Murray Seamounts (Fig. **F2**) (Rea, Basov, Janecek, Palmer-Julson, et al., 1993). Terrigenous turbidites, gravelly to diatomaceous mud, and claystone of the Surveyor Fan overlie marine chalk, barren clay, and basaltic basement of Pacific plate crust (Fig. **F14**) (Kulm and von Huene, 1973). The Chirikof and Surveyor Channel systems control present-day Surveyor Fan morphology and sediment distribution, but unlike other large deep-sea channels, they are not associated with a major fluvial system or submarine canyon (Fig. **F7**) (Ness and Kulm, 1973; Stevenson and Embley, 1987; Carlson et al., 1996; Reece et al., in press). The Surveyor Channel is >700 km

long with three major tributaries (Ness and Kulm, 1973; Stevenson and Embley, 1987; Carlson et al., 1996; Reece et al., in press). Early studies divided the Surveyor Fan into two major sequences (Ness and Kulm, 1973; von Huene and Kulm, 1973; Stevenson and Embley, 1987), termed "upper" and "lower," that were based on sedimentation rates and differences in acoustic facies imaged in two-dimensional (2-D) seismic reflection profiles. The boundary between the two sequences hypothetically represented a shift from a lower coarser grained facies to an upper finer grained facies possibly associated with Surveyor Channel inception and its control on fan sediment distribution during deposition of the upper sequence (Ness and Kulm, 1973; Stevenson and Embley, 1987). Reece et al. (in press) used reprocessed U.S. Geological Survey (USGS) and recently acquired high-resolution and crustal-scale seismic reflection data to correlate stratigraphic changes and fan morphology through time. In contrast to the previous interpretation of two seismic sequences within the fan, they recognized three sequences that are regionally extensive deposits likely related to increases in exhumation on land and regional response to global changes in climate (Figs. **F14, F15**). Sequences I and II exhibit laminated, laterally semicontinuous reflectors consistent with turbiditic deposition (Reece et al., in press) (Fig. **F15**). Sequence III is thinly laminated and contains reflectors that are laterally continuous, flatter, and smoother than those in the other sequences (Fig. **F15**). This seismic facies is especially prominent on the bathymetric high at Site GOA16-1A (Fig. **F16**). Stratal relationships at the sequence boundaries are highly variable and greatly influenced by basement topography and the presence of a mass transport deposit at the base of Sequence III in the northwestern portion of the fan (Fig. **F15**). Sequence II onlaps Sequence I in the in areas where Sequence I exhibits topography but is conformable in other locations. Sequence III onlaps sequence II in the proximal fan and downlaps it in the distal fan, where both sequences pinch out farther from the sediment source (Reece et al., in press). TWTT thickness (isopach maps) for the three sequences show a varying depositional history on the Surveyor Fan (Fig. **F17**) (Reece et al., in press). Sequence I depocenters are prevalent in topographic lows between basement highs, showing no significant spatial variation, which reflects infilling of preexisting Pacific plate topography. Deposits of Sequences II and III exhibit a distinct change in the locus of accumulation to shelf proximal depocenters that thicken into the Yakutat slope, with Sequence III thicker and covering a much larger area.

The correlation between seismic reflection profiles projected into the stratigraphy at DSDP Site 178 places tentative ages on sequence boundaries (Fig. **F14**). The Sequence I/II boundary occurs at ~330 m depth at Site 178, within a section of fine-grained sand to silty turbidites and interbedded diatomaceous ooze and mud with increasing dia-

mictite upsection (Reece et al., in press; The Shipboard Scientific Party, 1973). The Sequence I/II boundary is placed at ~5 Ma, near the beginning of Glacial Interval A, based on $^{40}Ar/^{39}Ar$ dating of ash layers (Hogan et al., 1978) (Fig. **F14**). At 130 m depth, the Sequence II/III boundary lies within an interval of changing fan lithology. The section from 96 to 141 m contains abundant diamicton interbedded with silty clay and diatom-rich intervals, whereas the section from 141 to 280 m contains less diamicton, much more silty clay, and a fewer diatoms (The Shipboard Scientific Party, 1973; Reece et al., in press). The Sequence II/III boundary is tentatively dated ~1 Ma based on correlation with a magnetic polarity reversal identified at Site 178 (von Huene et al., 1973) (Fig. **F14**), making it coincident with the onset of Glacial Interval C. Both sequence boundaries are synchronous with a doubling in terrigenous sediment flux observed at ODP Site 887 at ~5 Ma and ~1 Ma, but no regional sequence boundary projected into Site 178 correlates with the onset of Glacial Interval B (Reece et al., in press).

Spatial variability in seismic facies and stratigraphy reveals the temporal evolution of fan stratigraphy. The thickening of Sequences II and III into the Yakutat terrane continental slope is evidence of the long-term connection of the Surveyor Fan to the Yakutat shelf (Stevenson and Embley, 1987; Reece et al., in press). Due to dextral transform motion of the Pacific plate and Yakutat terranes along the Queen Charlotte-Fairweather Fault, Surveyor Fan provenance likely varies from southern Coast Mountains sources in older fan sediment to St. Elias Range in younger fan sediment, similar to the sedimentary strata on the Yakutat microplate (Fig. **F18**) (Perry et al., 2009). The onset of Glacial Interval A led to a reorganization of fan sedimentation by spurring Surveyor Channel genesis (Reece et al., in press). The youngest phases of the Surveyor Channel created shelf-proximal depocenters at the base of the Yakutat terrane slope. Glacial Interval C, with its corresponding ice advances to the shelf edge, extended the Surveyor Channel across the Alaskan Abyssal Plain and markedly increased sediment flux to the Surveyor Fan. The Surveyor Channel system is a unique deepwater sediment delivery pathway because of its glacial source and trench terminus, both of which may contribute to the Surveyor's ability to maintain a major channel and evade avulsion over long periods of time (Stevenson and Embley, 1987; Reece et al., in press).

Tectonic-climate interactions

The climatic influence on the width, structural style, and distribution of deformation in mountain belts is well established through analog, numerical, and analytical mod-

eling studies based on critical wedge theory (Willett, 1999; Roe et al., 2006; Stolar et al., 2006; Whipple, 2009). Generally, an increase in erosional intensity through glacial or fluvial processes is predicted to accelerate rock uplift and decrease orogen width and relief (Whipple and Meade, 2004; Roe et al., 2006). In the Chugach-St. Elias mountains, the observed spatial patterns along the windward side of the orogen of increased exhumation rates and more deeply exhumed rocks, a relative deficiency of activity along the leeward side, and relatively shallow particle exhumation pathways are all indicative of a coupled tectonic-climate "wet prowedge" system (Fig. **F6**) (Berger et al., 2008a, 2008b; Meigs et al., 2008). Based on apatite (U-Th)/He thermochronometry, in conjunction with offshore seismic data and modeling results, Berger et al. (2008a) proposed that a structural reorganization of the St. Elias orogen occurred associated with the onset of Glacial Interval C and the MPT. The proposed structural reorganization includes initiation of a large-scale backthrust onshore and deactivation of faults in the offshore frontal portion of the wedge (Fig. **F6**). However, offshore faulting has remained active in the St. Elias Range, primarily associated with the Pamplona zone fold-and-thrust deformation front (Bruns and Schwab, 1983; Chapman et al., 2008; Plafker et al., 1994; Meigs et al., 2008). Recent modeling (Malavieille, 2010; Simpson, 2010) suggests that the extent of active faulting and folding in a frontal wedge is highly dependent on the details of mass redistribution by climate drivers and the magnitude of incoming sediment load.

However, the localization of exhumation solely along the windward equilibrium line altitude (ELA) as indicated by apatite (U-Th)/He thermochronometry (Berger et al. 2008b) has been questioned based on reinterpretation of bedrock samples and observations of detrital thermochronometry from glaciers draining from the St. Elias Range (Enkelmann et al., 2008, 2010). A purely tectonic explanation has been proposed for the observed patterns of exhumation. These patterns are interpreted not to reflect a temporal increase in exhumation rates over the Pleistocene, but rather are simply driven by a southward progression of the Yakutat fold and thrust belt, perhaps influenced by the westward arrival of the leading edge of the thicker sedimentary cover and crust of the Yakutat terrane (Meigs et al., 2008; Enklemann et al., 2009, 2010; Christenson et al., 2010; Worthington et al., submitted). Although, onshore thermochronometry data alone cannot uniquely distinguish between orographically versus tectonically controlled temporal changes in erosion (Meigs et al., 2008).

Gulf of Alaska paleoceanography

The Gulf of Alaska, located in the subarctic northeast Pacific Ocean, is an important component of Northern Hemisphere climate variability. Modern observations indicate linkages between ALPS atmospheric conditions, North Pacific circulation, and marine ecosystem productivity, yet paleoceanographic data describing past changes in this system are sparse. Previous paleoceanographic studies of the Gulf of Alaska have been limited to lower temporal resolution records retrieved from lower sediment accumulation rate locales that were sampled to avoid dilution by turbidites and remain above the regionally high carbonate-compensation depth (CCD) (Zahn et al., 1991; McDonald et al., 1999; Galbraith et al., 2007; Gebhardt et al., 2008). The late Pleistocene millennial-scale climate change typical of the North Atlantic has been inferred from earlier work in the Gulf of Alaska but has only recently been confirmed for the Expedition 341 region (Barron et al., 2009; Davies et al., 2011; Addison et al., submitted).

Core EW0408-85JC, collected on Khitrov Ridge at Expedition 341 proposed Site KB-1A, has provided a detailed record of the last deglacial period to the present based on lithofacies analyses, siliceous microfossils, organic matter composition and biogenic silica concentrations, redox-sensitive metals, and oxygen isotope data from planktonic and benthic foraminifers, all tied to a high-resolution age model (44 ^{14}C dates spanning 17,400 y) (Fig. **F19**). Surface water freshening likely due to glacial meltwater input began at 16,650 ± 170 cal y BP during an interval of relatively ice proximal sedimentation probably sourced from the Bering Glacier (Davies et al., 2011). A sharp lithofacies transition from diamict to laminated hemipelagic sediments indicates retreat of regional outlet glaciers onto land or into coastal fjords at 14,790 ± 380 cal y BP. A sudden warming and/or freshening of the Gulf of Alaska surface waters corresponds with this lithofacies transition and coincides with the Bølling interstadial of Northern Europe and Greenland. Cooling and/or higher surface water salinities returned during the Allerød interval, coincident with the Antarctic Cold Reversal, and continued until 11,740 ± 200 cal y BP, when onset of warming coincided with the end of the Younger Dryas (Davies et al., 2011). Two laminated opal-rich intervals (deglacial Bølling-Allerød [B-A] and the early Holocene) reveal discrete periods of enhanced water column productivity that likely correlate to similar features observed elsewhere on the margins of the North Pacific and are coeval with episodes of rapid sea level rise (Barron et al., 2009; Davies et al., 2011; Addison et al., submitted). Proxies for Holocene productivity are consistently higher than during the colder periods of expanded regional glacial activity. The finding of low productivity during the glacial and stadial

intervals is consistent with previous findings from the open Gulf of Alaska, but are inconsistent with the hypothesis that such changes are the result of higher upper-ocean stratification during cold intervals (Sigman et al., 2004; Jaccard et al., 2005). The B-A interval is laminated and enriched in redox-sensitive metals, suggesting productivity-driven dysoxic-to-anoxic conditions in the water column. Enriched sedimentary $\delta^{15}N$ ratios are present in these laminated intervals, suggesting a link between productivity and N cycle dynamics (Addison et al., submitted). Remobilization of iron from newly inundated continental shelves may have helped to fuel these episodes of elevated primary productivity and sedimentary anoxia (Davies et al., 2011; Addison et al., submitted).

A temporal correspondence exists between water column and sedimentation events observed in Core EW0408-85JC and global last deglacial–early Holocene climate. In addition to the Bølling interstadial diamict–laminated facies transition, an early termination of the Bølling-Allerød warm interval observed in Core EW0408- 85JC relative to the North Atlantic appears in a number of high-latitude North Pacific records (Davies et al., 2011). When compared to the $\delta^{18}O$ ice core records from Antarctica (Ruth et al., 2007) and Greenland (Andersen et al., 2006; Rasmussen et al., 2006; Svensson et al., 2006), the planktonic oxygen isotope pattern of Core EW0408-85JC bears some similarity to both of these records, lending support to the idea that North Pacific climate records reflect both North Atlantic and Southern Ocean forcing (Mix et al., 1999; Davies et al., 2011).

Site survey data acquisition

In 2004, 1800 km of high-resolution MCS reflection profiles were collected in the Gulf of Alaska aboard the R/V *Maurice Ewing* (Fig. **F2**). The sources were dual 45/45 in^3 GI (generator-injector [GI]) air guns with 3–5 m vertical resolution. For the lines over the Surveyor Fan, dual 105/105 in^3 GI guns were used. Processing included trace regularization, normal move-out correction, bandpass filtering, muting, f-k (frequency-wave number) filtering, stacking, water-bottom muting, and finite-difference migration (Gulick et al., 2007; Berger et al., 2008a).

In 2008, ~1250 km of MCS reflection data and ~500 km of wide-angle seismic refraction data were acquired in the Gulf of Alaska as part of the St. Elias Erosion and Tectonics Project (STEEP; Fig. **F2**). The primary tectonic survey targets included the offshore Yakutat-North America deformation front, the offshore St. Elias orogenic wedge, known as the Pamplona zone fold-thrust belt, and the Dangerous River zone

(DRZ). The survey also targeted the transition fault (results presented in Christeson et al., 2010) and the offshore zone of seismicity in the Pacific plate known as the Gulf of Alaska shear zone (Gulick et al., 2007; preliminary STEEP results presented in Reece et al., 2009). Primary stratigraphic targets included mapping the shelf and Surveyor Fan sediments to basement.

In 2011, ~3022 km of MCS reflection and ~600 km of wide-angle seismic refraction data were acquired with supporting sonobuoy refraction data. The purpose of the Gulf of Alaska seismic mapping program was to image the distal parts of the Surveyor and Baranof Fans and the northern Pacific plate crustal structure that these sediment bodies interact with. The program was funded through the USGS as part of the United States assessment of Article 76 of the Law of the Sea Convention. The survey design targeted two areas for assessment and a series of science targets to better understand the tectonic-sedimentary system within the Gulf of Alaska. The two regions where the Alaskan deep-sea fans cross the U.S. Exclusive Economic Zone are where the Surveyor Fan system interacts with Aja Fracture Zone, potentially forming a thickened deposit, and the distal Baranof Fan. Science targets include the Surveyor Channel and its interaction with the Aleutian subduction zone, the Aja Fracture Zone, the Chirikof Channel, and the channels of the Baranof Fan (Horizon, North, etc.). Expedition 341 Sites GOAL-18A, GOA18-1A, and GOA18-2A are in the imaged distal part of the Surveyor Fan to the north and west of Surveyor Channel.

Acquisition parameters for both the 2008 and 2011 seismic reflection data included a seismic source of 36 Bolt air guns with a total volume of 6600 in^3 fired every 50 m. Receivers were located in an 8 km long solid streamer at 12.5 m spacing. Common midpoint spacing was 6.25 m. Seismic data processing included trace regularization, normal move-out correction, bandpass filtering, muting, stacking and frequency-wave number migration using Paradigm Geophysical FOCUS software (detailed seismic processing work flow in Worthington, 2010). Vertical resolution at the seafloor for this data set is 20–30 m.

Wide-angle reflection and refraction data were recorded along two profiles: STEEP01 is oriented west-east, crossing the offshore Yakutat microplate from near the Bering Glacier to east of the DRZ (Fig. **F4**); STEEP02 is oriented north-south and crosses the Yakutat shelf, the Transition fault, and the adjacent Pacific plate (Fig. **F2**). For Profile STEEP01, 25 ocean bottom seismometers (OBS) were deployed at ~15 km spacing across the profile. Data acquisition was simultaneous for the MCS and wide-angle data across STEEP01, with shot spacing of 50 m. Data were recovered from 21 instruments. Processing and survey details for Profile STEEP02 are presented in Christeson et al. (2010).

Locations of a 1975 USGS survey and a 1979 survey by Western Geophysical are shown in Figures **F2** and **F17.** These seismic profiles provide ~30 m vertical resolution and reliably image up to 4 s TWTT of the subsurface, ~3.5 km at 1750 m/s seismic velocity. These profiles image major faults, fault-related folds, and unconformities, roughly illustrating stratigraphic and structural relationships along the margin (Bruns, 1983, 1985; Bruns and Schwab, 1983; Lagoe et al., 1993; Zellers, 1995). Processing of the 1970s USGS data used in Reece et al. (in press) and Worthington et al. (2010) included bandpass filtering, muting, normal move-out correction, and stacking. The 1980s USGS data processing included trace editing and balancing, muting, and bandpass filtering.

In addition to MCS data, high-resolution subbottom profiles and multibeam bathymetry exist for the Expedition 341 region. High-resolution subbottom profiles were collected during the 2004 R/V *Maurice Ewing* cruise using a Bathy 2000-P CHIRP subbottom profiler. High-resolution (5–20 m^2) multibeam sonar data were collected at the proposed drill sites. At shallower depths (<800 m) a SIMRAD EM1002 midwater high-resolution multibeam sonar was used, and in deeper water (i.e., Site GOAL-16B), a STN ATLAS Hydrosweep DS-2 multibeam sonar was used. Additionally, in 2005, more than 162,000 km^2 of high-resolution (~100 m^2) multibeam sonar data were collected along the base of the Yakutat slope in the Gulf of Alaska in support of the United Nations Law of the Sea extended continental shelf investigation. Data were collected aboard the R/V *Kilo Moana* and post-processed at the University of New Hampshire Center for Coastal Studies (Mayer et al., 2005; Gardner et al., 2006). Vertical accuracy is ~0.3%–0.5% of the water depth. Additional high-resolution SeaBeam multibeam data were collected in 1988 by NOAA on the continental slope and proximal Surveyor Fan southwest of Kayak Island.

The supporting site survey data for Expedition 341 are archived at the **IODP Site Survey Data Bank.**

Scientific objectives

The aim of drilling the southern Alaska margin is to obtain a Neogene-to-recent sedimentary record of NCIS glaciation and its influence on tectonic processes and relationship with regional and global paleoclimatic changes. Focus is placed on establishing the timing and locus of NCIS expansion during the Pliocene and Pleistocene and its impact on surface processes and freshwater and sediment fluxes to the

subarctic Pacific Ocean. Erosion and sediment redistribution during glacial–interglacial cycles may have a direct effect on mountain building and deformation; thus, a goal is to determine the timing of changes in deformation patterns and sedimentary fluxes to the continental shelf and the adjacent deep-sea sediment fan. Priority is placed on documenting the NCIS response to global climate forcing. A unique component of Expedition 341 is the availability of extensive adjacent onland studies of glacial and tectonic processes and existing seismic coverage on the margin, which, when coupled with the age and stratigraphic controls provided by drilling, will allow for a more complete source-to-sink study of the depositional history, glacial record, and sequence stratigraphic significance of these strata. Sampling the rapidly accumulating Neogene glacimarine sediments will document the spatial and temporal behavior of the geomagnetic field at extremely high temporal resolution. Such data are missing from this part of the planet and are required to assess the geodynamo processes that control secular variation and geomagnetic polarity reversals.

To address these objectives we will core, log, and analyze sedimentary records from a potential five-site depth transect from the distal Surveyor Fan to the zone of active deformation on the outer shelf to recover strata that contain a record of the most significant climate and tectonic events of the southern Alaska continental margin with varying temporal resolution and stratigraphic completeness. Of particular note are stratigraphic intervals that have the potential of preserving records of the key phases of the evolution of the NCIS, such as the late Miocene inception of tidewater glaciation, warm early Pliocene events, large-scale early Pleistocene expansion of glacial coverage, and the mid-Pleistocene glacial intensification leading to the onset of highly erosive ice streams (Fig. **F3**). The expected chronostratigraphy and integrated multidisciplinary sediment provenance and climatic proxy record–based reconstructions of glacial dynamics are fundamental to understanding tectonic-climate interplay and the processes responsible for developing high-latitude continental margin stratigraphy.

Specific scientific objectives

1. *Document the tectonic response of an active orogenic system to Pliocene and mid-Pleistocene climate change.*

Our fundamental hypothesis is that the St. Elias orogen has undergone perturbation that has markedly changed the patterns and rates of deformation and exhumation in the orogenic wedge (Figs. **F3, F6**). Enhanced glacial erosion associated with the MPT

and the establishment of highly erosive ice streams lead to substantial mass redistribution in the wedge, shutting down existing regions of active deformation and refocusing the deformation and exhumation patterns of the orogen (Berger et al., 2008a; Worthington et al., 2008; 2010; Chapman et al., 2008). Testing the hypothesis that the MPT led to rapid intensification of erosion along the windward side of the mountain range first requires that we establish the baseline erosion conditions in the orogen prior to this climate perturbation, which involves integration of results of the Surveyor Fan seismic reflection data sets (Fig. **F17**) and sediment mass fluxes and provenance records from the most distal proposed Site GOA18-2A. Documenting climatic influence on enhanced exhumation requires establishing a connection between a change in sediment provenance to more windward source rocks (e.g., Prince William and Yakutat terranes) and establishing glacial conditions, which will require sediment accumulation rates and provenance records from Sites GOA16-1A and GOA18-2A, as they likely contain a proximal and a distal (and complete) record of the Surveyor Fan sequences, respectively, but that are still within a reasonable drilling depth. Lastly, addressing the hypothesis that the onset of ice streams has completely altered the deformation and exhumation patterns in the orogenic wedge (Berger et al., 2008a) will require age control, sediment accumulation rates, and provenance records from the more proximal Sites GOAL-15C, GOA16-1A, and GOAL-17B near the Bering Glacier, where tectonic deformation patterns have been shown to evolve with sedimentation (Worthington et al., 2010). Drilling also will allow testing the alternative hypothesis that rates of exhumation and erosion have not changed in the past 5 m.y. and that the locus of exhumation has steadily progressed southeastward with the encroachment of thicker crust (Enkelmann et al., 2008, 2009, 2010).

2. *Establish the timing of Neogene advance and retreat phases of the northwestern Cordilleran ice sheet to test its relation to global ice sheet dynamics.*

Previous scientific drilling on glaciated margins similar to southern Alaska has provided a rich and detailed examination of global Neogene ice dynamics including DSDP Leg 18 (Kulm, von Huene, et al., 1973), DSDP Leg 28 (Hayes, Frakes, et al., 1975), ODP Leg 105 (Srivastava, Aurthur, Clement, et al., 1987), ODP Leg 113 (Barker, Kennett, et al., 1988), ODP Leg 119 (Barron, Larsen, et al., 1989), ODP Leg 145 (Rea, Basov, Janecek, Palmer-Julson, et al., 1993), ODP Leg 152 (Larsen, Saunders, Clift, et al., 1994), ODP Leg 178 (Barker, Camerlenghi, Acton, et al., 2002), ODP Leg 188 (O'Brien, Cooper, Richter, et al., 2001), and IODP Expedition 318 (Escutia, Brinkhuis, Klaus, et al., 2011). We expect that drilling on this glaciated margin will complement these expeditions by filling a substantial gap in knowledge of North American ice dy-

namics by establishing the timing of advance and retreat phases of the NCIS throughout the Quaternary. Establishing the timing of NCIS advance–retreat cycles will address a major challenge in Quaternary paleoclimatology, which is to know the extent to which glacial-age climate change was a synchronous worldwide event and what the driving mechanisms were for potentially propagating millennial-scale warming–cooling cycles around the globe (oceanic, atmospheric, or both) (Clapperton, 2000; Mix et al., 2001; Hill et al., 2006). Although many records (Clark and Bartlein, 1995; Behl and Kennett, 1996; Hendy and Kennett, 1999; Grigg et al., 2001; Hendy and Cosma, 2008; Davies et al., 2011) provide strong evidence for millennial-scale climate change in the northeast Pacific in the Quaternary, the timing and character of these variations in relation to North Atlantic or Southern Ocean records are still unknown, largely due to uncertainties resulting from the scarcity of high-resolution records from the region. The proposed study area is an ideal one to address these issues because the regional climate and oceanography are highly sensitive to atmospheric-oceanic dynamics in the North Pacific (Bartlein et al., 1998). The Expedition 341 drilling program will provide a higher-resolution chronology and a more complete record of glacial activity in the St. Elias orogen, which will allow us to assess the timing of the changes relative to the established records of global forcing (i.e., global $\delta^{18}O$ stack).

3. *Conduct an expanded source-to-sink study of the complex interactions between glacial, tectonic, and oceanographic processes responsible for creation of Neogene high-latitude continental margin sequences.*

The Gulf of Alaska margin offers the opportunity for expanded study of the complex interactions between glacial, tectonic, and oceanographic processes responsible for creation of one of the thickest, most complete Neogene high-latitude continental margin sequences (Stevenson and Embley, 1987; Lagoe et al., 1993; Reece et al., in press). In southern Alaska, high sediment accumulation rates driven by the interaction of glacial processes with a dynamic tectonic setting have resulted in the substantial growth of this continental margin (Figs. **F11, F12, F17**) (Lagoe et al., 1993; Plafker, 1994; Willems, 2009; Worthington et al., 2010), and the proposed drilling coupled with the onshore work accomplished as part of STEEP to examine sediment production and transfer will allow us to document the depositional history, glaciological record, and sequence stratigraphic significance of these strata in a source-to-sink context. To test hypothetical models of glacial-sequence formation for temperate glacimarine settings (Dunbar et al., 2008) and those specific to Alaska (Fig. **F11**) (Powell and Cooper, 2002; Willems, 2009), we will make use of the extensive seismic coverage

on the shelf and the age and stratigraphic controls provided by our drilling program. Emphasis will be placed on documenting how the sedimentary "signals" of tectonic and climate induced changes in sediment production vary through the morphodynamic elements of glacimarine sediment dispersal systems.

4. *Understand the dynamics of productivity, nutrients, freshwater input to the ocean, and surface and subsurface circulation in the Northeast Pacific, and their role in the global carbon cycle.*

Drilling on the Gulf of Alaska continental margin will create a high-resolution (millennial) view of variability in productivity and water column circulation under a range of different forcings, including global-scale factors such as insolation, CO_2, and regional factors such as sea ice and runoff. The North Pacific is currently a low-salinity region, which inhibits large-scale intermediate and deep-water formation (Emile-Geay et al., 2003). However, evidence exists for enhanced Pacific meridional overturning circulation (PMOC) that has antiphase activity with Atlantic meridional overturning circulation (AMOC) (Okazaki et al., 2010; Menviel et al., in press). The dynamics of Northern Hemisphere freshwater and precipitation fluxes to the respective Atlantic and Pacific Oceans may be the primary control on large-scale intermediate and deep water-column circulation in the Pacific. Drilling also will allow us to compare and contrast the magnitude and scales of variability in water column productivity between glacial, interstadial, and interglacial conditions, which differ in detail such as insolation forcing, sea level, and so on. Productivity maxima events are widespread around the rim of the North Pacific (e.g., Mix et al., 1999). At Site KB-2A, a high-resolution chronology based on nearby shallow piston coring links these events locally to episodes of global sea level rise, leading Davies et al. (2011) to conclude that remobilization of iron and other limiting nutrients from continental shelves and inundated estuaries during sea level rise (e.g., Lam and Bishop, 2008; Severmann et al., 2010) contributes to events of productivity and hypoxia around the margins of the North Pacific. Assessing this hypothesis will require finding similar events associated with earlier sea level rises in the region.

A consequence of this episodic enhancement of productivity coupled with glacial-induced changes in terrigenous carbon supply is variability on a range of timescales and forcing conditions in the fluxes and burial of C, N, and Si and plankton assemblages on the Gulf of Alaska margin (Davies et al., 2011; Addison et al., submitted). In general, the paleoproductivity questions addressed by this expedition are fairly unique and significant because this understudied region is very productive and hosts important fisheries and ecosystems (Stabeno et al., 2004). Drilling offers a unique opportu-

nity to study how the past Gulf of Alaska marine ecosystem behaved during earlier periods of warmth, several of which are likely models for future warming trends.

5. *Document the spatial and temporal behavior during the Neogene of the geomagnetic field at extremely high temporal resolution in an undersampled region of the globe.*

Over the last decade, our understanding of the paleomagnetic record during the Pliocene–Pleistocene has improved substantially, providing new techniques and significantly improving stratigraphic resolution and reliability. Resulting largely from ODP/IODP drilling of ocean sediments, we now know that the strength of the Earth's magnetic field (paleointensity) varies globally on suborbital timescales for at least the last 1.5 m.y. (e.g., Channell et al., 2009), that short-duration (millennial or less) geomagnetic polarity events (magnetic excursions) are not only real, but common components of field behavior (e.g., Lund et al., 2001, 2005; Channell et al., 2002), and that polarity transitions display complex though reproducible behaviors (e.g. Channell et al., 1998; Clement et al., 2004; Mazaud et al., 2009), all hinting at the dynamics that drive geomagnetic change. New records have also resulted in improved chronologies (Channell et al., 2008), allowing increasingly reliable temporal calibrations and improved resolution of magnetic stratigraphic techniques. Global relative paleointensity (RPI) stacks providing orbital resolution tuning targets extend back over 2 m.y. (Valet et al., 2005), suborbital resolution stacks extend back over 1.5 m.y. (Channell et al., 2009), and multi-millennial records are available for the last 75 k.y. (Laj et al., 2004). Though constrained by fewer records, a western Pacific regional stack since 3 Ma (Yamazaki and Oda, 2005) provides additional tuning targets that may prove to be globally applicable. The RPI record is being refined through ongoing IODP research, and its integration with other stratigraphic and absolute dating techniques was a primary objective of North Atlantic IODP Expeditions 303 and 306 (e.g., Channell, Kanamatsu, Sato, Stein, Alvarez Zarikian, Malone, et al., 2006). RPI, together with the recognition of short-duration polarity events (e.g., Lund et al., 1998, 2001; Guyodo and Valet, 1999; Channell et al., 2002; Singer et al., 2002), provides additional stratigraphic opportunities through what has been termed the geomagnetic instability timescale (Singer et al., 2002).

Yet, much of this understanding is derived from data obtained from a limited part of the world. Historical data, dynamo models, and some paleomagnetic records attest to the importance of regions of concentrated flux that result in longitudinal asymmetry of the geomagnetic field. These asymmetries include subdued secular variation in the Pacific relative to the Atlantic hemisphere and regions of concentrated geomagnetic

flux (flux lobes or bundles) over Canada and Siberia at ~60°N latitude (Fig. **F20**). If truly long-lived, these imply that the structure of the geodynamo reflects lower mantle control, possibly through regulation of the long-term heat flux from the core (Bloxham and Gubbins, 1987; Bloxham, 2000). As such, these mantle-controlled non-axisymmetric flux concentrations could provide organizing structures that may control much of the dynamics of the geomagnetic field.

The ability to develop magnetic stratigraphies that allow regional to global correlation over a range of timescales will be important to the success of IODP drilling in southern Alaska. Preliminary paleomagnetic results from the Gulf of Alaska (Davies et al., unpubl. data) suggest that the proposed sites record geomagnetic field variability consistent on submillennial scales with independently dated Holocene paleosecular variation records from Alaskan lakes (Geiss and Banerjee, 2003) and across North America (Lund, 1996). Long paleomagnetic time series constrained by independent chronologies from radiocarbon dating, tephrachronology, and stable isotope stratigraphies would allow Pacific paleomagnetic secular variation and relative paleointensity to be compared with the many records from the Atlantic (e.g., Channell, 1999, 2006; Stoner et al., 2000; Lund et al., 2005). Outside of reversals and excursions, few of these studies have focused on the directional record, having concentrated on relative paleointensity. By linking paleomagnetic directions and intensity between these regions, we will be able to assess geomagnetic persistence, a signature of the mantle's influence on the geodynamo and the paleomagnetic record (Gubbins et al., 2007; Stoner, 2009; Amit et al., 2010), and to facilitate a test of the hypothesis that heterogeneities of the lowermost mantle influence the structure of the geodynamo and, therefore, the behavior of the geomagnetic field (Cox and Doell, 1964).

Drilling and coring strategy

We propose to drill a depth transect in Miocene–modern continental margin clastic strata (continental margin glacimarine, turbidites, and hemipelagic and diatomaceous clastic strata) using a combination of sites in water depths from 178 to 4218 m and drilled to ~150–1158 m depths. The operations plan and time estimates for the primary and alternate sites are summarized in Tables **T2** and **T3,** respectively. Time estimates are based on formation lithologies and depths inferred from seismic and regional geological interpretations, including prior drilling in this area (Leg 18 and industry; Risely et al., 1992). After departing from Victoria, British Columbia, Canada, we will transit for ~4 days to the Gulf of Alaska and prepare for drilling operations.

The proposed drilling strategy begins with drilling at proposed Site KB-2A followed by proposed Sites GOAL-15C, GOAL-17B, GOA16-1A, and GOA18-2A.

At Site KB-2A, three holes will be cored with the advanced piston corer (APC) to refusal or ~200 meters below seafloor (mbsf). A fourth hole will be cored with the APC/extended core barrel (XCB) ~400 mbsf. Nonmagnetic core barrels will be used in all APC sections, and the orientation of APC cores will be measured with the FlexIt tool in Hole A.

At Sites GOAL-15C and GOAL-17B, the first hole at each site (Hole A) will be APC cored to refusal (~250 mbsf) followed by XCB coring to ~1112 mbsf (GOAL-15C) or ~1032 mbsf (GOAL-17B). We are approved by the Environmental Protection and Safety Panel (EPSP) to drill 10% deeper than these depths in case the velocity estimates are incorrect. Nonmagnetic core barrels will be used in all APC sections. The orientation of APC cores will be measured with the FlexIt tool at Site GOAL-17B.

At Site GOA16-1A, three holes will be cored with the APC to ~200 mbsf. A fourth hole will be APC/XCB cored to ~978 mbsf. At Site GOA18-2A, two holes will be cored with the APC to ~200 mbsf. A third hole will be APC/XCB cored to ~780 mbsf. A fourth hole will be APC/XCB cored to ~425 mbsf. While drilling/coring in Hole A for both these sites, a number of advanced piston coring temperature tool (APCT-3) and sediment temperature tool (SET) measurements will be made, as formation conditions permit, to complement existing data. Nonmagnetic core barrels will be used in all APC sections, and the orientation of APC cores will be measured with the FlexIt tool in Hole A.

After coring is completed at each site, holes will be conditioned, displaced with logging mud, and logged as per the logging plan (see **"Downhole measurements strategy"**).

Drilling operations in shallow water require special precautions to ensure safety for crew and equipment. Weather conditions (particularly sea state and resulting heave behavior of the vessel) are critical (see **"Risks and contingency"**).

Risks and contingency

There are a number of risks to achieving the objectives of this program. Weather and the nature of the sediments in the Gulf of Alaska may present operational risks that could negatively impact coring/logging operations, hole stability, core recovery, core

quality, and rate of penetration. Expedition 341 has been scheduled to take place during the summer, the optimum weather season; however, severe weather may still occur and could adversely impact operational efficiency and transit speed. Additionally, the possible presence of ice rafted debris, chert layers, and glacial deposits could lead to bent core barrels and damaged APC shoes and XCB bits. A series of alternate sites are available for contingency operations.

Downhole measurements strategy

Wireline logging

We plan to acquire wireline logs from all sites proposed in the primary operations plan. Three standard IODP tool string configurations will be deployed in the deepest hole at each site. These are the triple combination (triple combo), Formation MicroScanner (FMS)-sonic, and Versatile Seismic Imager (VSI) tool strings (Fig. **F21**).

At each site logged the first tool string deployed will be the triple combo, which will measure density, neutron porosity, resistivity, and natural and spectral gamma ray, along with caliper. The caliper log provided by the density tool will allow an assessment of hole conditions and the potential for success of subsequent logging runs. The second run will be the FMS-sonic and will record gamma ray, sonic velocity (for compressional and shear waves), and high-resolution electrical images. The compressional velocity logs will be combined with the density logs to generate synthetic seismograms for detailed seismic-log correlations. To calibrate the integration of well and seismic data, the third run in each hole will be a vertical seismic profile (VSP), recorded with the VSI, which will require use of a seismic sound source. The expected spacing between stations will be 50 m over the entire open interval of each hole logged. Spacing could be reduced for specific targets or adjusted for hole conditions. The seismic sound source used during the check shot/VSP survey will be subject to the IODP marine mammal policy and may have to be postponed or cancelled if certain policy conditions are not met. For more information on specific logging tools, please refer to **iodp.ldeo.columbia.edu/TOOLS_LABS.**

At three of the five primary sites we plan to deploy the high-resolution Lamont Doherty Earth Observatory (LDEO) magnetic properties tool string. This consists of the Magnetic Susceptibility Sonde (MSS) in combination with the Multisensor Magnetometer Module (MMM). These tools will acquire total field and three-axis magnetic field measurements and magnetic susceptibility. The MMM and MSS are currently un-

der development at LDEO-Borehole Research Group (BRG), and it is anticipated that they will be available for deployment during Expedition 341.

At sites (GOAL-17B and GOAL-15C) where the magnetic properties tool string is not deployed, the triple combo will be modified to replace the Dual Induction Tool (DIT-E) resistivity tool with the MSS; this is called the "paleo-combo" (Fig. **F22**).

Formation temperature measurements

The downhole measurement plan includes a depth series of reconnaissance temperature measurements at Sites GOA16-1A and GOA18-2A within the Surveyor Fan, principally using the APCT-3 tool, supplemented by the SET if necessary where sediments are more consolidated. The scientific objective of the temperature measurement plan is to provide sufficient data to reconstruct the thermal gradient at each site. This information will help constrain the subduction inputs and the history of burial diagenesis.

Sampling and data sharing strategy

Shipboard and shore-based researchers should refer to the IODP Sample, Data, and Obligations Policy (**www.iodp.org/program-policies/**). This document outlines the policy for distributing IODP samples and data. It also defines the obligations incurred by sample and data recipients. All requests for data and core samples must be approved by the Sample Allocation Committee (SAC). The SAC is composed of the Co-Chief Scientists, Expedition Project Manager, and IODP Curator on shore and curatorial representative in place of the Curator onboard the ship.

Every member of the science party is obligated to carry out scientific research for the expedition and publish it. For this purpose, shipboard and shore-based scientists are expected to submit sample requests (at **smcs.iodp.org/**) detailing their science plan at least 3 months before the beginning of the expedition. Based on sample requests submitted by this deadline and input from the scientific party, the SAC will prepare a tentative sampling plan that will be revised on the ship as dictated by recovery and cruise objectives. The sampling plan will be subject to modification depending upon the actual material recovered and collaborations that may evolve between scientists during the expedition. This planning process is necessary to coordinate the research to be conducted and to ensure that the scientific objectives are achieved.

Minimizing the overlap of measurements among the shipboard party and identified shore-based collaborators will be a factor in evaluating sample requests. Success will require collaboration, integration of complementary data sets, and consistent methods of analysis. Substantial collaboration and cooperation are highly encouraged.

Shipboard sampling will be restricted to acquiring ephemeral data types and to low-resolution sampling, mainly so that we can rapidly produce age model data critical to the overall objectives of the expedition and for planning for higher resolution sampling postcruise. Whole-round samples will be taken for pore fluid chemistry, physical properties, and possibly microbiological experiments. Sampling for the bulk of individual scientists' personal research will be postponed until a shore-based sampling party to be implemented ~4 months after the expedition at the Gulf Coast Repository (College Station, Texas, USA).

All collected data and samples will be protected by a 1 y moratorium period following the completion of the sampling party, during which time data and samples are available only to the Expedition 341 science party and approved shore-based participants. Modifications to the sampling plan during the expedition and the moratorium period require the approval of the SAC.

There may be considerable demand for samples from a limited amount of cored material for some critical intervals. Critical intervals may require special handling, a higher sampling density, reduced sample size, or continuous core sampling for a set of particular high-priority research objectives. The SAC may require an additional formal sampling plan before critical intervals are sampled and a special sampling plan will be developed to maximize scientific participation and to preserve some material for future studies. The SAC can decide at any stage during the expedition or during the moratorium period which recovered intervals should be considered as critical.

At Sites KB-2A, GOA16-1A, and GOA18-2A we plan to split and describe on the ship only some of the holes acquired at each site and preserve selected intervals as whole-round cores. Immediately following the expedition, the unsplit cores will be sent to shore-based laboratories to be scanned by computed tomography. Splitting and description of these cores will be accomplished last at the IODP Gulf Coast Repository.

References

Addison, J.A., Finney, B.P., Dean, W.E., Davies, M.H., Mix, A.C., and Jaeger, J.M., submitted. Productivity maxima and sedimentary $\delta^{15}N$ during the Last Glacial Maximum termination in the Gulf of Alaska. *Paleoceanography*.

Amit, H., Aubert, J., and Hulot, G., 2010. Stationary, oscillating, or drifting mantle–driven geomagnetic flux patches? *J. Geophys. Res., [Solid Earth],* 115:B07108–B07121. **doi:10.1029/2009JB006542**

Andersen, K.K., Svensson, A., Johnsen, S.J., Rasmussen, S.O., Bigler, M., Röthlisberger, R., Ruth, U., Siggaard-Andersen, M.-L., and Steffensen, J.P., 2006. The Greenland ice core chronology 2005, 15–42 ka, Part 1: Constructing the timescale. *Quat. Sci. Rev.,* 25(23–24):3246–3257. **doi:10.1016/j.quascirev.2006.08.002**

Barker, P.F., Camerlenghi, A., Acton, G.D., et al., 1999. *Proc. ODP, Init. Repts.,* 178: College Station, TX (Ocean Drilling Program). **doi:10.2973/odp.proc.ir.178.1999**

Barker, P.F, Kennett, J.P., et al., 1988. *Proc. ODP, Init. Repts.,* 113: College Station, TX (Ocean Drilling Program). **doi:10.2973/odp.proc.ir.113.1988**

Barron, J.A., Basov, I.A., Beaufort, L., Dubuisson, G., Gladenkov, A.Y., Morley, J.J., Okada, M., Ólafsson, D.K., Pak, D.K., Roberts, A.P., Shilov, V.V., and Weeks, R.J., 1995. Biostratigraphic and magnetostratigraphic summary. *In* Rea, D.K., Basov, I.A., Scholl, D.W., and Allan, J.F. (Eds.), *Proc. ODP, Sci. Results,* 145: College Station, TX (Ocean Drilling Program), 559–575. **doi:10.2973/odp.proc.sr.145.145.1995**

Barron, J.A., Bukry, D., Dean, W.E., Addison, J.A., and Finney, B., 2009. Paleoceanography of the Gulf of Alaska during the past 15,000 years: results from diatoms, silicoflagellates, and geochemistry. *Mar. Micropaleontol.,* 72(3–4):176–195. **doi:10.1016/j.marmicro.2009.04.006**

Barron, J., Larsen, B., et al., 1989. *Proc. ODP, Init. Repts.,* 119: College Station, TX (Ocean Drilling Program). **doi:10.2973/odp.proc.ir.119.1989**

Bartlein, P.J., Anderson, K.H., Anderson, P.M., Edwards, M.E., Mock, C.J., Thompson, R.S., Webb, R.S., Webb, T., III, and Whitlock, C., 1998. Paleoclimate simulations for North America over the past 21,000 years: features of the simulated climate and comparisons with paleoenvironmental data. *Quat. Sci. Rev.,* 17(6–7):549–585. **doi:10.1016/S0277-3791(98)00012-2**

Behl, R.J., and Kennett, J.P., 1996. Brief interstadial events in the Santa Barbara Basin, NE Pacific, during the last 60 kyr. *Nature (London, U. K.),* 379(6562):243–246. **doi:10.1038/379243a0**

Berger, A.L., Gulick, S.P.S., Spotila, J.A., Upton, P., Jaeger, J.M., Chapman, J.B., Worthington, L.A., Pavlis, T.L., Ridgway, K.D., Willems, B.A., and McAleer, R.J., 2008a. Quaternary tectonic response to intensified glacial erosion in an orogenic wedge. *Nat. Geosci.,* 1:793–799. **doi:10.1038/ngeo334**

Berger, A.L., Spotila, J.A., Chapman, J.B., Pavlis, T.L., Enkelmann, E., Ruppert, N.A., and Buscher, J.T., 2008b. Architecture, kinematics, and exhumation of a convergent orogenic wedge: a thermochronoligical investigation of tectonic–climatic interactions within the central St. Elias orogen, Alaska. *Earth Planet. Sci. Lett.,* 270(1–2):13–24. **doi:10.1016/j.epsl.2008.02.034**

Bloxham, J., 2000. The effect of thermal core–mantle interactions on the palaeomagnetic secular variation. *Philos. Trans. R. Soc., A,* 358(1768):1171–1179. **doi:10.1098/rsta.2000.0579**

Bloxham, J., and Gubbins, D., 1987. Thermal core–mantle interactions. *Nature (London, U. K.),* 325:511–513. **doi:10.1038/325511a0**

Boyd, P.W., Law, C.S., Wong, C.S., Nojiri, Y., Tsuda, A., Levasseur, M., Takeda, S., Rivkin, R., Harrison, P.J., Strzepek, R., Gower, J., McKay, R.M., Abraham, E., Arychuk, M., Barwell-Clarke, J., Crawford, W., Crawford, D., Hale, M., Harada, K., Johnson, K., Kiyosawa, H., Kudo, I., Marchetti, A., Miller, W., Needoba, J., Nishioka, J., Ogawa, H., Page, J., Robert, M., Saito, H., Sastri, A., Sherry, N., Soutar, T., Sutherland, N., Taira, Y., Whitney, F., Wong, S.-K.E., and Yoshimura, T., 2004. The decline and fate of an iron-induced subarctic phytoplankton bloom. *Nature (London U. K.),* 428(6982):549–553. **doi:10.1038/nature02437**

Briner, J.P., Kaufman, D.S., Werner, A., Caffee, M., Levy, L., Manley, W.F., Kaplan, M.R., and Finkel, R.C., 2002. Glacier readvance during the late glacial (Younger Dryas?) in the Ahklun Mountains, southwestern Alaska. *Geology,* 30(8):679–682. **doi:10.1130/0091-7613(2002)030<0679:GRDTLG>2.0.CO;2**

Brocher, T.M., Fuis, G.S., Fisher, M.A., Plafker, G., Moses, M.J., Taber, J.J., and Christensen, N.I., 1994. Mapping the megathrust beneath the northern Gulf of Alaska using wide-angle seismic data. *J. Geophys. Res., [Solid Earth],* 99(B6):11663–11685. **doi:10.1029/94JB00111**

Bruhn, R.L., Pavlis, T.L., Plafker, G., and Serpa, L., 2004. Deformation during terrane accretion in the Saint Elias orogen, Alaska. *Geol. Soc. Am. Bull.,* 116(7–8):771–787. **doi:10.1130/B25182.1**

Bruns, T.R., 1983. Model for the origin of the Yakutat block, an accreting terrane in the northern Gulf of Alaska. *Geology,* 11(12):718–721. **doi:10.1130/0091-7613(1983)11<718:MFTOOT>2.0.CO;2**

Bruns, T.R., 1985. Tectonics of the Yakutat block, an allochthonous terrane in the northern Gulf of Alaska. *Open-File Rep.–U.S. Geol. Surv.,* 85-13. **http://www.dggs.alaska.gov/webpubs/usgs/of/text/of85-0013.PDF**

Bruns, T.R., and Schwab, W.C., 1983. Structure maps and seismic stratigraphy of the Yakataga segment of the continental margin, northern Gulf of Alaska. *U.S. Geol. Surv.,* MF-1424.

Calkin, P.E., Wiles, G.C., and Barclay, D.J., 2001. Holocene coastal glaciation of Alaska. *Quat. Sci. Rev.,* 20(1–3):449–461. **doi:10.1016/S0277-3791(00)00105-0**

Carlson, P.R., 1989. Seismic reflection characteristics of glacial and glacimarine sediment in the Gulf of Alaska and adjacent fjords. *Mar. Geol.,* 85(2–4):391–416. **doi:10.1016/0025-3227(89)90161-8**

Carlson, P.R., Bruns, T.R., Molnia, B.F., and Schwab, W.C., 1982. Submarine valleys in the northeastern Gulf of Alaska: characteristics and probable origin. *Mar. Geol.,* 47(3–4):217–242. **doi:10.1016/0025-3227(82)90070-6**

Carlson, P.R., Stevenson, A.J., Bruns, T.R., Mann, D.M., and Huggett, Q., 1996. Sediment pathways in the Gulf of Alaska from beach to abyssal plain. *In* Gardner, J.V., Field, M.E., and Twichell, D.C. (Eds.), *Geology of the United States' Seafloor: The View from GLORIA:* Cambridge, (Cambridge Univ.), 255–278. **doi:10.1017/CBO9780511529481.021**

Channell, J.E.T., 1999. Geomagnetic paleointensity and directional secular variation at Ocean Drilling Program (ODP) Site 984 (Bjorn Drift) since 500 ka: comparisons with ODP Site 983 (Gardar Drift). *J. Geophys. Res., [Solid Earth],* 104(B10):22937–22951. **doi:10.1029/1999JB900223**

Channell, J.E.T., Hodell, D.A., McManus, J., and Lehman, B., 1998. Orbital modulation of the Earth's magnetic field intensity. *Nature (London, U. K.),* 394:464–468. **doi:10.1038/28833**

Channell, J.E.T., Kanamatsu, T., Sato, T., Stein, R., Alvarez Zarikian, C.A., Malone, M.J., and the Expedition 303/306 Scientists, 2006. *Proc. IODP,* 303/306: College Station, TX (Integrated Ocean Drilling Program Management International, Inc.). **doi:10.2204/iodp.proc.303306.2006**

Channell, J.E.T., Mazaud, A., Sullivan, P., Turner, S., and Raymo, M.E., 2002. Geomagnetic excursions and paleointensities in the Matuyama Chron at Ocean Drilling Program Sites 983 and 984 (Iceland Basin). *J. Geophys. Res., [Solid Earth],* 107(B6):2114–2127. **doi:10.1029/2001JB000491**

Channell, J.E.T., Xuan, C., and Hodell, D.A., 2009. Stacking paleointensity and oxygen isotope data for the last 1.5 Myr (PISO-1500). *Earth Planet. Sci. Lett.,* 283(1–4):14–23. **doi:10.1016/j.epsl.2009.03.012**

Chapman, J.B., Pavlis, T.L., Gulick, S., Berger, A., Lowe, L., Spotila, J., Bruhn, R., Vorkink, M., Koons, P., Barker, A., Picomell, C., Ridgway, K., Hallet, B., Jaeger, J., and McCalpin, J., 2008. Neotectonics of the Yakutat collision: changes in deformation driven by mass redistribution. *In* Freymueller, J.T., Haeussler, P.J., Wesson, R., and Ekstrom, G. (Eds.), *Active Tectonics and Seismic Potential of Alaska*. Geophys. Monogr., 179:65–81.

Chase, Z., Strutton, P.G., and Hales, B., 2007. Iron links river runoff and shelf width to phytoplankton biomass along the U.S. West Coast. *Geophys. Res. Lett.,* 34:L04607–L04613. **doi:10.1029/2006GL028069**

Childers, A.R., Whitledge, T.E., and Stockwell, D.A., 2005. Seasonal and interannual variability in the distribution of nutrients and chlorophyll a across the Gulf of Alaska shelf: 1998–2000. *Deep-Sea Res., Part II,* 52(1–2):193–216. **doi:10.1016/j.dsr2.2004.09.018**

Christeson, G.L., Gulick, S.P.S., van Avendonk, H.J.A, Worthington, L.L., Reece, R.S., and Pavlis, T.L., 2010. The Yakutat terrane: dramatic change in crustal thickness across the Transition fault, Alaska. *Geology,* 38(10):895–898. **doi:10.1130/G31170.1**

Clapperton, C., 2000. Interhemispheric synchroneity of marine oxygen isotope Stage 2 glacier fluctuations along the American cordilleras transect. *J. Quat. Sci.,* 15(4):435–468. **doi:10.1002/1099-1417(200005)15:4<435::AID-JQS552>3.0.CO;2-R**

Clark, P.U., and Bartlein, P.J., 1995. Correlation of late Pleistocene glaciation in the western United States with North Atlantic Heinrich events. *Geology,* 23(6):483–486. **doi:10.1130/0091-7613(1995)023<0483:COLPGI>2.3.CO;2**

Clement, B.M., 2004. Dependence of the duration of geomagnetic polarity reversals on site latitude. *Nature (London, U. K.),* 428:637–640. **doi:10.1038/nature02459**

Cowan, D.S., 1982. Geological evidence for post–40 m.y. B.P. large-scale northwestward displacement of part of southeastern Alaska. *Geology,* 10(6):309–313. **doi:10.1130/0091-7613(1982)10<309:GEFPMB>2.0.CO;2**

Cowan, E.A., Brachfeld, S.A., Powell, R.D., and Schoolfield, S.C., 2006. Terrane-specific rock magnetic characteristics preserved in glacimarine sediment from southern coastal Alaska. *Can. J. Earth Sci.,* 43(9):1269–1282. **doi:10.1139/e06-042**

Cox, A., and Doell, R.R., 1964. Long period variations of the geomagnetic field. *Bull. Seismol. Soc. Am.,* 54(6B):2243–2270.

Dahlgren, K.I.T., Vorren, T.O., Stoker, M.S., Nielsen, T., Nygård, A., and Sejrup, H.P., 2005. Late Cenozoic prograding wedges on the NW European continental margin: their formation and relationship to tectonics and climate. *Mar. Pet. Geol.,* 22(9–10):1089–1110. **doi:10.1016/j.marpetgeo.2004.12.008**

Davies, M.H., Mix, A.C., Stoner, J.S., Addison, J.A., Jaeger, J., Finney, B., and Wiest, J., 2011. The deglacial transition on the southeastern Alaskan Margin: meltwater input, sea level

rise, marine productivity, and sedimentary anoxia. *Paleoceanography,* 26:PA2223–PA2240. **doi:10.1029/2010PA002051**

DeMets, C., and Dixon, T.H., 1999. New kinematic models for Pacific-North America motion from 3 Ma to present, I: evidence for steady motion and biases in the NUVEL-1A model. *Geophys. Res. Lett.,* 26(13):1921–1924. **doi:10.1029/1999GL900405**

Donnelly, T.W., 1982. Worldwide continental denudation and climatic deterioration during the late Tertiary: evidence from deep-sea sediments. *Geology,* 10(9):451–454. **doi:10.1130/0091-7613(1982)10<451:WCDACD>2.0.CO;2**

Dumoulin, J.A., 1987. Sandstone composition of the Valdez and Orca groups, Prince William Sound, Alaska. *U.S. Geol. Surv. Bull.,* 1774. **http://www.dggs.dnr.state.ak.us/webpubs/usgs/b/text/b1774.PDF**

Dunbar, G.B., Naish, T.R., Barrett, P.J., Fielding, C.R., and Powell, R.D., 2008. Constraining the amplitude of late Oligocene bathymetric changes in western Ross Sea during orbitally-induced oscillations in the East Antarctic Ice Sheet, 1. Implications for glacimarine sequence stratigraphic models. *Palaeogeogr., Palaecoclimatol., Palaeoecol.,* 260(1–2):50–65. **doi:10.1016/j.palaeo.2007.08.018**

Eberhart-Philips, D., Christensen, D.H., Brocher, T.M., Hansen, R., Ruppert, N.A., Haeussler, P.J., and Abers, G.A., 2006. Imaging the transition from Aleutian subduction to Yakutat collision in central Alaska, with local earthquakes and active source data. *J. Geophys. Res., [Solid Earth],* 111:B11303–B11333. **doi:10.1029/2005JB004240**

Eidvin, T., Jansen, E., and Riis, F., 1993. Chronology of Tertiary fan deposits off the western Barents Sea: implications for the uplift and erosion history of the Barents shelf. *Mar. Geol.,* 112(1–4):109–131. **doi:10.1016/0025-3227(93)90164-Q**

Elliott, J.L., Larsen, C.F., Freymueller, J.T., and Motyka, R.J., 2010. Tectonic block motion and glacial isostatic adjustment in southeast Alaska and adjacent Canada constrained by GPS measurements. *J. Geophys. Res., [Solid Earth],* 115:B09407–B09427. **doi:10.1029/2009JB007139**

Elverhøi, A., Andersen, E.S., Dokken, T., Hebbeln, D., Spielhagen, R., Svendsen, J.I., Sørflaten, M., Rørnes, A., Hald, M., and Forsberg, C.F., 1995. The growth and decay of the Late Weichselian ice sheet in western Svalbard and adjacent areas based on provenance studies of marine sediments. *Quat. Res.*, 44(3):303–316. **doi:10.1006/qres.1995.1076**

Emile-Geay, J., Cane, M.A., Naik, N., Seager, R., Clement, A.C., and van Geen, A., 2003. Warren revisited: atmospheric freshwater fluxes and "why is no deep water formed in the North Pacific?" *J. Geophys. Res., [Oceans],* 108:3178–3189. **doi:10.1029/2001JC001058**

Engstrom, D.R., Hansen, B.C.S., and Wright, H.E., Jr., 1990. A possible Younger Dryas record in southeastern Alaska. *Science,* 250(4986):1383–1385. **doi:10.1126/science.250.4986.1383**

Enkelmann, E., Garver, J.I., and Pavlis, T.L., 2008. Rapid exhumation of ice-covered rocks of the Chugach–St. Elias orogen, southeast Alaska. *Geology,* 36(12):915–918. **doi:10.1130/G2252A.1**

Enkelmann, E., Zeitler, P.K., Garver, J.I., Pavlis, T.L., and Hooks, B.P., 2010. The thermochronological record of tectonic and surface process interaction at the Yakutat–North American collision zone in southeast Alaska. *Am. J. Sci.,* 310:231–260. **doi:10.2475/04.2010.01**

Enkelmann, E., Zeitler, P.K., Pavlis, T.L., Garver, J.I., and Ridgway, K.D., 2009. Intense localized rock uplift and erosion in the St. Elias orogen of Alaska. *Nat. Geosci.,* 2:360–363. **doi:10.1038/ngeo502**

Escutia, C., Brinkhuis, H., Klaus, A., and the Expedition 318 Scientists, 2011. *Proc. IODP,* 318: Tokyo (Integrated Ocean Drilling Program Management International, Inc.). **doi:10.2204/iodp.proc.318.2011**

Eyles, C.H., Eyles, N., and Lagoe, M.B., 1991. The Yakataga formation: a late Miocene to Pleistocene record of temperate glacial marine sedimentation in the Gulf of Alaska. *In* Anderson, J.B., and Ashley, G.M. (Eds.), *Glacial Marine Sedimentation: Paleoclimatic Significance.* Spec. Pap.—Geol. Soc. Am., 261:159–180.

Feely, R.A., Baker, E.T., Schumacher, J.D., Massoth, G.J., and Landing, W.M., 1979. Processes affecting the distribution and transport of suspended matter in the northeast Gulf of Alaska. *Deep-Sea Res., Part A,* 26(4):445–464. **doi:10.1016/0198-0149(79)90057-8**

Ferris, A., Abers, G.A., Christensen, D.H., and Veenstra, E., 2003. High resolution image of the subducted Pacific (?) plate beneath central Alaska, 50–150 km depth. *Earth Planet. Sci. Lett.,* 214(3–4):575–588. **doi:10.1016/S0012-821X(03)00403-5**

Finzel, E.S., Trop, J.M., Ridgway, K.D., and Enkelmann, E., 2011. Upper plate proxies for flat-slab subduction processes in southern Alaska. *Earth Planet. Sci. Lett.,* 303(3–4):348–360. **doi:10.1016/j.epsl.2011.01.014**

Foster, H.L., Keith, T.E.C., and Menzie, W.D., 1994. Geology of the Yukon-Tanana area of east-central Alaska. *In* Plafker, G., and Berg, H.C. (Eds.), *The Geology of North America* (Vol. G): *The Geology of Alaska:* Boulder, Colorado (Geol. Soc. Am.), 205–240.

Galbraith, E.D., Jaccard, S.L., Pedersen, T.F., Sigman, D.M., Haug, G.H., Cook, M., Southon, J.R., and Francois, R., 2007. Carbon dioxide release from the North Pacific abyss during the last deglaciation. *Nature (London, U. K.),* 449:890–893. **doi:10.1038/nature06227**

Gardner, J.V., Mayer, L.A., and Armstrong, A., 2006. Mapping supports potential submission to U.N. Law of the Sea. *Eos, Trans. Am. Geophys. Union,* 87(16):157. **doi: 10.1029/2006EO160002**

Gebhardt, H., Sarnthein, M., Grootes, P.M., Kiefer, T., Kuehn, H., Schmieder, F., and Röhl, U., 2008. Paleonutrient and productivity records from the subarctic North Pacific for Pleistocene glacial terminations I to V. *Paleoceanography,* 23:PA4212–PA4232. **doi:10.1029/2007PA001513**

Gehrels, G.E., and Berg, H.C., 1994. Geology of southeastern Alaska. *In* Plafker, G., and Berg, H.C. (Eds.), *The Geology of North America: The Geology of Alaska* (Vol. G-1): Boulder, CO (Geol. Soc. Am.), 451–468.

Gehrels, G.E., and Saleeby, J.B., 1987. Geologic framework, tectonic evolution, and displacement history of the Alexander terrane. *Tectonics,* 6(2):151–173. **doi:10.1029/TC006i002p00151**

Geiss, C.E., and Banerjee, S.K., 2003. A Holocene–late Pleistocene geomagnetic inclination record from Grandfather Lake, SW Alaska. *Geophys. J. Int.,* 153(2):497–507. **doi:10.1046/j.1365-246X.2003.01921.x**

Gilhousen, D.B., Quayle, R.G., Baldwin, R.G., Karl, T.R., and Brines, R.O., 1983. *Climatic Summaries for NOAA Data Buoys:* Asheville, NC (National Climatic Data Center).

Grigg, L.D., Whitlock, C., and Dean, W.E., 2001. Evidence for millennial-scale climate change during marine isotope Stages 2 and 3 at Little Lake, western Oregon, U.S.A. *Quat. Res.,* 56(1):10–22. **doi:10.1006/qres.2001.2246**

Gubbins, D., Jones, A.L., and Finlay, C.C., 2006. Fall in Earth's magnetic field is erratic. *Science,* 312(5775):900–902. **doi:10.1126/science.1124855**

Gubbins, D., and Kelly, P., 1993. Persistent patterns in the geomagnetic field over the last 2.5 Myr. *Nature (London, U. K.),* 365:829–832. **doi:10.1038/365829a0**

Gubbins, D., Willis, A.P., and Sreenivasan, B., 2007. Correlation of Earth's magnetic field with lower mantle thermal and seismic structure. *Phys. Earth Planet. Inter.,* 162(3–4):256–260. **doi:10.1016/j.pepi.2007.04.014**

Gulick, S.P.S., Lowe, L.A., PavIis, T.L., Gardner, J.V., and Mayer, L.A., 2007. Geophysical insights into the Transition fault debate: propagating strike slip in response to stalling Yakutat block subduction in the Gulf of Alaska. *Geology,* 35(8):763–766. **doi:10.1130/G23585A.1**

Guyodo, Y., and Valet, J.-P., 1999. Global changes in intensity of the Earth's magnetic field during the past 800 kyr. *Nature (London, U. K.),* 399(6733):249–252. **doi:10.1038/20420**

Hallet, B., Hunter, L., and Bogen, J., 1996. Rates of erosion and sediment evacuation by glaciers: a review of field data and their implications. *Global Planet. Change,* 12(1–4):213–235. **doi:10.1016/0921-8181(95)00021-6**

Haeussler, P.J., Gehrels, G.E., and Karl, S.M., 2006. Constraints on the age and provenance of the Chugach accretionary complex from detrital zircons in the Sitka graywacke near Sitka, Alaska. *U.S. Geol. Surv. Prof. Pap.,* 1709-F. **http://pubs.usgs.gov/pp/pp1709f/**

Harrison, P.J., Boyd, P.W., Varela, D.E., Takeda, S., Shiomoto, A., and Odate, T., 1999. Comparison of factors controlling phytoplankton productivity in the NE and NW subarctic Pacific gyres. *Prog. Oceanogr.,* 43(2–4):205–234. **doi:10.1016/S0079-6611(99)00015-4**

Hay, W.W., Soeding, E., DeConto, R.M., and Wold, C.N., 2002. The late Cenozoic uplift—climate change paradox. *Int. J. Earth Sci.,* 91(5):746–774. **doi:10.1007/s00531-002-0263-1**

Hayes, D.E., Frakes, L.A., et al., 1975. *Init. Repts. DSDP,* 28: Washington, DC (U.S. Govt. Printing Office). **doi:10.2973/dsdp.proc.28.1975**

Hayes, S.P., 1979. Variability of current and bottom pressure across the continental shelf in the northeast Gulf of Alaska. *J. Phys. Oceanogr.,* 9(1):88–103. **doi:10.1175/1520-0485(1979)009<0088:VOCABP>2.0.CO;2**

Hayes, S.P., and Schumacher, J.D., 1976. Description of wind, current, and bottom pressure variations on continental shelf in northeast Gulf of Alaska from February to May 1975. *J. Geophys. Res., [Oceans],* 81(36):6411–6419. **doi:10.1029/JC081i036p06411**

Hendy, I.L., and Cosma, T., 2008. Vulnerability of the Cordilleran Ice Sheet to iceberg calving during late Quaternary rapid climate change events. *Paleoceanography,* 23:PA2101–PA2108. **doi:10.1029/2008PA001606**

Hendy, I.L., and Kennett, J.P., 1999. Latest Quaternary North Pacific surface-water responses imply atmosphere-driven climate instability. *Geology,* 27(4):291–294. **doi:10.1130/0091-7613(1999)027<0291:LQNPSW>2.3.CO;2**

Hill, H.W., Flower, B.P., Quinn, T.M., Hollander, D.J., and Guilderson, T.P., 2006. Laurentide Ice Sheet meltwater and abrupt climate change during the last glaciation. *Paleoceanography,* 21: PA1006–PA1014. **doi:10.1029/2005PA001186**

Hogan, L.G., Scheidegger, K.F., Kulm, L.D., Dymond, J., and Mikkelsen, N., 1978. Biostratigraphic and tectonic implications of ^{40}Ar-^{39}Ar dates of ash layers from the northeast Gulf of Alaska. *Geol. Soc. Am. Bull.,* 89(8):1259–1264. **doi:10.1130/0016-7606(1978)89<1259:BATIOA>2.0.CO;2**

Hoth, S., Adam, J., Kukowski, N., and Oncken, O., 2006. Influence of erosion on the kinematics of bivergent orogens: results from scaled sandbox simulations. *Spec. Pap.—Geol. Soc. Am.,* 398:201–225. **doi:10.1130/2006.2398(12)**

Hu, F.S., Nelson, D.M., Clarke, G.H., Rühland, K.M., Huang, Y., Kaufman, D.S., and Smol, J.P., 2006. Abrupt climatic events during the last glacial–interglacial transition in Alaska. *Geophys. Res. Lett.,* 33:L18708–L18713. **doi:10.1029/2006GL027261**

Jaccard, S.L., Haug, G.H., Sigman, D.M., Pedersen, T.F., Thierstein, H.R., and Röhl, U., 2005. Glacial/interglacial changes in subarctic North Pacific stratification. *Science,* 308(5724):1003–1006. **doi:10.1126/science.1108696**

Jaeger, J.M., Nittrouer, C.A., Scott, N.D., and Milliman, J.D., 1998. Sediment accumulation along a glacially impacted mountainous coastline: north-east Gulf of Alaska. *Basin Res.,* 10(1):155–173. **doi:10.1046/j.1365-2117.1998.00059.x**

Jaeger, J.M., Rosen, G.P., Kramer, B., Stoner, J., Cowan, E.A., and Channell, J., 2008. Cross-margin signal transfer in a glacial source-to-sink sedimentary system: Bering Glacier, southern Alaska [presented at the 2008 Ocean Sciences Meeting, Orlando, Florida, 2–7 March 2008].

Jones, D.L., Silberling, N.J., and Hillhouse, J., 1977. Wrangellia—a displaced terrane in northwestern North America. *Can. J. Earth Sci.,* 14(11):2565–2577. **doi:10.1139/e77-222**

Keigwin, L.D., and Cook, M.S., 2007. A role for North Pacific salinity in stabilizing North Atlantic climate. *Paleoceanography,* 22:PA3102–PA3106. **doi:10.1029/2007PA001420**

Koons, P.O., 1995. Modeling the topographic evolution of collisional belts. *Annu. Rev. Earth Planet. Sci.,* 23:375–408. **doi:10.1146/annurev.ea.23.050195.002111**

Kreemer, C., Holt, W.E., and Haines, A.J., 2003. An integrated global model of present-day plate motions and plate boundary deformation. *Geophys. J. Int.,* 154(1):8–34. **doi:10.1046/j.1365-246X.2003.01917.x**

Krissek, L.A., 1995. Late Cenozoic ice-rafting records from Leg 145 sites in the North Pacific: late Miocene onset, late Pliocene intensification, and Pliocene–Pleistocene events. *In* Rea, D.K., Basov, I.A., Scholl, D.W., and Allan, J.F. (Eds.), *Proc. ODP, Sci. Results,* 145: College Station, TX (Ocean Drilling Program), 179–194. **doi:10.2973/odp.proc.sr.145.118.1995**

Kulm, L.D., von Huene, R., et al., 1973. *Init. Repts. DSDP,* 18: Washington, DC (U.S. Govt. Printing Office). **doi:10.2973/dsdp.proc.18.1973**

Kusky, T.M., Bradley, D.C., and Haeussler, P., 1997. Progressive deformation of the Chugach accretionary complex, Alaska, during a Paleogene ridge-trench encounter. *J. Struct. Geol.,* 19(2):139–157. **doi:10.1016/S0191-8141(96)00084-3**

Landis, P.S., 2007. Stratigraphic framework and provenance of the Eocene–Oligocene Kulthieth formation, Alaska: implications for paleogeography and tectonics of the early Cenozoic continental margin of northwestern North America [M.S. thesis]. Purdue Univ., West Lafayette, Indiana.

Lagoe, M.B., Eyles, C.H., Eyles, N., and Hale, C., 1993. Timing of late Cenozoic tidewater glaciation in the far North Pacific. *Geol. Soc. Am. Bull.,* 105(12):1542–1560. **doi:10.1130/0016-7606(1993)105<1542:TOLCTG>2.3.CO;2**

Lagoe, M.B., and Zellers, S.D., 1996. Depositional and microfaunal response to Pliocene climate change and tectonics in the eastern Gulf of Alaska. *Mar. Micropaleontol.,* 27(1–4):121–140. **doi:10.1016/0377-8398(95)00055-0**

Laj, C., Kissel, C., and Beer, J., 2004. High-resolution global paleointensity stack since 75 kyr (GLOPIS-75) calibrated to absolute values. *In* Channell, J.E.T., Kent, D.V., Lowrie, W., and Meert, J. (Eds.), *Timescales of the Internal Geomagnetic Field.* Geophys. Monogr., 145:255–266.

Lam, P.J., and Bishop, J.K.B., 2008. The continental margin is a key source of iron to the HNLC North Pacific Ocean. *Geophys. Res. Lett.,* 35:L07608–L07612. **doi:10.1029/2008GL033294**

Larsen, H.C., Saunders, A.D., Clift, P.D., et al., 1994. *Proc. ODP, Init. Repts.,* 152: College Station, TX (Ocean Drilling Program). **doi:10.2973/odp.proc.ir.152.1994**

Lisiecki, L.E., and Raymo, M.E., 2005. A Pliocene–Pleistocene stack of 57 globally distributed benthic $\delta^{18}O$ records. *Paleoceanography,* 20(1):PA1003–PA1019. **doi:10.1029/2004PA001071**

Lund, S.P., 1996. A comparison of Holocene paleomagnetic secular variation records from North America. *J. Geophys. Res.,* 101(B4):8007–8024. **doi:10.1029/95JB00039**

Lund, S.P., Acton, G.D., Clement, B., Hastedt, M., Okada, M., Williams, T., and ODP Leg 172 Scientific Party, 1998. Geomagnetic field excursions occurred often during the last million years. Eos, Trans. Am. Geophys. Union, 79(14):179. doi:10.1029/98EO00134

Lund, S.P., Acton, G.D., Clement, B., Okada, M., and Williams, T., 2001. Paleomagnetic records of Stage 3 excursions, Leg 172. *In* Keigwin, L.D., Rio, D., Acton, G.D., and Arnold, E. (Eds.), *Proc. ODP, Sci. Results,* 172: College Station, TX (Ocean Drilling Program), 1–20. **doi:10.2973/odp.proc.sr.172.217.2001**

Lund, S.P., Schwartz, M., Keigwin, L., and Johnson, T., 2005. Deep-sea sediment records of the Laschamp geomagnetic field excursion (~41,000 calendar years before present). *J. Geophys. Res., [Solid Earth],* 110:B04101–B04115. **doi:10.1029/2003JB002943**

Lund, S., Stoner, J.S., Channell, J.E.T., and Acton, G., 2006. A summary of Brunhes paleomagnetic field variability recorded in Ocean Drilling Program cores. *Phys. Earth Planet. Int.,* 156(3–4):194–204. **doi:10.1016/j.pepi.2005.10.009**

Mahowald, N.M., Baker, A.R., Bergametti, G., Brooks, N., Duce, R.A., Jickells, T.D., Kubilay, N., Prospero, J.M., and Tegen, I., 2005. Atmospheric global dust cycle and iron inputs to the ocean. *Global Biogeochem. Cycles,* 19:GB4024–GB4038. **doi:10.1029/2004GB002402**

Malavieille, J., 2010. Impact of erosion, sedimentation, and structural heritage on the structure and kinematics of orogenic wedges: analog models and case studies. *GSA Today,* 20(1):4–10. **doi:10.1130/GSATG48A.1**

Manley, W., and Kaufman, D.S., 2002. *Alaska Paleoglacier Atlas:* Boulder, CO (Inst. Arct. Alp. Res., Univ. Colorado). **http://instaar.colorado.edu/QGISL/ak_paleoglacier_atlas/**

Mann, D.H., Crowell, A.L., Hamilton, T.D., and Finney, B.P., 1998. Holocene geologic and climatic history around the Gulf of Alaska. *Arct. Anthropol.,* 35(1):112–131. **http://www.jstor.org/pss/40316459**

Mann, D.H., and Peteet, D.M., 1994. Extent and timing of the Last Glacial Maximum in southwestern Alaska. *Quat. Res.,* 42(2):136–148. **doi:10.1006/qres.1994.1063**

Mayer, L.A., Gardner, J.V., Armstrong, A., Calder, B.R., Malik, M., Angwenyi, C., Karlpata, S., Montoro-Dantes, H., Morishita, T., Mustapha, A., van Waes, M., Wood, D., and Withers, A., 2005. New views of the Gulf of Alaska Margin mapped for UNCLOS applications. *Eos, Trans. Am. Geophys. Union,* 88(52)(Suppl.):T13D-0500. (Abstract) **http://www.agu.org/meetings/fm05/waisfm05.html**

Mazaud, A., Channell, J.E.T., Xuan, C., and Stoner, J.S., 2009. Upper and lower Jaramillo polarity transitions recorded in IODP Expedition 303 North Atlantic sediments: implications for transitional field geometry. *Phys. Earth Planet. Inter.,* 172(3–4):131–140. **doi:10.1016/j.pepi.2008.08.012**

Mazzotti, S., and Hyndman, R.D., 2002. Yakutat collision and strain transfer across the northern Canadian cordillera. *Geology,* 30(6):495–498. **doi:10.1130/0091-7613(2002)030<0495:YCASTA>2.0.CO;2**

McDonald, D., Pedersen, T.F., and Crusius, J., 1999. Multiple late Quaternary episodes of exceptional diatom production in the Gulf of Alaska. *Deep-Sea Res., Part II,* 46(11–12):2993–3017. **doi:10.1016/S0967-0645(99)00091-0**

Meigs, A., Johnston, S., Garver, J., and Spotila, J., 2008. Crustal-scale structural architecture, shortening, and exhumation of an active, eroding orogenic wedge (Chugach/St. Elias Range, southern Alaska). *Tectonics,* 27:TC4003–TC4028. **doi:10.1029/2007TC002168**

Menviel, L., Timmermann, A., Timm, O.E., Mouchet, A., Abe-Ouchi, A., Chikamoto, M.O., Harada, N., Ohgaito, R., and Okazaki, Y., in press. Removing the North Pacific halocline: effects on global climate, ocean circulation and the carbon cycle. *Deep-Sea Res., Part II.* **doi:10.1016/j.dsr2.2011.03.005**

Mix, A.C., Bard, E., and Schneider, R., 2001. Environmental processes of the ice age: land, oceans, glaciers (EPILOG). *Quat. Sci. Rev.,* 20(4):627–657. **doi:10.1016/S0277-3791(00)00145-1**

Mix, A.C., Lund, D.C., Pisias, N.G., Bodén, P., Bornmalm, L., Lyle, M., and Pike, J., 1999. Rapid climate oscillations in the Northeast Pacific during the last deglaciation reflect Northern and Southern Hemisphere sources. *In* Webb, R.S., Clark, P.U., and Keigwin, L. (Eds.), *Mechanisms of Millennial-scale Global Climate Change.* Geophys. Monogr., 112:127–148.

Molnar, P., 2004. Late Cenozoic increase in accumulation rates of terrestrial sediment: how might climate change have affected erosion rates? *Annu. Rev. Earth Planet. Sci.,* 32:67–89. **doi:10.1146/annurev.earth.32.091003.143456**

Molnar, P., and England, P., 1990. Late Cenozoic uplift of mountain ranges and global climate change: chicken or egg? *Nature (London, U. K.),* 346:29–34. **doi:10.1038/346029a0**

Molnia, B.F., 1986. Late Wisconsin glacial history of the Alaskan continental margin. *In* Hamilton, T.D., Reed, K.M., and Thorson, R.M. (Eds.), *Glaciation in Alaska: The Geologic Record:* Anchorage, AK (Alaska Geol. Soc.), 219–236.

Molnia, B.F., and Sangrey, D.A., 1979. Glacially derived sediments in the northern Gulf of Alaska—geology and engineering characteristics. *Proc.—Annu. Offshore Technol. Conf.,* 1:647–655. **doi:10.4043/3433-MS**

Neal, E.G., Hood, E., and Smikrud, K., 2010. Contribution of glacier runoff to freshwater discharge into the Gulf of Alaska. *Geophys. Res. Lett.,* 37:L06404–L06408. **doi:10.1029/2010GL042385**

Ness, G.E., and Kulm, L.D., 1973. Origin and development of Surveyor Deep-Sea Channel. *Geol. Soc. Am. Bull.,* 84(10):3339–3354. **doi:10.1130/0016-7606(1973)84<3339:OADOSD>2.0.CO;2**

Nokleberg, W.J., Parfenov, L.M., Monger, J.W.H., Norton, I.O., Khanchuk, A.I., Stone, D.B., Scotese, C.R., Scholl, D.W., and Fujita, K., 2000. Phanerozoic tectonic evolution of the circum-North Pacific. *Geol. Surv. Prof. Pap. U.S.,* 1626. **http://pubs.usgs.gov/pp/2000/1626/**

O'Brien, P.E., Cooper, A.K., Richter, C., et al., 2001. *Proc. ODP, Init. Repts.,* 188: College Station, TX (Ocean Drilling Program). **doi:10.2973/odp.proc.ir.188.2001**

Okazaki, Y., Timmermann, A., Menviel, L., Harada, N., Abe-Ouchi, A., Chikamoto, M.O., Mouchet, A., and Asahi, H., 2010. Deepwater formation in the North Pacific during the Last Glacial Termination. *Science,* 329(5988):200–204. **doi:10.1126/science.1190612**

Pavlis, T.L., Hamburger, M.W., and Pavlis, G.L., 1997. Erosional processes as a control on the structural evolution of an actively deforming fold and thrust belt: an example from the Pamir-Tien Shan region, central Asia. *Tectonics,* 16(5):810–822. **doi:10.1029/97TC01414**

Pavlis, T.L., Picornell, C., Serpa, L., Bruhn, R.L., and Plafker, G., 2004. Tectonic processes during oblique collision: insights from the St. Elias orogen, northern North American cordillera. *Tectonics,* 23(3):TC3001–TC3014. **doi:10.1029/2003TC001557**

Perry, S.E., Garver, J.I., and Ridgway, K.D., 2009. Transport of the Yakutat terrane, Southern Alaska: evidence from sediment petrology and detrital zircon fission-track and U/Pb double dating. *J. Geol.,* 117(2):156–173. **doi:10.1086/596302**

Peteet, D.M., 2007. Muskeg archives of vegetation, migration, and climate history in the Gulf of Alaskan arc. *Abstr.—Geol. Soc. Am.* **http://gsa.confex.com/gsa/2007CD/finalprogram/abstract_120879.htm**

Peteet, D.M., and Mann, D.H., 1994. Late-glacial vegetation, tephra, and climatic history of southwestern Kodiak Island, Alaska. *Ecoscience*, 1:255–267.

Pinter, N., and Brandon, M.T., 1997. How erosion builds mountains. *Sci. Am.,* 276(4):74–79. **doi:10.1038/scientificamerican0497-74**

Plafker, G., 1987. Regional geology and petroleum potential of the northern Gulf of Alaska continental margin. *In* Scholl, D.W., Grantz, A., and Vedder, J.G. (Eds.), *Petroleum Geology Potential of the Continental Margin of Western North America and Adjacent Ocean Basins.* Earth Sci. Ser. (N. Y.), 6:229–268.

Plafker, G., Moore, J.C., and Winkler, G.R., 1994. Geology of the southern Alaska margin. *In* Plafker, G., and Berg, H.C. (Eds.), *The Geology of North America: The Geology of Alaska* (Vol. G-1): Boulder, CO (Geol. Soc. Am.), 389–449.

Powell, R.D., and Cooper, J.M., 2002. A glacial sequence stratigraphic model for temperate, glaciated continental shelves. *In* Dowdeswell, J.A., and Ó'Cofaigh, C. (Eds.), *Glacier-Influenced Sedimentation on High-Latitude Continental Margins.* Geol. Soc. Spec. Publ., 203:215–244. **doi:10.1144/GSL.SP.2002.203.01.12**

Powell, R.D., and Molnia, B.F., 1989. Glacimarine sedimentatary processes, facies and morphology of the south-southeast Alaska shelf and fjords. *Mar. Geol.,* 85(2–4):359–390. **doi:10.1016/0025-3227(89)90160-6**

Prueher, L.M., and Rea, D.K., 1998. Rapid onset of glacial conditions in the subarctic North Pacific region at 2.67 Ma: clues to causality. *Geology,* 26(11):1027–1030. **doi:10.1130/0091-7613(1998)026<1027:ROOGCI>2.3.CO;2**

Rasmussen, S.O., Andersen, K.K., Svensson, A.M., Steffensen, J.P., Vinther, B.M., Clausen, H.B., Siggaard-Andersen, M.-L., Johnsen, S.J., Larsen, L.B., Dahl- Jensen, D., Bigler, M., Röthlisberger, R., Fischer, H., Goto-Azuma, K., Hansson, M.E., and Ruth, U., 2006. A new Greenland ice core chronology for the Last Glacial Termination. *J. Geophys. Res., [Atmospheres],* 111:D06102–D06118. **doi:10.1029/2005JD006079**

Rea, D.K., Basov, I.A., Janecek, T.R., Palmer-Julson, A., et al., 1993. *Proc. ODP, Init. Repts.,* 145: College Station, TX (Ocean Drilling Program). **doi:10.2973/odp.proc.ir.145.1993**

Rea, D.K., and Snoeckx, H., 1995. Sediment fluxes in the Gulf of Alaska: paleoceanographic record from Site 887 on the Patton-Murray Seamount platform. *In* Rea, D.K., Basov, I.A., Scholl, D.W., and Allan, J.F. (Eds.), *Proc. ODP, Sci. Results,* 145: College Station, TX (Ocean Drilling Program), 247–256. **doi:10.2973/odp.proc.sr.145.122.1995**

Redfield, T.F., Scholl, D.W., Fitzgerald, P.G., and Beck, M.E., Jr., 2007. Escape tectonics and the extrusion of Alaska: past, present, and future. *Geology,* 35(11):1039–1042. **doi:10.1130/G23799A.1**

Reece, R.S., Gulick, S.P.S., Horton, B.K., Christeson, G.L., and Worthington, L.L., in press. Tectonic and climatic influence on the evolution of the Surveyor fan and channel system, Gulf of Alaska. *Geosphere.*

Reece, R.S., Gulick, S.P.S., Jaeger, J.M., Christeson, G., Worthington, L.L., and Pavlis, T.L., 2009. Erosion and deposition by cross-shelf glacial advance as a mechanism for channel

inception in the Surveyor Fan, Gulf of Alaska. *Abstr. Programs Geol. Soc. Am.,* 41(7):305. **http://gsa.confex.com/gsa/2009AM/finalprogram/abstract_165472.htm**

Richter, D.H., Preller, C.C., Labay, K.A., and Shrew, N.B., 2006. Geologic map of the Wrangell–Saint Elias National Park and Preserve, Alaska. *Sci. Invest. Rep. (U. S. Geol. Surv.),* SIM-2877. **http://pubs.usgs.gov/sim/2006/2877/**

Riis, F., 1992. Dating and measuring of erosion, uplift and subsidence in Norway and the Norwegian shelf in glacial periods. *Nor. Geol. Tiddskr. (1905–2000),* 72(3):325–331. **http://www.npd.no/Global/Norsk/3 - Publikasjoner/Forskningsartikler/Riis_1992.pdf**

Risley, D.E., Martin, G.C., Lynch, M.B., Flett, T.O., Larson, J.A., Horowitz, W.L., and Turner, R.F., 1992. Geologic report for the Gulf of Alaska planning area. *MMS Rep.,* 92-0065.

Roe, G.H., Stolar, D.B., and Willett, S.D., 2006. Response of a steady-state critical wedge orogen to changes in climate and tectonic forcing. *Spec. Pap.—Geol. Soc. Am.,* 398:227–239. **doi:10.1130/2005.2398(13)**

Royer, T.C., 1981. Baroclinic transport in the Gulf of Alaska, Part II. Fresh water driven coastal current. *J. Mar. Res.,* 39:251–266.

Royer, T.C., 1982. Coastal fresh water discharge in the northeast Pacific. *J. Geophys. Res., [Oceans],* 87(C3):2017–2021. **doi:10.1029/JC087iC03p02017**

Royer, T.C., 2005. Hydrographic responses at a coastal site in the northern Gulf of Alaska to seasonal and interannual forcing. *Deep-sea Res., Part II,* 52(1–2):267–288. **doi:10.1016/j.dsr2.2004.09.022**

Ruth, U., Barnola, J.-M., Beer, J., Bigler, M., Blunier, T., Castellano, E., Fischer, H., Fundel, F., Huybrechts, P., Kaufmann, P., Kipfstuhl, S., Lambrecht, A., Morganti, A., Oerter, H., Parrenin, F., Rybak, O., Severi, M., Udisti, R., Wilhelms, F., and Wolff, E., 2007. "EDML1": a chronology for the EPICA deep ice core from Dronning Maud Land, Antarctica, over the last 150,000 years. *Clim. Past,* 3:475–484. **doi:10.5194/cp-3-475-2007**

Schroth, A.W., Crusius, J., Sholkovitz, E.R., and Bostick, B.C., 2009. Iron solubility driven by speciation in dust sources to the ocean. *Nat. Geosci.,* 2:337–340. **doi:10.1038/ngeo501**

Severmann S., McManus, J., Berelson, W.M., and Hammond, D.E., 2010. The continental shelf benthic iron flux and its isotope composition. *Geochim. Cosmochim. Acta,* 74(14):3984–4004. **doi:10.1016/j.gca.2010.04.022**

Shackleton, N.J., Hall, M.A., and Pate, D., 1995. Pliocene stable isotope stratigraphy of Site 846. *In* Pisias, N.G., Mayer, L.A., Janecek, T.R., Palmer-Julson, A., and van Andel, T.H. (Eds.), *Proc. ODP, Sci. Results,* 138: College Station, TX (Ocean Drilling Program), 337–355. **doi:10.2973/odp.proc.sr.138.117.1995**

Sheaf, M.A., Serpa, L., and Pavlis, T.L., 2003. Exhumation rates in the St. Elias Mountains, Alaska. *Tectonophysics,* 367(1–2):1–11. **doi:10.1016/S0040-1951(03)00124-0**

Siddall, M., Stocker, T.F., and Clark, P.U., 2009. Constraints on future sea level rise from past sea level change. *Nat. Geosci.,* 2:571–575. **doi:10.1038/ngeo587**

Sigman, D.M., Jaccard, S.L., and Haug, G.H., 2004. Polar ocean stratification in a cold climate. *Nature (London, U. K.),* 428(6978):59–63. **doi:10.1038/nature02357**

Simpson, G.D.H., 2010. Formation of accretionary prisms influenced by sediment subduction and supplied by sediments from adjacent continents. *Geology,* 38(2):131–134. **doi:10.1130/G30461.1**

Singer, B.S., Relle, M.K., Hoffman, K.A., Battle, A., Laj, C., Guillou, H., and Carracedo, J.C., 2002. Ar/Ar ages from transitionally magnetized lavas on La Palma, Canary Islands, and the geomagnetic instability timescale. *J. Geophys. Res., [Solid Earth],* 107(B11):2307–2327. **doi:10.1029/2001JB001613**

Smith, W.H.F., and Sandwell, D.T., 1997. Global sea floor topography from satellite altimetry and ship depth soundings. *Science,* 277(5334):1956–1962. **doi:10.1126/science.277.5334.1956**

Spotila, J.A., and Berger, A.L., 2010. Exhumation at orogenic indentor corners under long-term glacial conditions: example of the St. Elias orogen, southern Alaska. *Tectonophysics,* 490(3–4): 241–256. **doi:10.1016/j.tecto.2010.05.015**

Spotila, J.A., Buscher, J.T., Meigs, A.J., and Reiners, P.W., 2004. Long-term glacial erosion of active mountain belts: example of the Chugach–St. Elias Range, Alaska. *Geology,* 32(6):501–504. **doi:10.1130/G20343.1**

Srivastava, S.P., Arthur, M., Clement, B., et al., 1987. *Proc. ODP, Init. Repts.,* 105: College Station, TX (Ocean Drilling Program). **doi:10.2973/odp.proc.ir.105.1987**

Stabeno, P.J., Bond, N.A., Hermann, A.J., Kachel, N.B., Mordy, C.W., and Overland, J.E., 2004. Meteorology and oceanography of the northern Gulf of Alaska. *Continent. Shelf Res.*, 24(7–8):859–897. **doi:10.1016/j.csr.2004.02.007**

Stabeno, P.J., Reed, R.K., and Schumacher, J.D., 1995. The Alaska Coastal Current: continuity of transport and forcing. *J. Geophys. Res., [Oceans],* 100(C2):2477–2485. **doi:10.1029/94JC02842**

Stevenson, A.J., and Embley, R., 1987. Deep-sea fan bodies, terrigenous turbidite sedimentation, and petroleum geology, Gulf of Alaska. *In* Scholl, D.W., Grantz, A., and Vedder, J.G. (Eds.), *Geology and Resource Potential of the Continental Margin of Western North America and Adjacent Ocean Basins—Beaufort Sea to Baja California.* Earth Sci. Ser. (N. Y.), 503–522.

Stolar, D.B., Willett, S.D., and Roe, G.H., 2006. Climatic and tectonic forcing of a critical orogen. *Spec. Pap.—Geol. Soc. Am.,* 398:241–50. **doi:10.1130/2006.2398(14)**

Stoner, J.S., 2009. Towards an understanding of paleomagnetic secular variation: observations from the North Atlantic, implications for the world? *Geol. Soc. Am. Abstr. Program,* 41(7):46. **http://gsa.confex.com/gsa/2009AM/finalprogram/abstract_166811.htm**

Stoner, J.S., Channell, J.E.T., Hillaire-Marcel, C., and Kissel, C., 2000. Geomagnetic paleointensity and environmental record from Labrador Sea Core MD95-2024: global marine sediment and ice core chronostratigraphy for the last 110 kyr. *Earth Planet. Sci. Lett.,* 183(1–2):161–177. **doi:10.1016/S0012-821X(00)00272-7**

Svensson, A., Andersen, K.K., Bigler, M., Clausen, H.B., Dahl-Jensen, D., Davies, S.M., Johnsen, S.J., Muscheler, R., Rasmussen, S.O., Röthlisberger, R., Steffensen, J.P., and Vinther, B.M., 2006. The Greenland ice core chronology 2005, 15–42 ka, Part 2. Comparison to other records. *Quat. Sci. Rev.,* 25(23–24):3258–3267. **doi:10.1016/j.quascirev.2006.08.003**

The Shipboard Scientific Party, 1973. Site 178. *In* Kulm, L., and von Huene, R., et al., *Init. Repts. DSDP,* 18: Washington, DC (U.S. Govt. Printing Office), 287–376. **doi:10.2973/dsdp.proc.18.109.1973**

Tomkin, J.H., 2007. Coupling glacial erosion and tectonics at active orogens: a numerical modeling study. *J. Geophys. Res., [Earth Surface],* 112:F02015–F02028. **doi:10.1029/2005JF000332**

Tomkin, J.H., and Roe, G.H., 2007. Climate and tectonic controls on glaciated critical-taper orogens. *Earth Planet. Sci. Lett.,* 262(3–4):385–397. **doi:10.1016/j.epsl.2007.07.040**

Trop, J.M., Ridgway, K.D., Manuszak, J.D., and Layer, P., 2002. Mesozoic sedimentary-basin development on the allochthonous Wrangellia composite terrane, Wrangell Mountains basin, Alaska: a long-term record of terrane migration and arc construction. *Geol. Soc. Am. Bull.,* 114(6):693–717. **doi:10.1130/0016-7606(2002)114<0693:MSBDOT>2.0.CO;2**

Tsuda, A., Kiyosawa, H., Kuwata, A., Mochizuki, M., Shiga, N., Saito, H., Chiba, S., Imai, K., Nishioka, J., and Ono, T., 2005. Responses of diatoms to iron-enrichment (SEEDS) in the western subarctic Pacific, temporal and special comparisons. *Prog. Oceanogr.,* 64(2–4):189–205. **doi:10.1016/j.pocean.2005.02.008**

Vagnes, E., Faleide, J.I., and Gudlaugsson, S.T., 1992. Glacial erosion and tectonic uplift in the Barents Sea. *Nor. Geol. Tidsskr. (1905–2000)*, 72(3):333–338.

Valet, J.-P., Meynadier, L., and Guyodo, Y., 2005. Geomagnetic dipole strength and reversal rate over the past two million years. *Nature (London, U. K.)*, 435(7043):802–805. **doi:10.1038/nature03674**

von Huene, R., and Kulm, L.D., 1973. Tectonic summary of Leg 18. *In* Kulm, L.D., von Huene, R., et al., *Init. Repts. DSDP,* 18: Washington (U.S. Govt. Printing Office), 961–976. **doi:10.2973/dsdp.proc.18.133.1973**

von Huene, R., Larson, E., and Crouch, J., 1973. Preliminary study of ice-rafted erratics as indicators of glacial advances in the Gulf of Alaska. *In* Kulm, L.D., von Huene, R., et al., *Init. Repts. DSDP,* 18: Washington (U.S. Govt. Printing Office), 835–842. **doi:10.2973/dsdp.proc.18.121.1973**

Weingartner, T.J., Danielson, S.L., and Royer, T.C., 2005. Freshwater variability and predictability in the Alaska Coastal Current. *Deep-Sea Res., Part II,* 52(1–2):161–191. **doi:10.1016/j.dsr2.2004.09.030**

Whipple, K.X., 2009. The influence of climate on the tectonic evolution of mountain belts. *Nat. Geosci.,* 2:97–104. **doi:10.1038/ngeo413**

Whipple, K.X., and Meade, B.J., 2004. Controls on the strength of coupling among climate, erosion, and deformation in two-sided, frictional orogenic wedges at steady state. *J. Geophys. Res., [Earth Surface],* 109:F01011–F01034. **doi:10.1029/2003JF000019**

White, J.M., Ager, T.A., Adam, D.P., Leopold, E.B., Liu, G., Jetté, H., and Schweger, C.E., 1997. An 18 million year record of vegetation and climate change in northwestern Canada and Alaska: tectonic and global climatic correlates. *Palaeogeogr., Palaeoclimatol., Palaeoecol.,* 130(1–4):293–306. **doi:10.1016/S0031-0182(96)00146-0**

Willems, B.A., 2009. Quaternary glacial and climatic history of southern Alaska using high-resolution seismic reflection records [Ph.D. dissert.]. Northern Illinois Univ., DeKalb.

Willett, S.D., 1999. Orogeny and orography: the effects of erosion on the structure of mountain belts. *J. Geophys. Res., [Solid Earth],* 104(B12):28957–28981. **doi:10.1029/1999JB900248**

Willett, S.D., 2010. Late Neogene erosion of the Alps: a climate driver? *Annu. Rev. Earth Planet. Sci.,* 38:411–437. **doi:10.1146/annurev-earth-040809-152543**

Witmer, J.W., Ridgway, K.D., Enkelmann, E., Brennan, P., and Valencia, V.A., 2009. Deposition, provenance, and exhumation of Neogene strata at the syntaxis of the Chugach–St. Elias Range, southeast Alaska. *Geol. Soc. Am. Abstr. Program,* 41(7):306. **http://gsa.confex.com/gsa/2009AM/finalprogram/abstract_165389.htm**

Worthington, L., 2010. New geophysical parameters for understanding the evolution of the St. Elias orogen, southern Alaska [Ph.D. dissert]. Univ. Texas, Austin.

Worthington, L.L., Gulick, S.P.S., and Pavlis, T.L., 2008. Identifying active structures in the Kayak Island and Pamplona zones: implications for offshore tectonics of the Yakutat microplate, Gulf of Alaska. *In* Freymueller, J.T., Haeussler, P.J., Wesson, R.L., and Ekström, G. (Eds.), *Active Tectonics and Seismic Potential of Alaska*. Geophys. Monogr., 179:257–268.

Worthington, L.L, Gulick, S.P.S., and Pavlis, T.L., 2010. Coupled stratigraphic and structural evolution of a glaciated orogenic wedge, offshore St. Elias orogen, Alaska. *Tectonics,* 29:TC6013–TC6039. **doi:10.1029/2010TC002723**

Worthington, L.L., Gulick, S.P.S., van Avendonk, H.J., Christeson, G.L., and Pavlis, T.L, submitted. Crustal structure of the Yakutat terrane: new constraints for understanding the evolution of subduction and collision in southern Alaska. *J. Geophys. Res.*

Wu, J., Aguilar-Islas, A., Rember, R., Weingertner, T., Danielson, S., and Whitledge, T., 2009. Size-fractionated iron distribution on the northern Gulf of Alaska. *Geophys. Res. Lett.,* 36:L11606. **doi:10.1029/2009GL038304**

Wu, X., Heflin, M.B., Schotman, H., Vermeersen, B.L.A., Dong, D., Gross, R.S., Ivins, E.R., Moore, A.W., and Owen, S.E., 2010. Simultaneous estimation of global present-day water transport and glacial isostatic adjustment. *Nat. Geosci.,* 3:642–646. **doi:10.1038/ngeo938**

Yamazaki, T., and Oda, H., 2005. A geomagnetic paleointensity stack between 0.8 and 3.0 Ma from equatorial Pacific sediment cores. *Geochem., Geophys., Geosyst.,* 6:Q11H20–Q11H43. **doi:10.1029/2005GC001001**

You, Y., Suginohara, N., Fukasawa, M., Yasuda, I., Kaneko, I., Yoritaka, H., and Kawamiya, M., 2000. Roles of the Okhotsk Sea and Gulf of Alaska in forming the North Pacific Intermediate Water. *J. Geophys. Res., [Oceans],* 105(C2):3253–3280. **doi:10.1029/1999JC900304**

Zachos, J., Pagani, M., Sloan, L., Thomas, E., and Billups, K., 2001. Trends, rhythms, and aberrations in global climate 65 Ma to present. *Science,* 292(5517):686–693. **doi:10.1126/science.1059412**

Zahn, R., Pedersen, T.F., Bornhold, B.D., and Mix, A.C., 1991. Water mass conversion in the glacial subarctic Pacific (54°N, 148°W): physical constraints and the benthic-planktonic stable isotope record. *Paleoceanography,* 6(5):543–560. **doi:10.1029/91PA01327**

Zeitler, P.K., Meltzer, A.S., Koons, P.O., Craw, D., Hallet, B., Chamberlain, C.P., Kidd, W.S.F., Park, S.K., Seeber, L., Bishop, M., and Shroder, J., 2001. Erosion, Himalayan geodynamics, and the geomorphology of metamorphism. *GSA Today,* January 2001:4–9. **doi:10.1130/1052-5173(2001)011<0004:EHGATG>2.0.CO;2**

Zellers, S.D., 1995. Foraminiferal sequence biostratigraphy and seismic stratigraphy of a tectonically active margin: the Yakataga Formation, northeastern Gulf of Alaska. *Mar. Micropaleontol.,* 26(1–4):255–271. **doi:10.1016/0377-8398(95)00031-3**

Zhang, P., Molnar, P., and Downs, W.R., 2001. Increased sedimentation rates and grain sizes 2–4 Myr ago due to the influence of climate change on erosion rates. *Nature (London, U. K.),* 410:891–897. **doi:10.1038/35073504**

Table T1. Interpreted horizons on shelf seismic profiles (Worthington et al., 2010). Horizon color after Zellers (1995).

Horizon	Age (Ma)	Definition	Color	References
H1	~1	Mid-Pleistocene Transition (MPT)—local angular erosional unconformity created by shelfal glacial advance	Violet	Worthington et al. (2008); Berger et al. (2008a)
H2	~1.8–1	Arbitrary time marker	Blue	—
H3	1.8	Pliocene–Pleistocene transition	Yellow	Zellers (1995)
H4	~5.9	Yakataga Poul Creek contact; generally defines onset of glaciation	Green	Zellers (1995)
H5		Acoustic basement; contact between shelf sediment and Yakutat basement crust	Purple	—

Table T2. Operations plan, primary sites.

Proposed site	Location (latitude, longitude)	Seafloor depth (mbrf)	Operations description	Transit (days)	Coring/ drilling (days)	Logging (days)
Victoria			Begin Expedition 5.0	port call days		
			Transit ~1037 nmi to KB-2A@ 10.5 knots	4.1		
KB-2A EPSP depth approved to 417 mbsf	59°31.93'N 144°8.03'W	721	Hole A: APC to ~200 mbsf with orientation		1.1	
			Hole B: APC to ~200 mbsf		0.6	
			Hole C: APC to ~200 mbsf		0.6	
			Hole D: APC/XCB to 400 mbsf; Log w/ Triple Combo, FMS Sonic, VSI, and MMM		1.6	1.2
			All APC sections begin with non-magnetic core barrels.			
			Sub-Total Days on Site: 5.1			
			Transit ~30 nmi to GOAL-15C@ 10.0 knots	0.1		
GOAL-15C EPSP depth approved to 1225 mbsf	59°41.34'N 143°12.06'W	261	Hole A: APC ~250 mbsf, XCB ~1112 mbsf; Log w/ Triple Combo, FMS Sonic, and VSI		4.5	1.5
			All APC sections begin with non-magnetic core barrels.			
			Sub-Total Days on Site: 6.0			
			Transit ~12 nmi to GOAL-17B@ 8.0 knots	0.1		
GOAL-17B EPSP depth approved to 1045 mbsf	59°30.44'N 143°2.74'W	738	Hole A: APC ~250 mbsf, XCB ~1032 mbsf w/orientation; Log w/ Triple Combo, FMS Sonic, and VSI		4.8	1.5
			All APC sections begin with non-magnetic core barrels.			
			Sub-Total Days on Site: 6.3			
			Transit ~62 nmi to GOA16-1A@ 10.5 knots	0.3		
GOA16-1A EPSP depth approved to 1100 mbsf	58°46.61'N 144°29.60'W	3703	Hole A: APC ~ 200 mbsf w/orientation and APCT3 measurements		1.8	
			Hole B: APC ~ 200 mbsf		1.3	
			Hole C: APC ~ 200 mbsf		1.3	
			Hole D: APC/XCB to 978 mbsf; Log w/ Triple Combo, FMS Sonic, VSI, and MMM		7.6	2.1
			All APC sections begin with non-magnetic core barrels.			
			Sub-Total Days on Site: 14.1			
			Transit ~137 nmi to GOA18-2A@ 10.5 knots	0.6		
GOA18-2A EPSP depth pending approval	56°57.60'N 147°6.60'W	4188	Hole A: APC ~ 200 mbsf w/orientation and APCT3 measurements		2.0	
			Hole B: APC ~ 200 mbsf		1.4	
			Hole C: APC/XCB ~780 mbsf; Log w/ Triple Combo, FMS Sonic, VSI, and MMM		5.9	2.4
			Hole D: APC/XCB to 425 mbsf		3.5	
			All APC sections begin with non-magnetic core barrels.			
			Sub-Total Days on Site: 15.2			
			Transit ~1032 nmi to Victoria@ 10.5 knots	4.1		
Victoria			End Expedition	9.3	38.0	8.7

Port Call Days:	5.0	Total Operating Days:	56.0
Sub-Total on Site Days:	46.7	Total Expedition Days:	61.0

APC = advanced piston coring, XCB = extended core barrel coring. FMS = Formation MicroScanner, VIS = Versatile Seismic Imager, MMM = Multisensor Magnetometer Module.

Table T3. Operations plan, alternate sites.

Proposed site	Location (latitude, longitude)	Seafloor depth (mbrf)	Operations description		Coring/ drilling (days)	Logging (days)
GOA15-1A	59°42.06'N	189	Hole A: APC ~250 mbsf, XCB ~1158 mbsf w/ APCT3; Log w/ Triple Combo, FMS Sonic, and VSI		4.7	1.5
EPSP depth approved to 1200 mbsf	143°7.20'W					
			All APC sections begin with non-magnetic core barrels.			
			Sub-Total Days on Site:	6.2		
GOA16-2A	58°46.35'N	3701	Hole A: APC ~200 mbsf, w/orientation and APCT3 measurements		1.8	
	144°30.12'W		Hole B: APC ~ 200 mbsf		1.4	
			Hole C: APC ~200 mbsf		1.3	
EPSP depth approved to 1100 mbsf			Hole D: APC/XCB to 962 mbsf; Log w/ Triple Combo, FMS Sonic, VSI, and MMM		7.4	2.1
			All APC sections begin with non-magnetic core barrels.			
			Sub-Total Days on Site:	14.0		
GOAL-16B	58°46.18'N	3701	Hole A: APC ~200 mbsf, w/orientation and APCT3 measurements		1.8	
	144°29.79'W		Hole B: APC ~200 mbsf		1.4	
			Hole C: APC ~200 mbsf		1.3	
EPSP depth approved to 1100 mbsf			Hole D: APC/XCB to 986 mbsf; Log w/ Triple Combo, FMS Sonic, VSI, and MMM		7.8	2.2
			All APC sections begin with non-magnetic core barrels.			
			Sub-Total Days on Site:	14.5		
GOAL-18A	56°57.38'N	4229	Hole A: APC ~200 mbsf, w/orientation and APCT3 measurements		2.0	
	147°8.25'W		Hole B: APC ~200 mbsf		1.4	
			Hole C: APC/XCB ~780 mbsf; Log w/Triple Combo, FMS Sonic, VSI, and MMM		5.9	2.1
EPSP depth approved to 856 mbsf			Hole D: APC/XCB to 500 mbsf		4.2	
			All APC sections begin with non-magnetic core barrels.			
			Sub-Total Days on Site:	15.6		
GOA18-1A	56°56.36'N	4273	Hole A: APC ~200 mbsf, w/orientation and APCT3 measurements		2.0	
	147°22.37'W		Hole B: APC ~200 mbsf		1.4	
			Hole C: APC/XCB ~758 mbsf; Log w/Triple Combo, FMS Sonic, VSI, and MMM		5.8	2.3
EPSP depth pending approval			Hole D: APC/XCB to 500 mbsf		4.2	
			All APC sections begin with non-magnetic core barrels.			
			Sub-Total Days on Site:	15.7		

APC = advanced piston coring, XCB = extended core barrel coring. FMS = Formation MicroScanner, VIS = Versatile Seismic Imager, MMM = Multisensor Magnetometer Module.

Figure F1. Conceptual model for the response of a one-sided critical taper wedge to a climate-driven erosional perturbation. Top: St. Elias orogen is in steady state during the Pliocene–late Pleistocene with tectonic influx and exhumation balanced by erosion and removal of material from the wedge. Lower: Mid-Pleistocene transition to longer-lived ice sheets and the formation of ice streams focuses erosion along the windward side at the glacial equilibrium line (ELA). Assuming that the tectonic influx remains steady, the onset of more intense glacial erosion increases exhumation rates (purple arrow) and rapid redistribution of mass to toe of orogenic wedge alters the internal stress loads, creating a new taper angle (β), shutting down active thrust sheets and repositioning active deformation to the new toe of the wedge (modified after Willet, 1999).

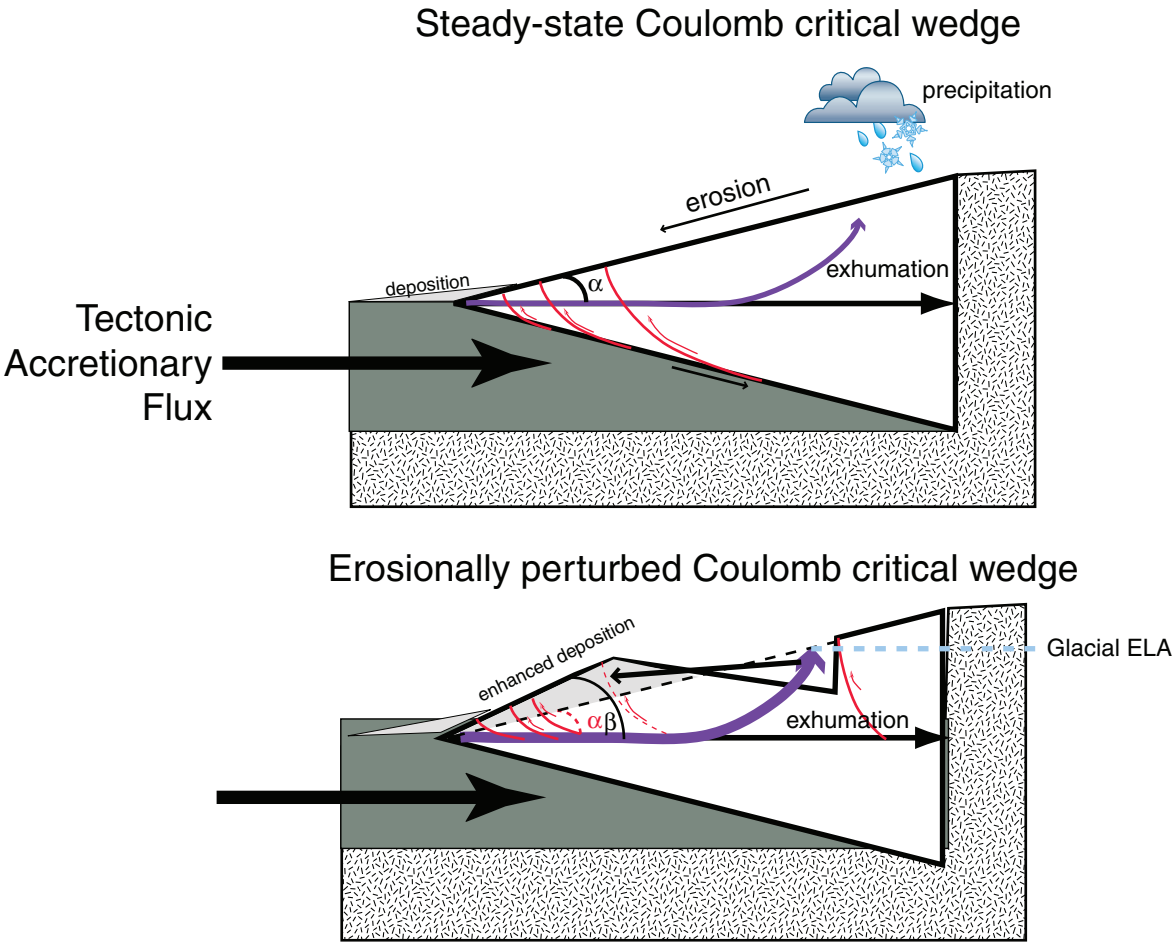

Figure F2. The Gulf of Alaska (GoA) region: geography and location of previous DSDP and ODP drilling locations (see inset) and the proposed drilling sites (GOAL/KB locations). There is significant regional coverage of seismic reflection data on the shelf. High-resolution multichannel seismic (MCS) lines collected in 2004 are shown in yellow. Reflection and refraction lines (green) were collected in summer 2008 as part of the STEEP program.

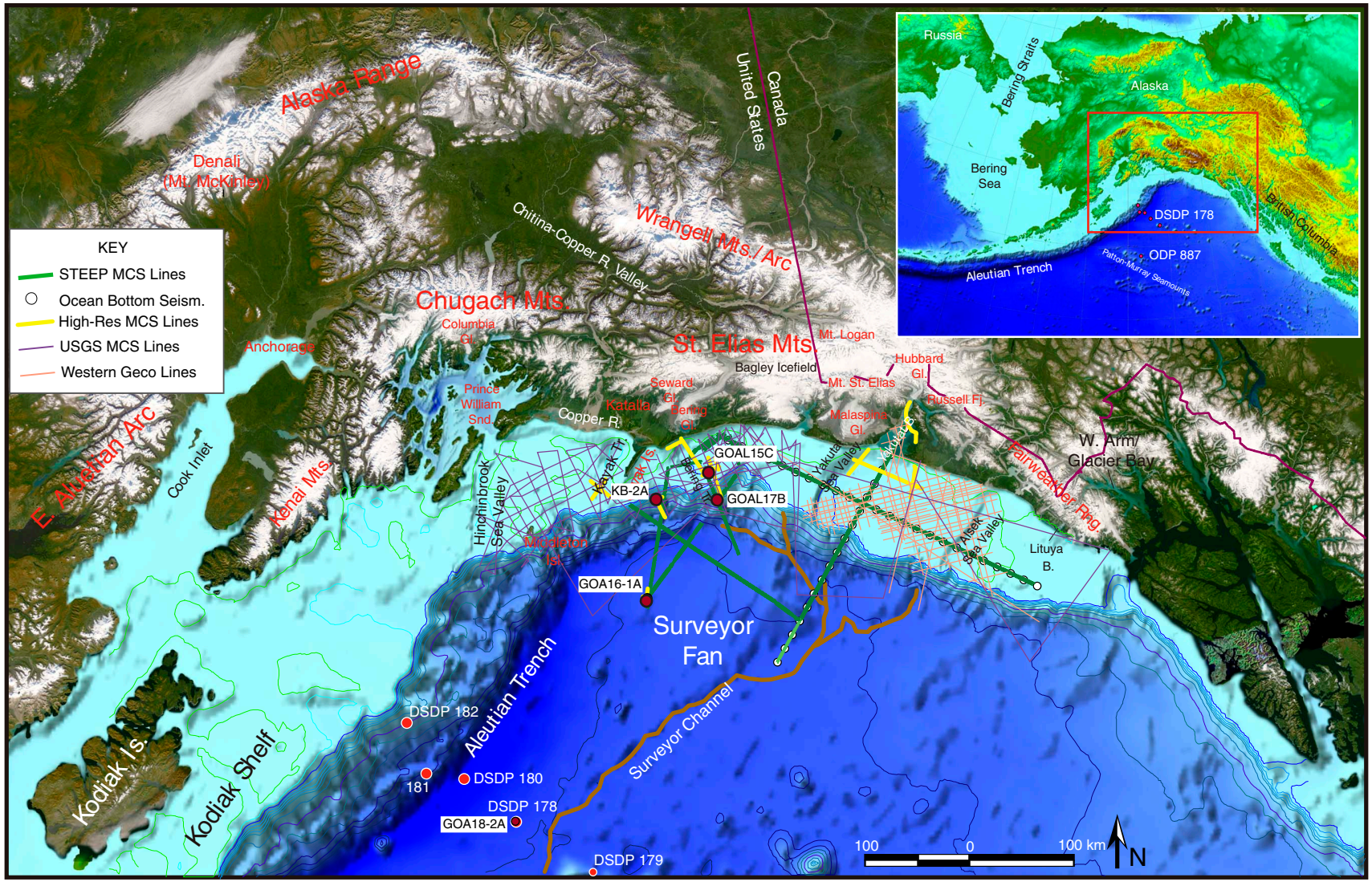

Figure F3. Stratigraphic, depositional, tectonic, and climatic history of the Gulf of Alaska and adjacent regions as modified from Lagoe et al. (1993) and Berger et al. (2008a). Lithologic data are from Lagoe et al. (1993), Rea and Snoeckx (1995), and Lagoe and Zellers (1996). Bedrock temperature paths vs. time from Berger et al. (2008a). Tectonic events from Lagoe et al. (1993), Stevenson and Embley (1987), Berger et al. (2008a, 2008b), Enkelmann et al. (2010), and Finzel et al. (2011). Oxygen isotope data from global stacks of Lisiecki and Raymo (2005) (black) and Zachos et al. (2001) (gray). IRD = ice-rafted debris.

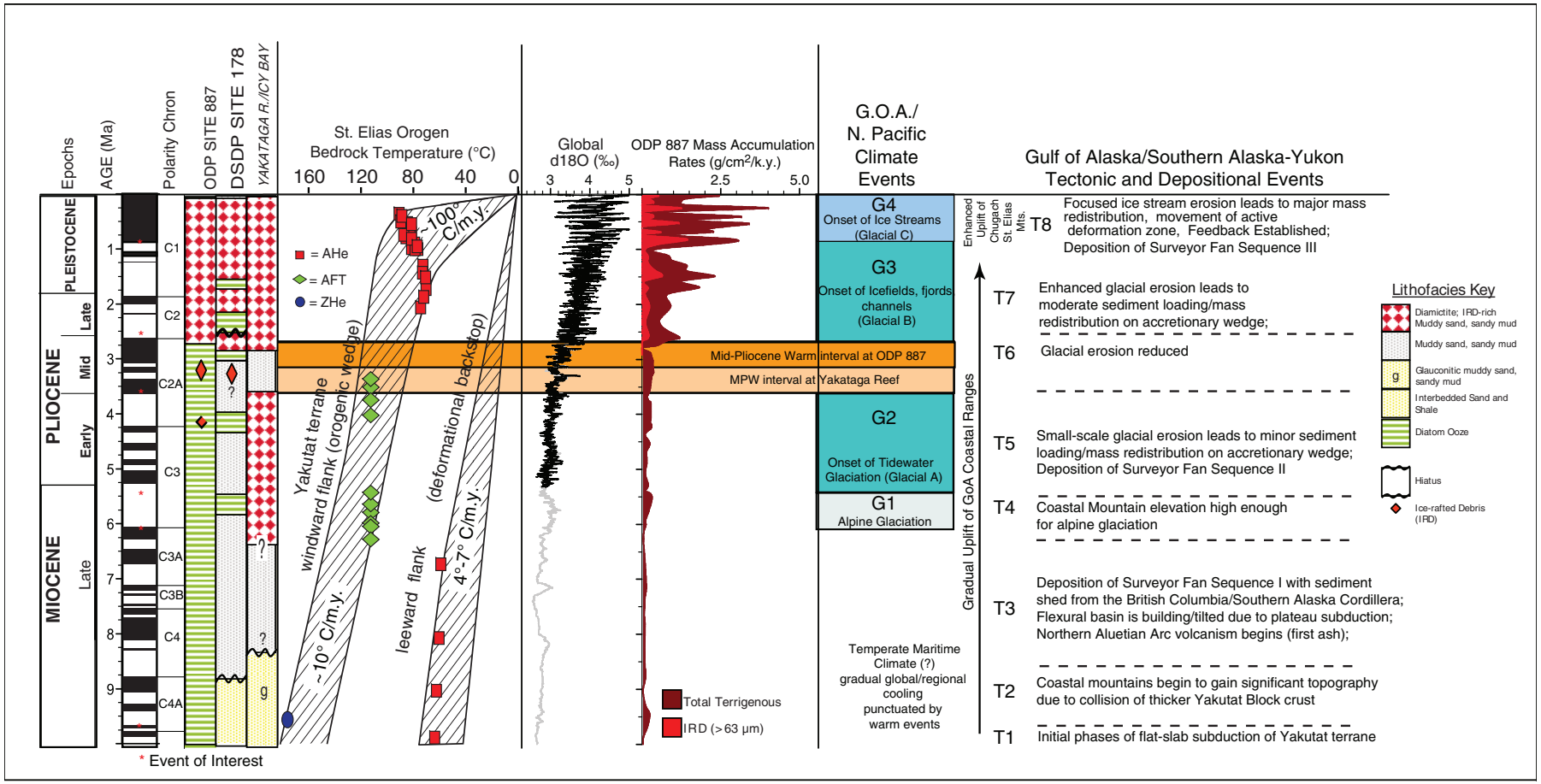

Figure F4. Regional tectonic map of southern Alaska showing major faults, topography, and geographic landmarks. Pacific plate velocity vector from Demets and Dixon (1999). Yakutat terrane velocity w.r.t. North America in red arrows (avg. = 47 mm/y from Elliot et al., 2010). Blue dashed line shows extent of subducted Yakutat slab from Eberhart-Phillips et al., (2006). Black dashed outline shows currently defined Yakutat terrane. Benioff zone depth contours at 50, 100, and 150 km. KIZ = Kayak Island zone, DRZ = Dangerous River zone, TACT = Trans-Alaska Crustal Transect. Figure from Worthington, 2010.

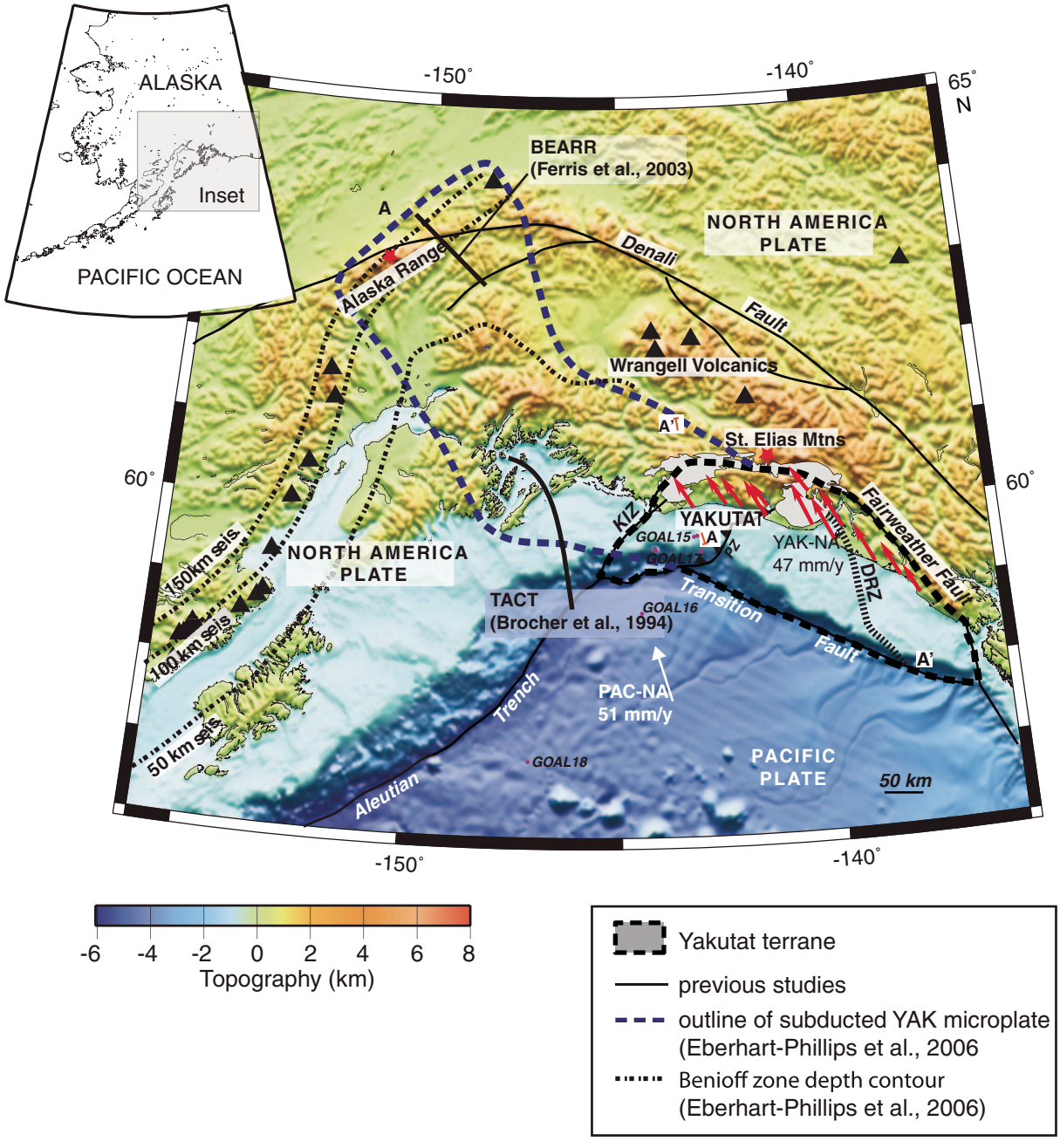

Figure F5. Terrane map of Alaska showing major tectonostratigraphic terranes. Modified from Nokleburg et al. (2001).

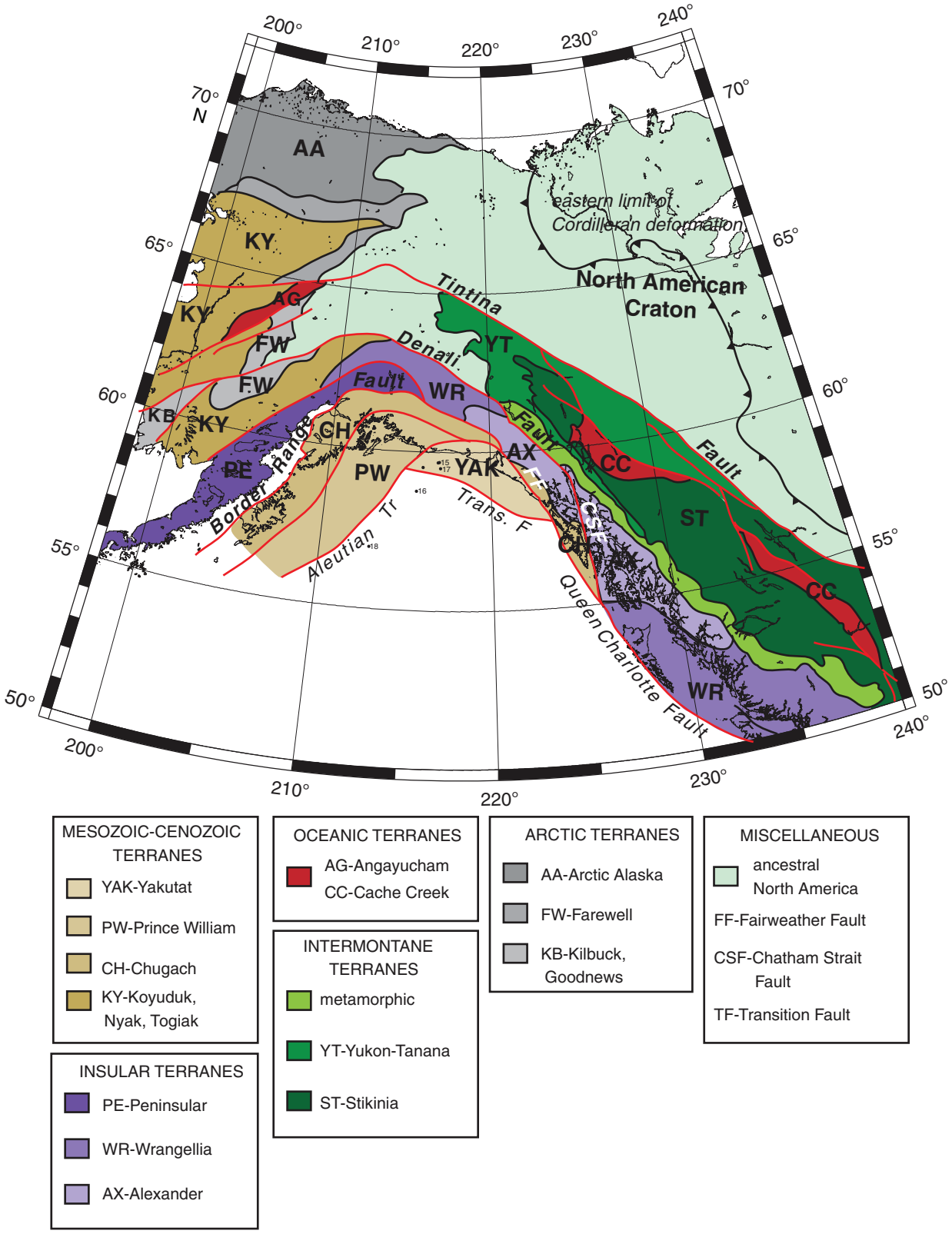

Figure F6. Proposed model of climate-related influences on orogen kinematics. **A.** Exhumational flux based on thermochronometry and architecture of the orogen prior to onset of glacial interval C, drawn along line A-A′ (Fig. F4) based on thermochronometry (Berger et al., 2008b; Spotila and Berger, 2010) and geologic data (Plafker et al., 1994; Bruhn et al., 2004). **B.** Exhumational flux based on thermochronometry and architecture of the orogen after the onset of glacial interval C. **C.** Interpretative model of the effect of glacial erosion and deposition on the St. Elias critical wedge. Before glacial interval C (left), the critical Coulomb wedge is wider and has greater relief. After the intensification of glaciation (right), increased glacial erosion and offshore deposition reduced relief, concentrated deformation, required enhanced back thrusting, and forced the termination of foreland structures, thereby narrowing the wedge. For A, B, and C, straight dashed lines depict structures with only minor amounts of slip and wavy dashed lines depict inactive structures. Gray, green, and brown strata along windward site reflect Kultieth, Poul Creek, and Yakataga Formations, respectively. Modified from Berger et al. (2008a, 2008b).

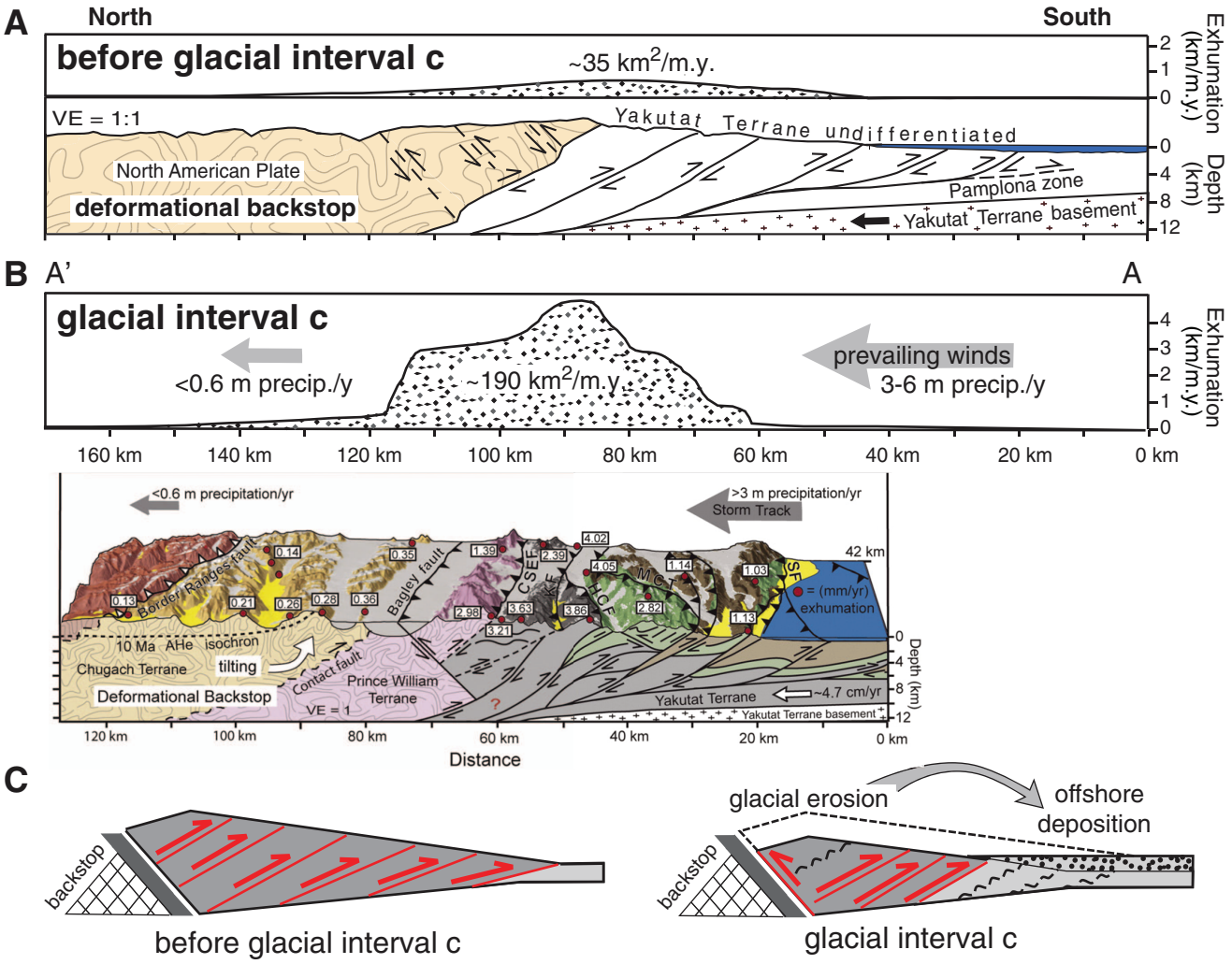

Figure F7. 3-D perspective view of the bathymetry/topography of the southern Alaska continental margin, showing tectonic boundaries, and the Surveyor Fan in high-resolution bathymetry. ASV = Alsek Sea Valley, BT = Bering Trough, GS = Giacomini Seamount, KT = Kayak Trough, PS = Pamplona Spur, YSV = Yakutat Sea Valley. Data sources: plate boundaries adapted from Gulick et al. (2007); high-resolution bathymetry (Gardner et al., 2006); remaining bathymetry (Smith and Sandwell, 1997); Yakutat terrane motion relative to North America (Elliott et al., 2010); Pacific plate motion (Kreemer et al., 2003). Inset: Location of Alaska Coastal Current (ACC; purple); Alaska Current (AC; orange); and NOAA wave buoy 4600 (red star). Modified from Reece et al., in press.

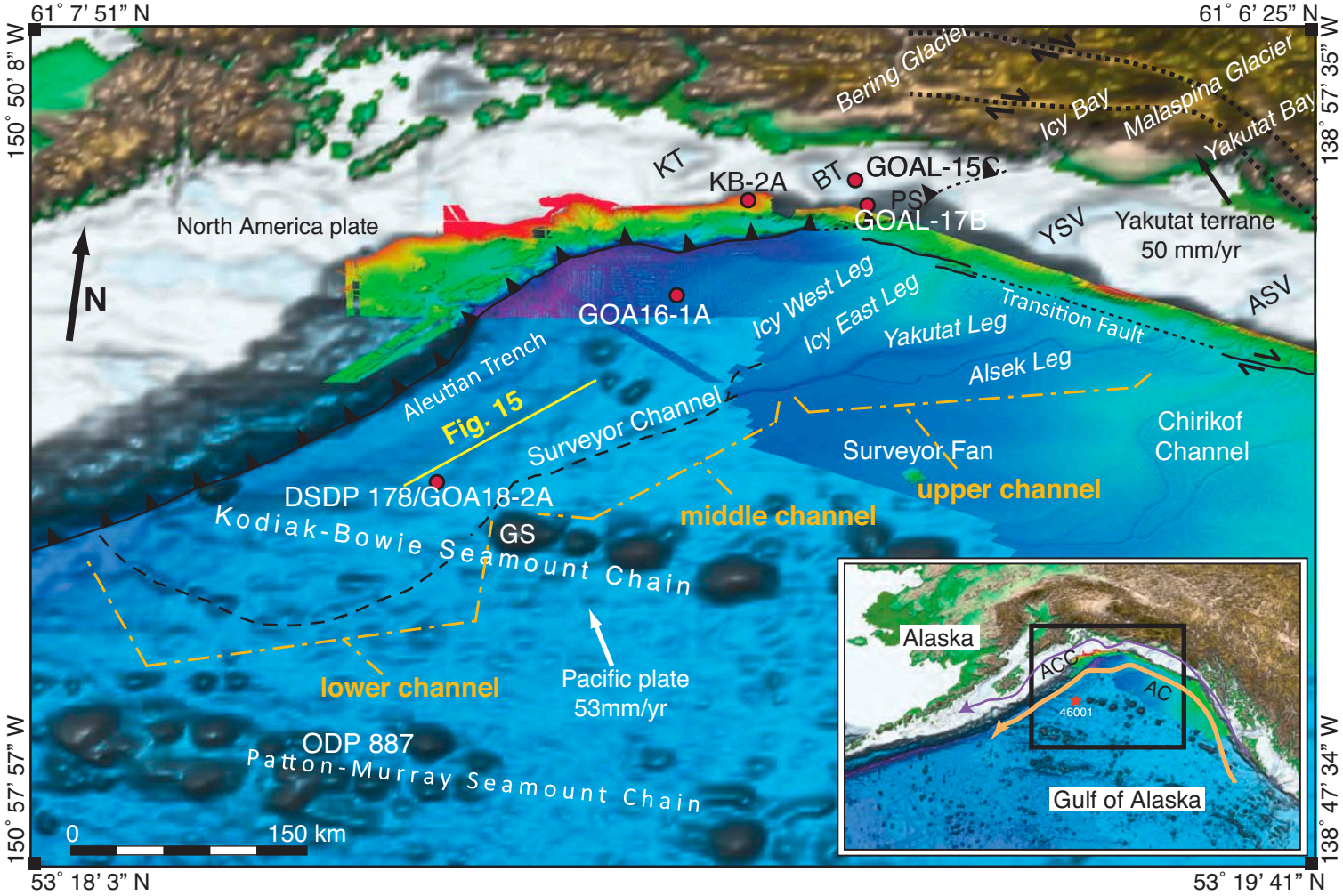

Figure F8. Alaska paleoglacier summary of Pleistocene glaciation across Alaska. Shown is the extent of glaciers during the late Wisconsin (LGM) glaciation and the maximum extent reached during the last 3 m.y. by valley glaciers, ice caps, and the NCIS. From Manley and Kaufmann (2002).

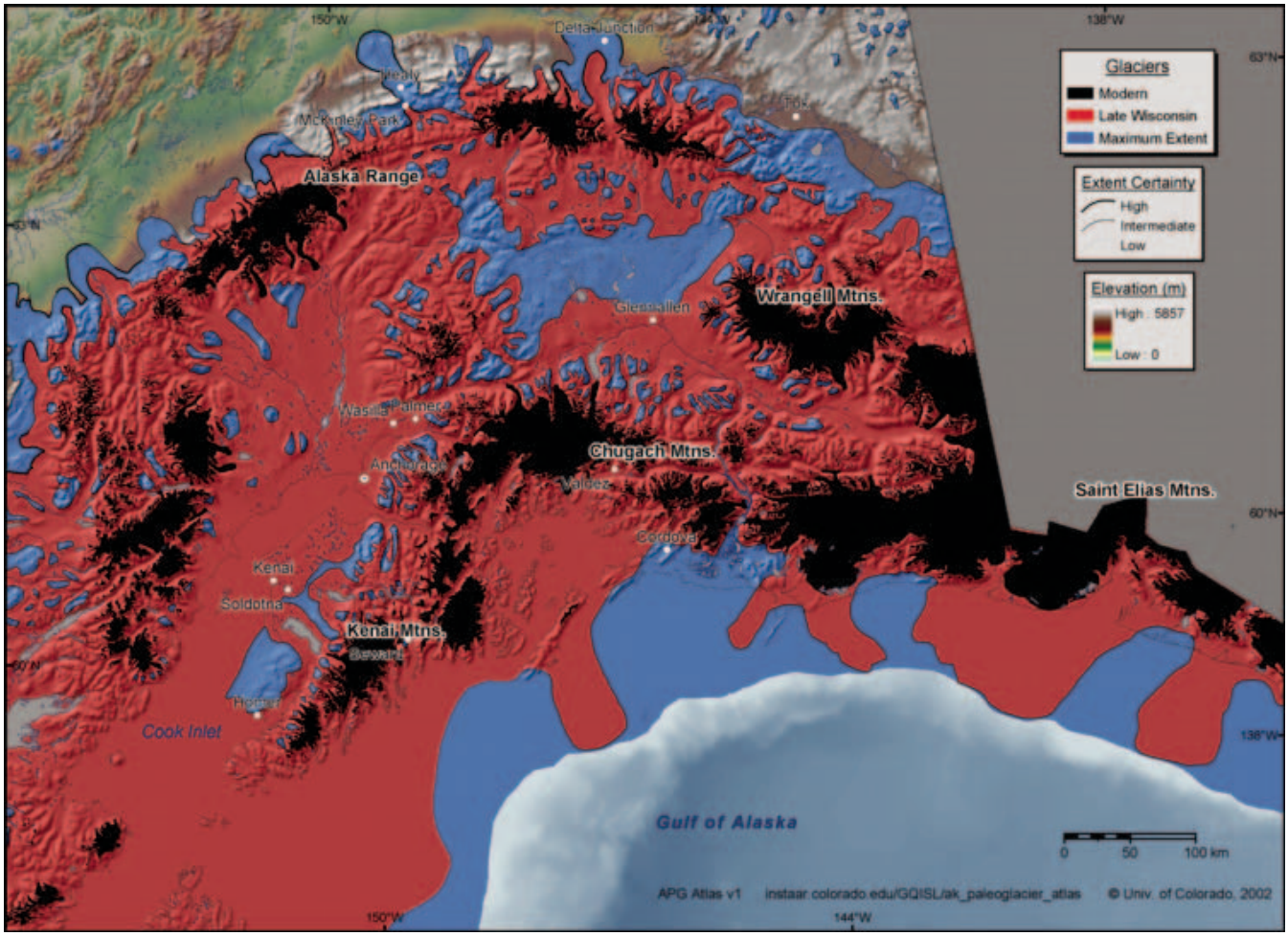

Figure F9. GOA-2505 seismic section, uninterpreted (top) and interpreted (bottom). Interpreted section shows structures BT4, BT5, and key horizons. Colored horizons are regional horizons interpreted throughout the study area. Black horizons are interpreted locally to define glacial depositional sequences in the upper 2 s of the record. From Worthington et al. (2010).

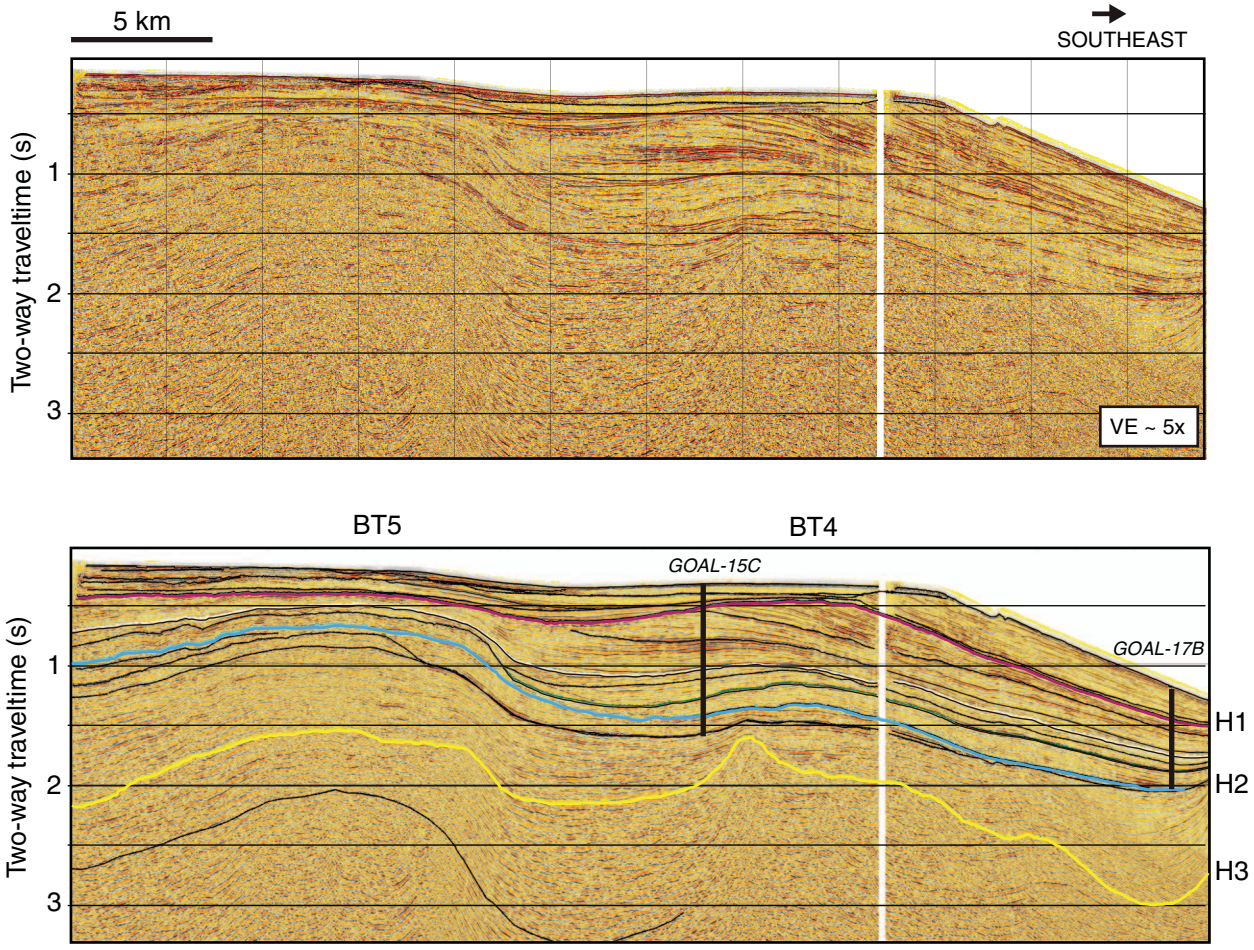

Figure F10. A. STEEP09 seismic section, uninterpreted (top) and interpreted (bottom). Interpreted section shows structures BT1, BT2, BT3, BT4, and key horizons. Colored horizons are regional horizons interpreted throughout the study area. Horizons A–F (black) are interpreted locally to define growth strata packages on fold limbs and glacial depositional sequences in the upper 2 s of the record. **B.** High-resolution (1002 m) bathymetry shows fault scarps on Yakutat slope associated with BT1 and BT2. Locations of seismic profiles STEEP09 (red) and GOA2505 (purple). From Worthington et al. (2010).

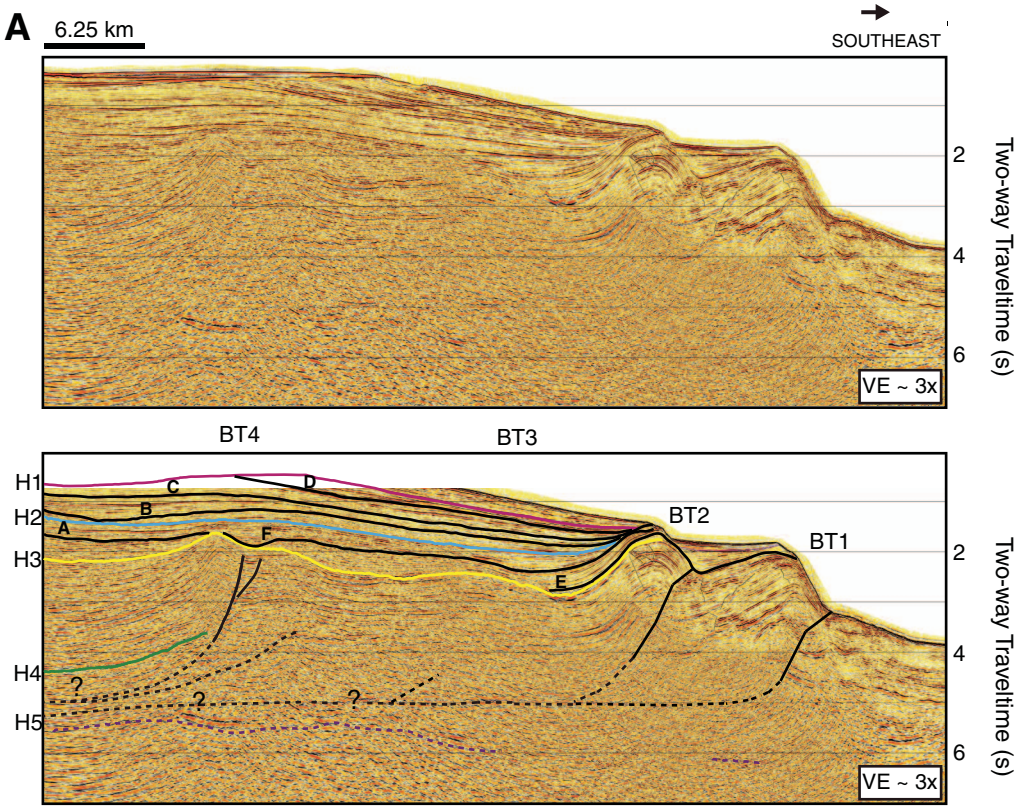

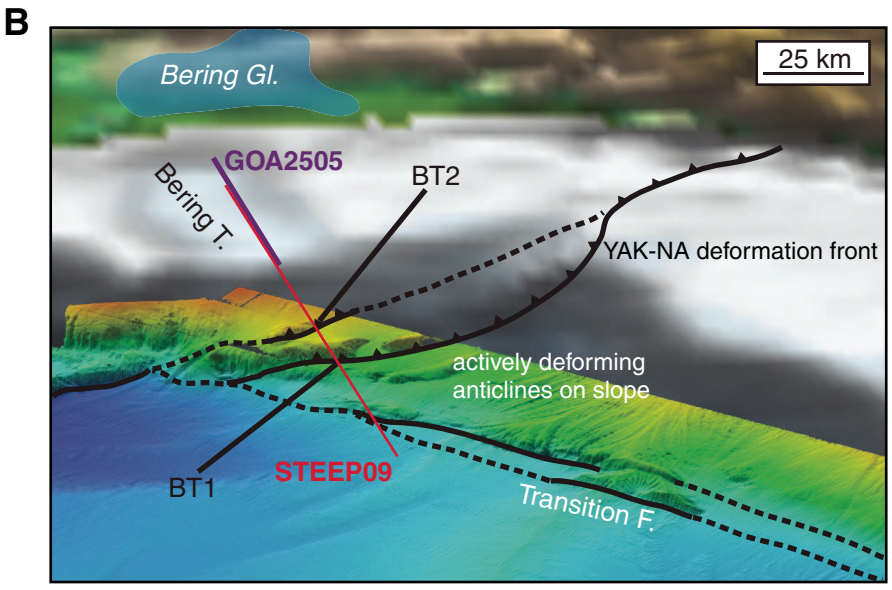

Figure F11. Glacial sequences and interpreted lithofacies of GOA-2505 seismic section based on glacial systems tracts at proposed drill sites. The GMiST includes sediment accumulated during interglacial periods. The GRST includes glacial sediment deposited at the glacial grounding-line, and the GMaST is composed of sediment deposited at the continental slope during glacial advance. Each proposed drill core should sample at least eight interglacial intervals with thicknesses up to 5 ms. Sequence geometries indicate a overall reduction in shelf accommodation space over the past 2 m.y. Such a reduction in accommodation space could be eustatic in nature and influenced by fluctuations of the Cordilleran ice sheet. After Willems (2009).

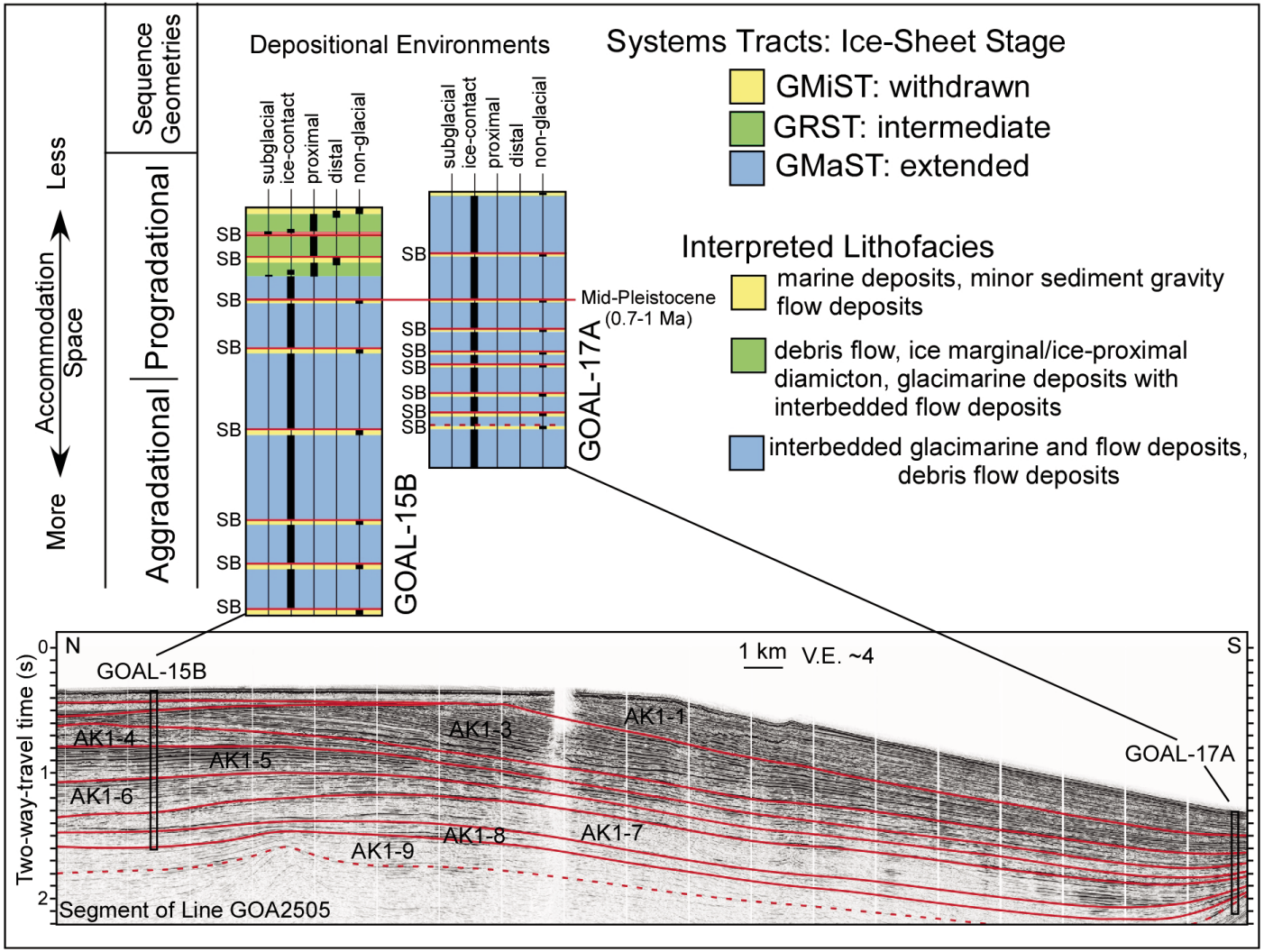

Figure F12. A. High-resolution seismic Profile GOA-2505 imaging Bering Trough showing a distinct change in margin architecture from tectonically to depositionally influenced at the labeled erosional unconformity. **B.** Interpretations for seismic Profile GOA-2505. Location of seismic profile shown in Figure F2. **C.** Schematic cross-section across frontal St. Elias wedge. Modified from Worthington et al., 2008, 2010.

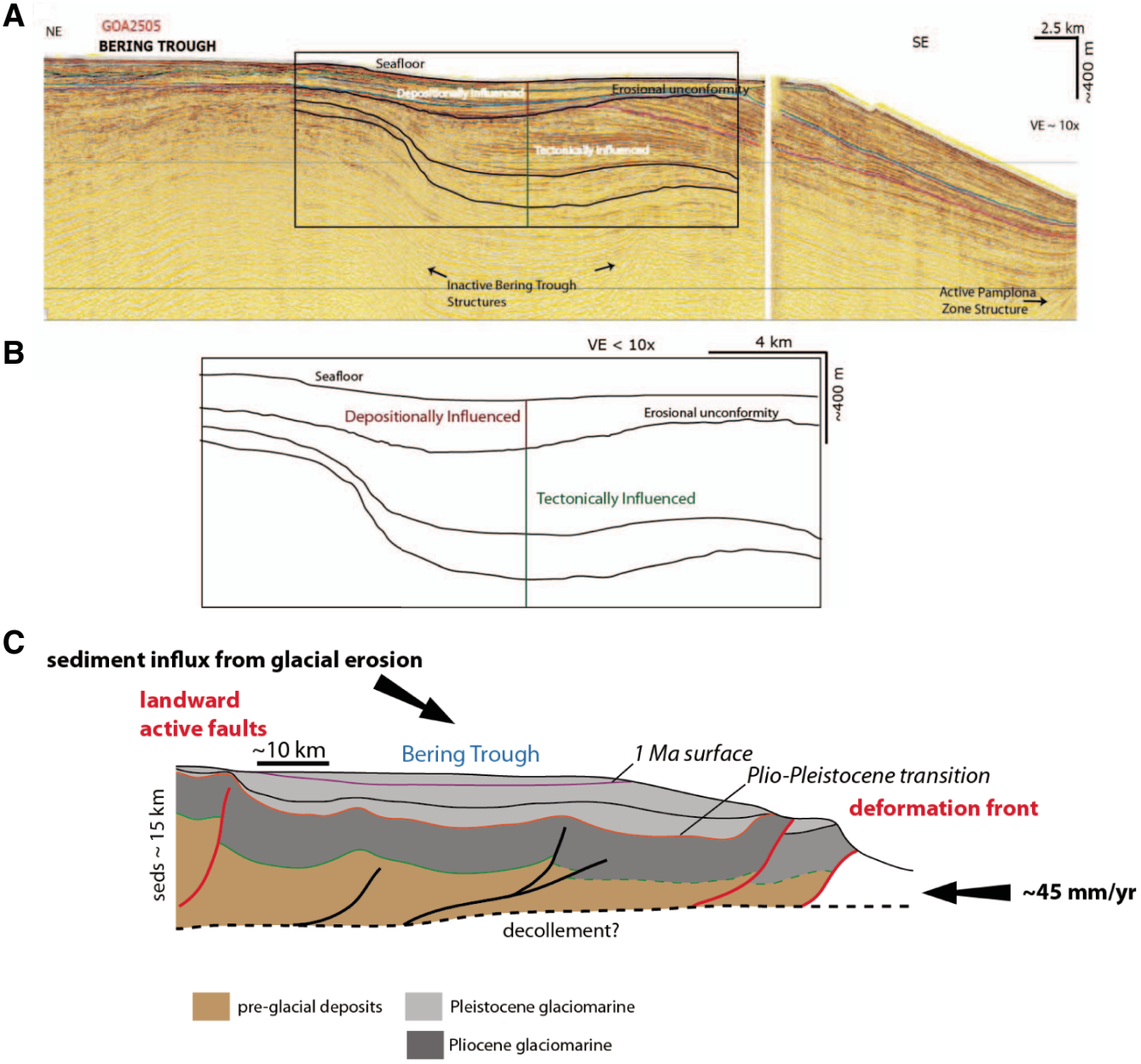

Figure F13. High-resolution seismic profile (**A**) GOA-3101 and GOA-3102 and (**B**) CHIRP imaging the shelf break at Khitrov Ridge. Active deformation and faulting at seafloor soles into a transtensional flower structure and the drill Site KB-2 is located upslope of these structures. Higher amplitude reflectors correspond in Core EW0408 85JC (located at the landward end of seismic Profile GOA3101) to diamict (Davies et al., 2011). LGM = Last Glacial Maximum.

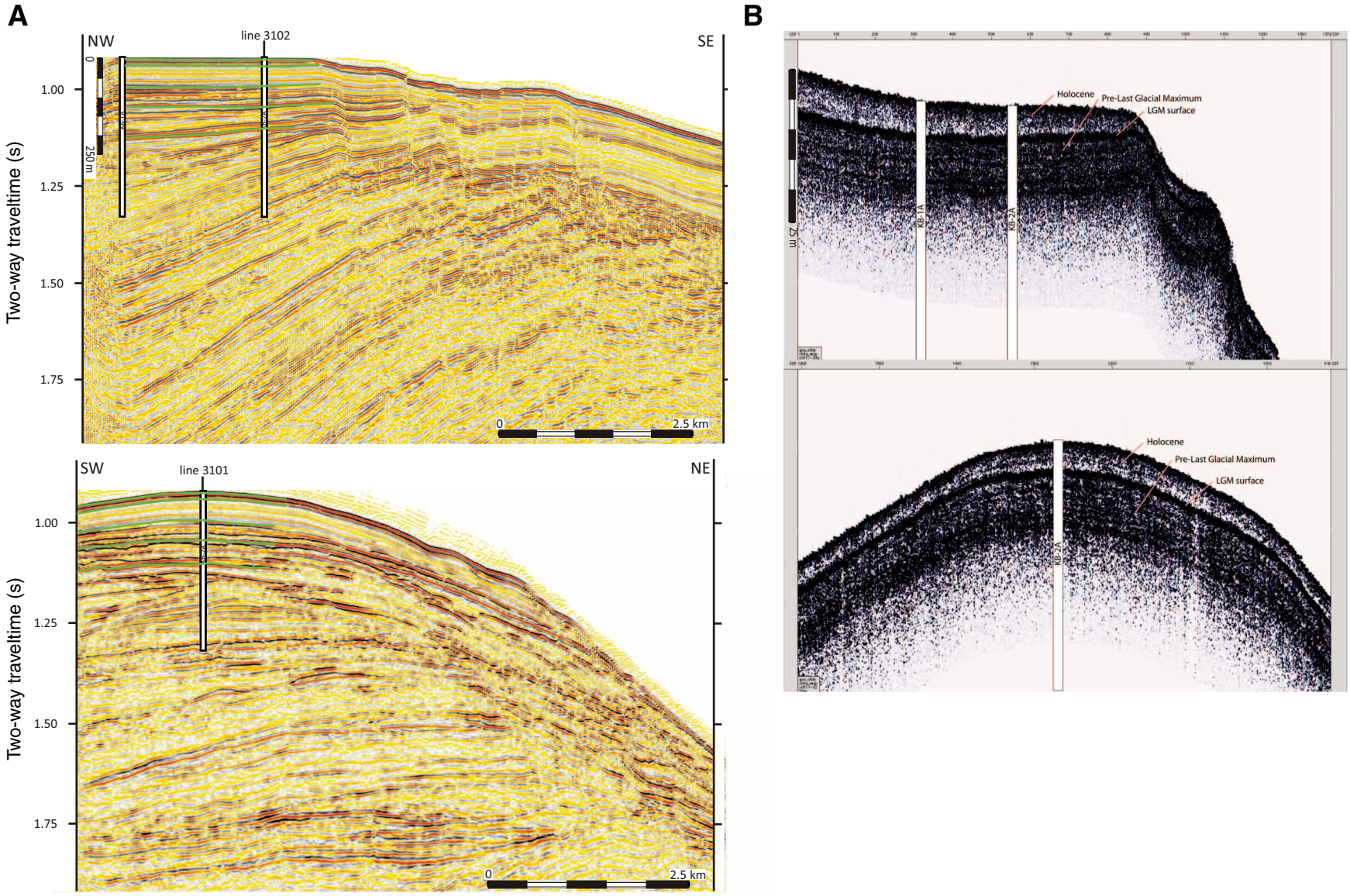

Figure F14. Lithology and age control for DSDP Site 178. Modified from Lagoe et al. (1993). Partial seismic section from Line 13 of 1989 USGS Survey F689 (Fig. F7). IRD = ice-rafted debris, Ja = Jaramillo, Oi = Olduvai. GI A, GI B, GI C = glacial Intervals A, B, and C. MPW = mid-Pliocene warm period. $^{40}Ar/^{39}Ar$ ages from Hogan et al. (1978). Magnetic polarity stratigraphy from von Huene et al. (1973). Modified from Reece et al., in press.

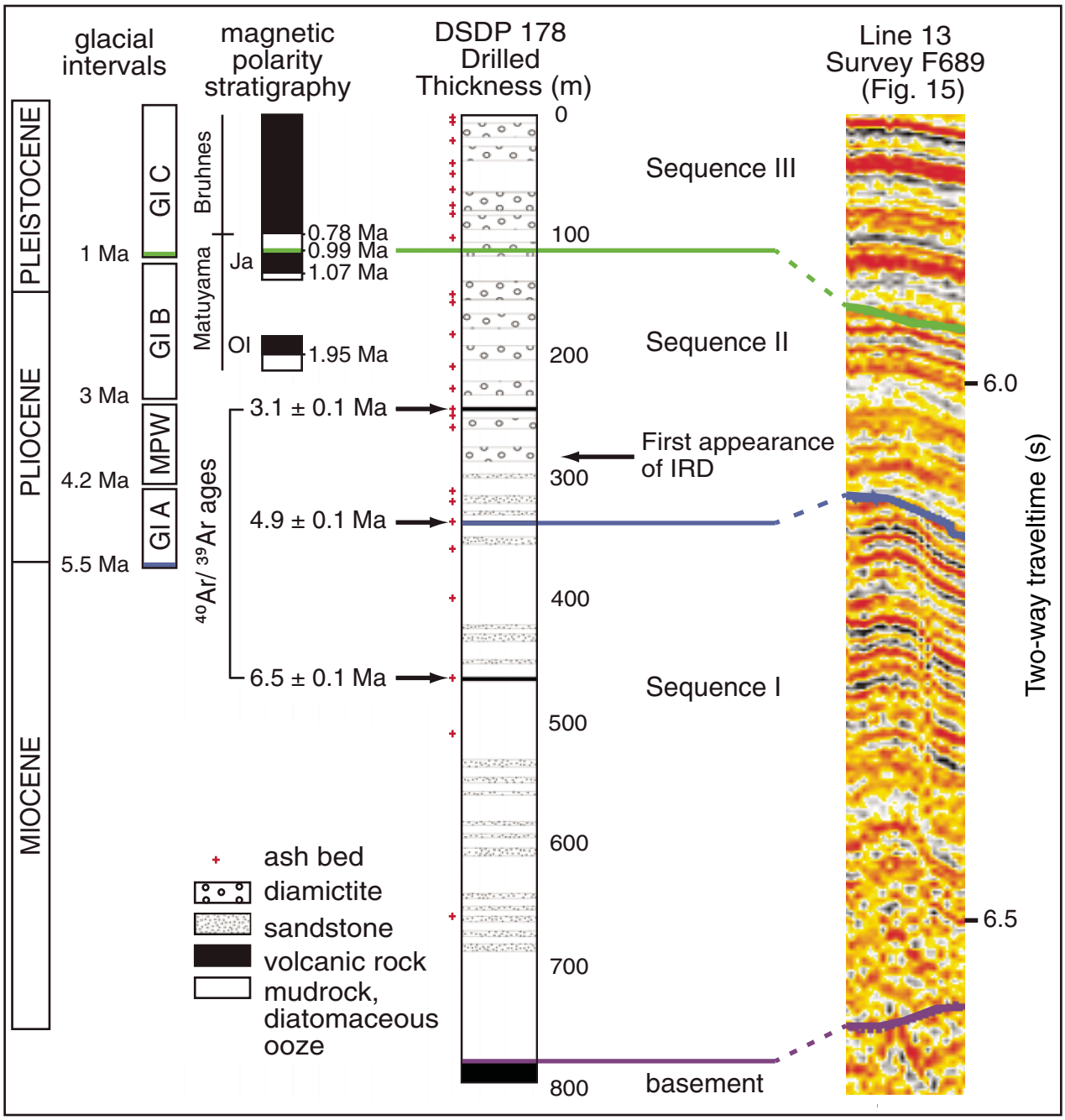

Figure F15. Seismic reflection Line 13 from 1989 USGS Survey F689 showing sequences newly defined by this study and approximate correlation to DSDP Site 178. See Figure F7 for line location. Vertical exaggeration assumes 2000 m/s sediment acoustic velocity. Modified from Reece et al., in press.

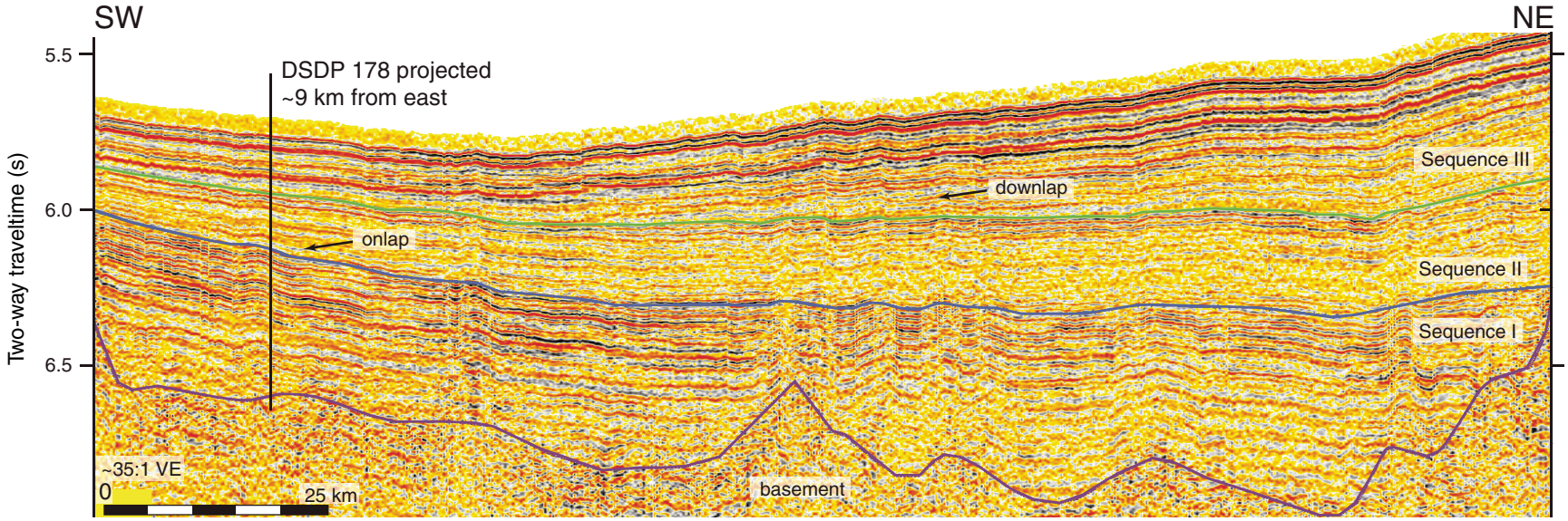

Figure F16. STEEP13 seismic section and high-resolution seismic Profile GOA-3201 (inset) showing typical seismic facies of Sequence III on the proximal Surveyor Fan. Proposed drill sites for the proximal fan penetrate all of Sequence III and bottom in a proposed mass transport deposit (MTD, Surveyor Slide) (Reece and Gulick, unpubl. data).

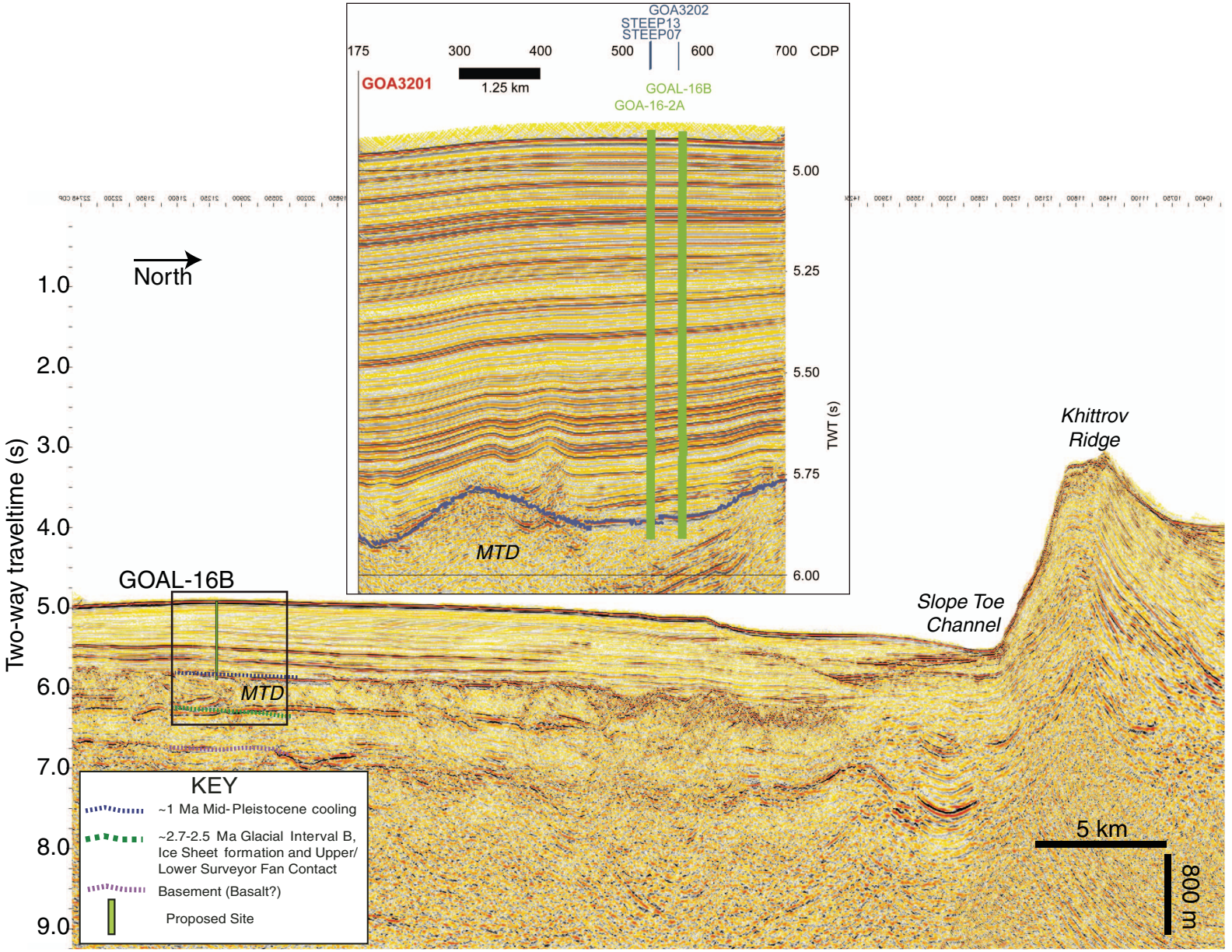

Figure F17. Two-way travel time thickness maps of (**A**) Sequence I, Pacific plate formation to ~5.5 Ma, (**B**) Sequence II, ~5.5–1 Ma, and (**C**) Sequence III, ~1 Ma to present. **D.** Seismic reflection data track lines used in the calculation. ASV = Alsek Sea Valley, BT = Bering Trough, KT = Kayak Trough, YSV = Yakutat Sea Valley. From Reece et al., in press.

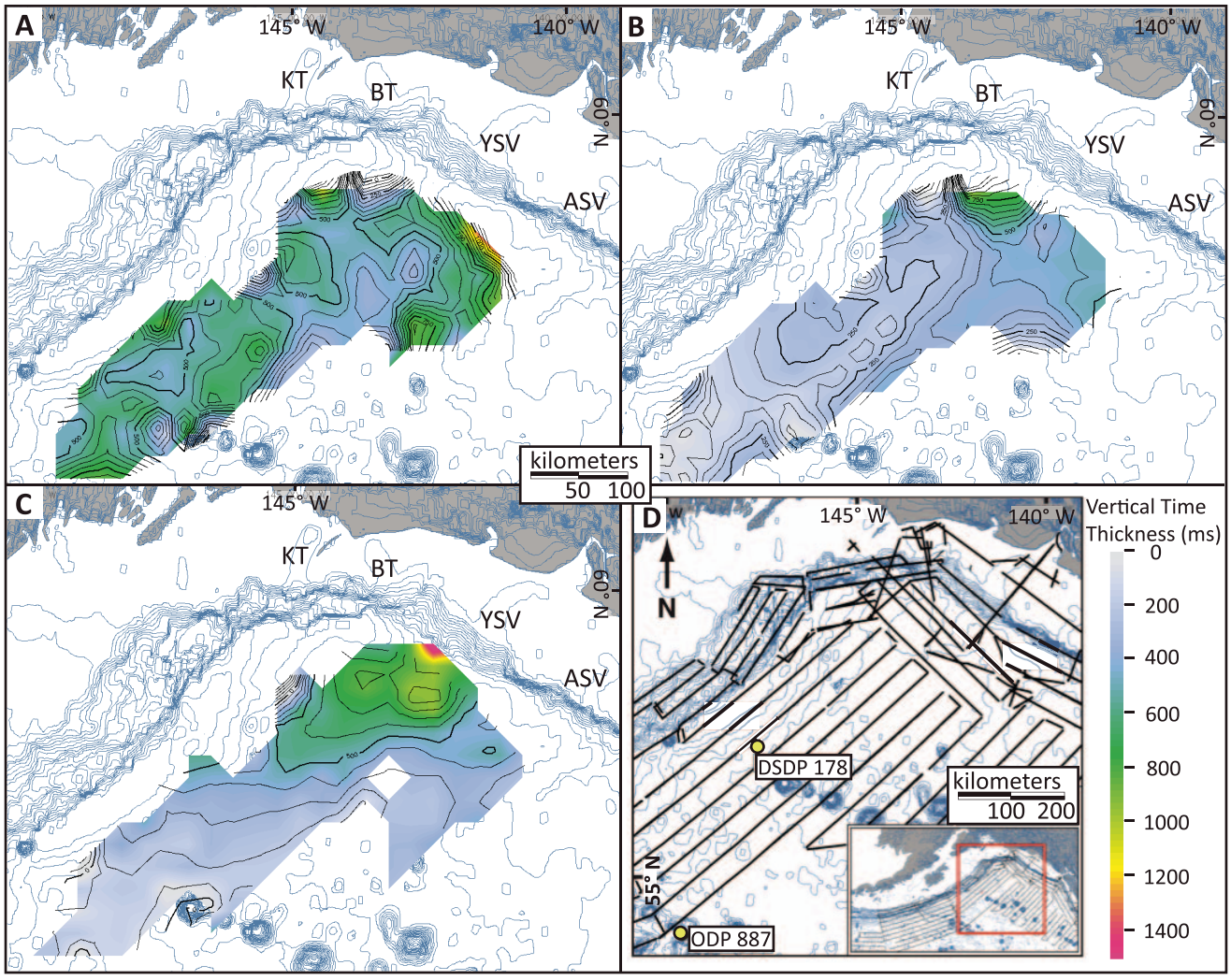

Figure F18. Schematic illustration of Surveyor Fan and southern Alaska margin sedimentary evolution over the last ~20 m.y. The area in gray on the seafloor represents the growth and evolution of the Surveyor Fan by channel-related processes. Red asterisk denotes the approximate location of Alsek Sea Valley through time. **A.** ~20–5.5 Ma. **B.** ~5.5 Ma. **C.** ~1 Ma. **D.** LGM–present. AT = Aleutian Trench, FWF = Fairweather Fault, IRD = ice-rafted debris, NA = North America, PSC = proto-Surveyor Channel, TF = transition fault, YAK = Yakutat terrane. From Reece et al. (in press).

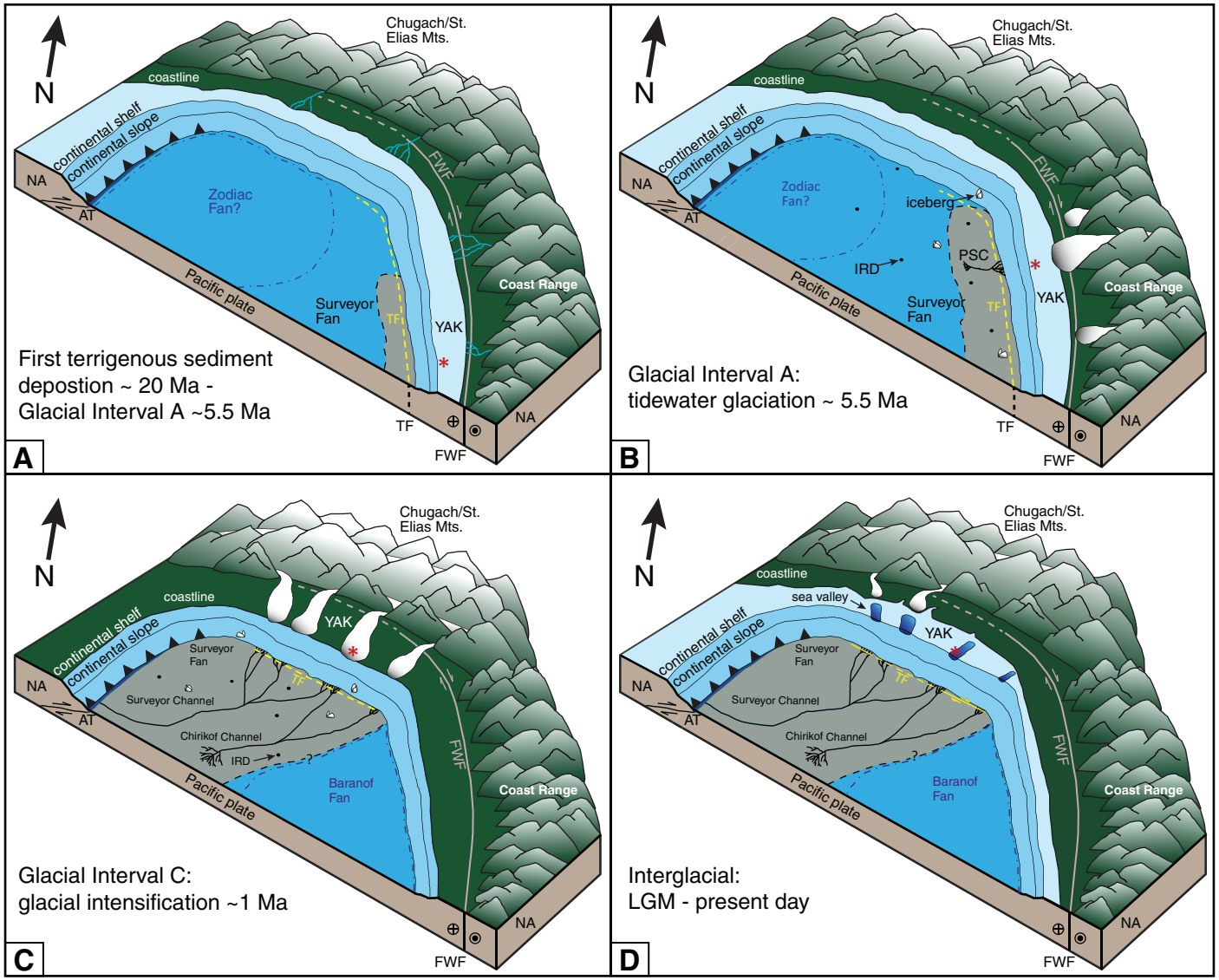

Figure F19. Lithofacies and paleoceanographic data from Core EW0408-85JC. **A.** Computed tomography (CT)-derived bulk density data. **B.** Opal (periods of lamination are delineated below the record by green bars). **C.** Planktonic $\delta^{18}O$ (dark blue = *Neogloboquadrina pachyderma*, light blue = *Globigerina bulloides*). **D.** Benthic $\delta^{18}O$ (solid squares = *Uvigerina peregrina*, open squares = *Cibicidoides wuellerstorfi* + 0.64, crossed squares = *Nonionella* sp. + 0.10). **E.** Planktonic-benthic $\delta^{18}O$ (light pink squares). **F.** Planktonic $\delta^{13}C$ (purple = *N. pachyderma* sinistral, pink-red = *G. bulloides*). **G.** Benthic $\delta^{13}C$ (orange = *U. peregrina* + 0.20, orange open canted triangles = *C. wuellerstorfi*). For global context these data are presented next to (**H**) the Greenland ice core $\delta^{18}O$ record (NGRIP; gray) (Andersen et al., 2006; Rasmussen et al., 2006; Svensson et al., 2006) and (**I**) the relative sea level (RSL) curve compiled in Sidall et al. (2009) (open blue squares). Timing of the North Atlantic Bølling-Allerød (B-A) and Younger Dryas (Y-D) climate anomalies is highlighted in yellow and blue, respectively, as well as meltwater pulse (MWP) 1A (yellow, coeval with the B-A), and 1B (green). From Davies et al. (2011). **(Figure shown on next page.)**

Figure F19 (continued). (Caption shown on previous page.)

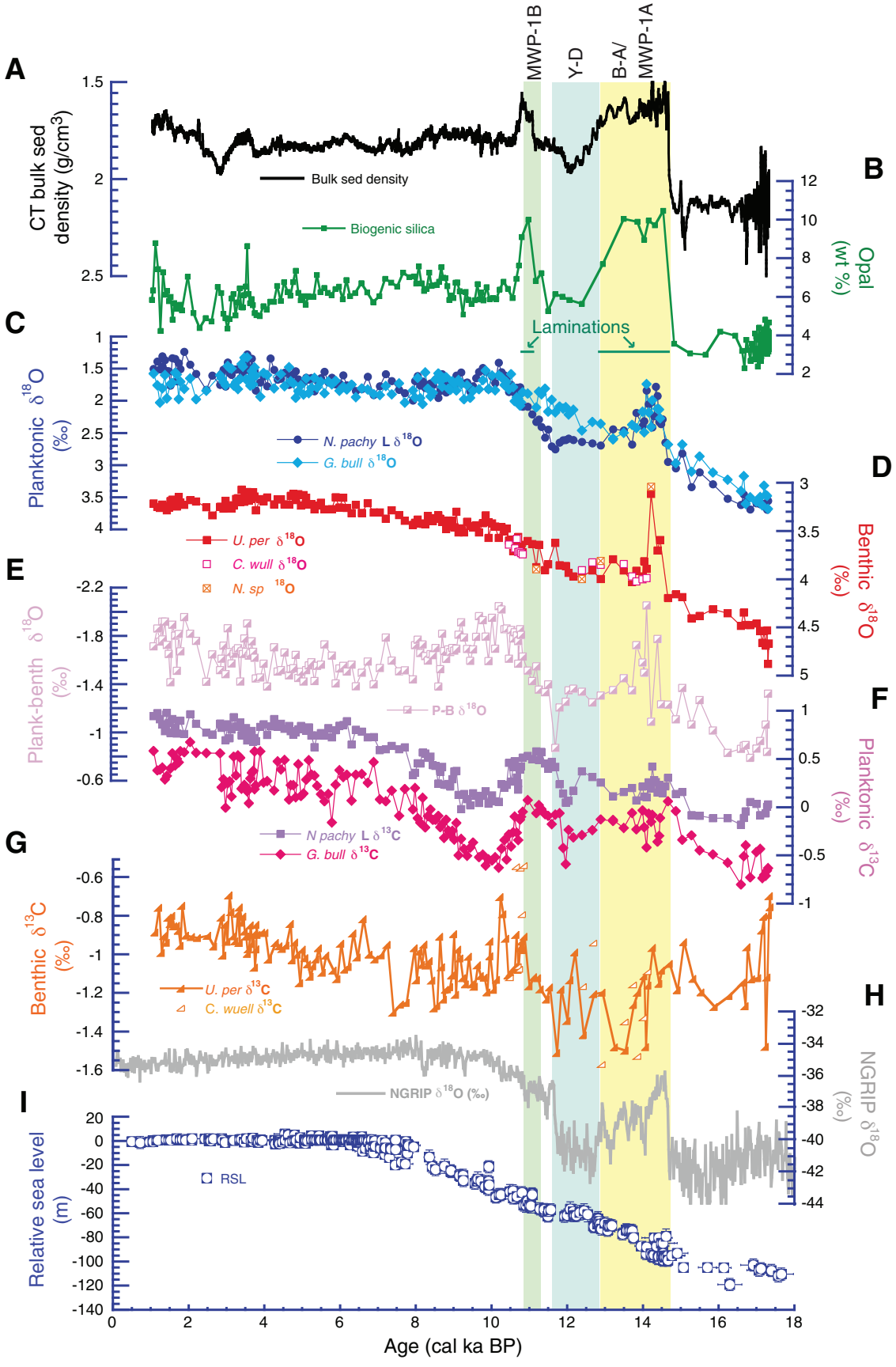

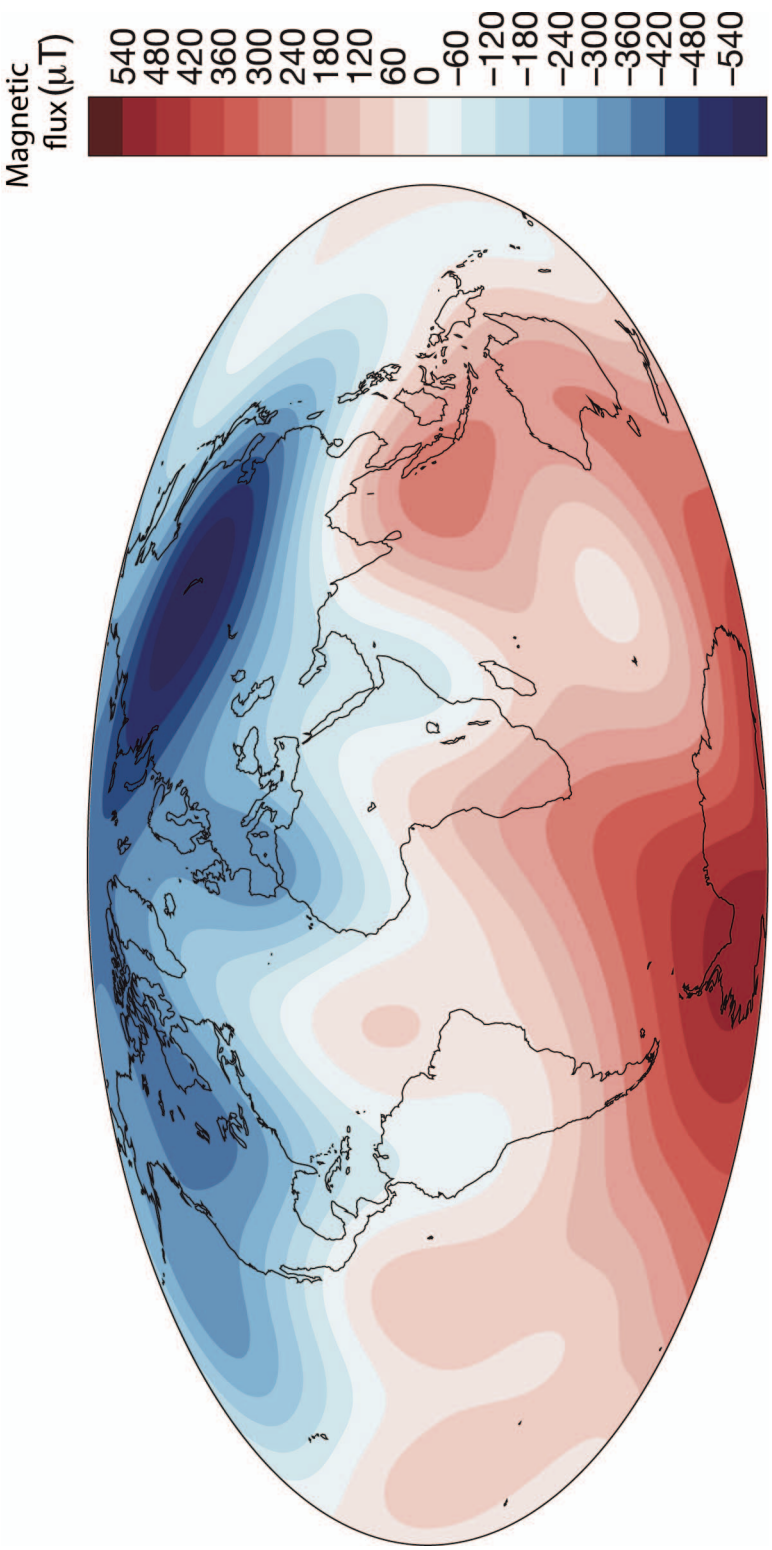

Figure F20. 5 m.y. time-averaged paleomagnetic field showing quasistationary nondipole features (Gubbins and Kelly, 1993).

Figure F21. Standard downhole logging tool strings. GPIT = general purpose inclinometry tool, HNGS = Hostile Environment Natural Gamma Ray Sonde, APS = Accelerator Porosity Sonde, HLDS = Hostile Environment Litho-Density Sonde, DIT-E = Dual Induction Tool, DSI = Dipole Sonic Imager, MEST-B = Microelectrical Scanner Tool, FMS = Formation MicroScanner, VSI = Versatile Seismic Imager.

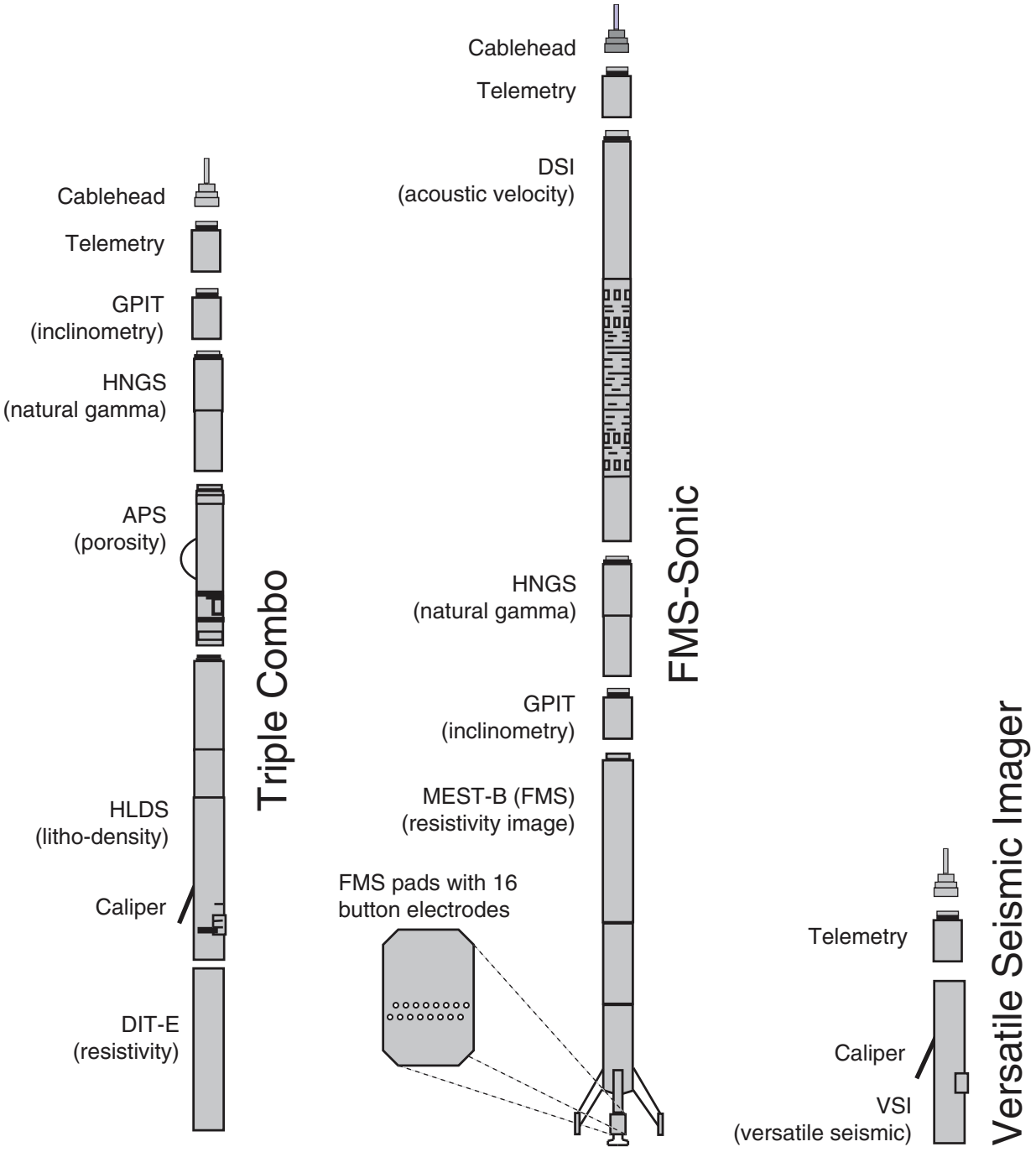

Figure F22. The "paleo combo" tool string is a variation of the triple combo tool string. GPIT = general purpose inclinometry tool, HNGS = Hostile Environment Natural Gamma Ray Sonde, APS = Accelerator Porosity Sonde, HLDS = Hostile Environment Litho-Density Sonde, MSS = Magnetic Susceptibility Sonde.

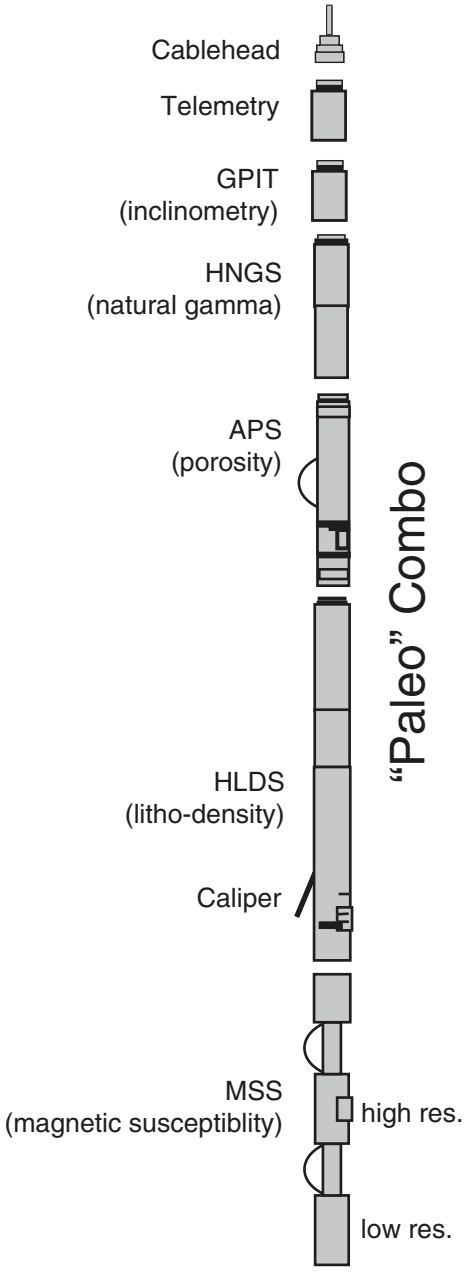

Site summaries

Proposed Site GOAL-15C

Priority:	Primary
Position:	59°41.3394′N, 143°12.0552′W
Water depth (mbrf):	261
Target drilling depth (mbsf):	1112
Approved maximum penetration (mbsf):	1225
Survey coverage:	Inline GOA2505 (CDP 2845), Xline GOA2502 (CDP 1137), MCS line STEEP09 (CDP 14018) (navigation and bathymetric maps Figs. **AF2, AF8;** seismic profiles Figs. **AF3, AF4, AF5**)
Objective:	Tectonic and climate history of the Bering Glacier and Trough
Drilling and coring program:	• Hole A: APC to ~250 mbsf with non-magnetic core barrels, XCB to ~1112 mbsf • See **"Drilling and coring strategy"** and Table **T2**
Downhole measurements program:	• Wireline logging with triple combo, FMS-sonic, and VSI tool strings • See **"Downhole measurements strategy"** and Table **T2**
Anticipated lithology:	Mud, silt, fine sand, volcanic ash, ice-rafted debris, diamict

Site summaries (continued)

Proposed Site GOA15-1A

Priority:	Alternate
Position:	59°42.0600′N, 143°7.2012′W
Water depth (mbrf):	189
Target drilling depth (mbsf):	1158
Approved maximum penetration (mbsf):	1200
Survey coverage:	Inline GOA2503 (CDP 2336), Xline GOA2502 (CDP 758) (navigation and bathymetric maps Figs. **AF6, AF8;** seismic profiles Figs. **AF5, AF7**)
Objective:	Tectonic and climate history of the Bering Glacier and Trough
Drilling and coring program:	• Hole A: APC to ~250 mbsf with non-magnetic core barrels, XCB to ~1158 mbsf • See **"Drilling and coring strategy"** and Table **T3**
Downhole measurements program:	• Wireline logging with triple combo, FMS-sonic, and VSI tool strings • See **"Downhole measurements strategy"** and Table **T3**
Anticipated lithology:	Mud, silt, fine sand, volcanic ash, ice-rafted debris, diamict

Site summaries (continued)

Proposed Site GOAL-17B

Priority:	Primary
Position:	59°30.4398′N, 143°2.7378′W
Water depth (mbrf):	738
Target drilling depth (mbsf):	1032
Approved maximum penetration (mbsf):	1045
Survey coverage:	Inline GOA2503 (CDP 576), Xline STEEP07B (CDP 2165) (navigation and bathymetric maps Figs. **AF9, AF11;** seismic profiles Figs. **AF7, AF10**)
Objective:	• Tectonic and climate history of the slope • Growth strata of active thrust
Drilling and coring program:	• Hole A: APC to ~250 mbsf with non-magnetic core barrels and core orientation, XCB to ~1032 mbsf • See **"Drilling and coring strategy"** and Table **T2**
Downhole measurements program:	• Wireline logging with triple combo, FMS-sonic, and VSI tool strings • See **"Downhole measurements strategy"** and Table **T3**
Anticipated lithology:	Mud, silt, sand, volcanic ash, ice-rafted debris, diamict

Site summaries (continued)

Proposed Site GOA16-1A

Priority:	Primary
Position:	58°46.6122′N, 144°29.5968′W
Water depth (mbrf):	3703
Target drilling depth (mbsf):	978
Approved maximum penetration (mbsf):	1100
Survey coverage:	Inline GOA3202 (CDP 510), Xline STEEP07 (CDP 3592) (navigation and bathymetric maps Figs. **AF12, AF13;** seismic profiles Figs. **AF15, AF16**)
Objective:	• Tectonic and climate history of upper Surveyor Fan and origin of Surveyor Fan sequence boundaries • Provenance of unroofed sediments
Drilling and coring program:	• Hole A: APC to ~200 mbsf with non-magnetic core barrels and core orientation • Hole B: APC to ~200 mbsf with non-magnetic core barrels • Hole C: APC to ~200 mbsf with non-magnetic core barrels • Hole D: APC/XCB to 978 mbsf • See **"Drilling and coring strategy"** and Table **T2**
Downhole measurements program:	• Hole A: APCT-3 (SET if needed) formation temperature measurements • Hole D: wireline logging with triple combo, FMS-sonic, VSI, and Magnetic Properties tool strings • See **"Downhole measurements strategy"** and Table **T2**
Anticipated lithology:	Mud (possibly diatom rich), silt, fine sand, volcanic ash, ice-rafted debris

Site summaries (continued)

Proposed Site GOA16-2A

Priority:	Alternate
Position:	58°46.3476′N, 144°30.1200′W
Water depth (mbrf):	3701
Target drilling depth (mbsf):	962
Approved maximum penetration (mbsf):	1100
Survey coverage:	Inline GOA3201 (CDP 535), STEEP07 (CDP 3478), Xline STEEP13 (CDP 21728) (navigation and bathymetric maps Figs. **AF12, AF13;** seismic profiles Figs. **AF14, AF16, AF17**)
Objective:	• Tectonic and climate history of upper Surveyor Fan and origin of Surveyor Fan sequence boundaries • Provenance of unroofed sediments
Drilling and coring program:	• Hole A: APC to ~200 mbsf with non-magnetic core barrels and core orientation • Hole B: APC to ~200 mbsf with non-magnetic core barrels • Hole C: APC to ~200 mbsf with non-magnetic core barrels • Hole D: APC/XCB to 962 mbsf • See **"Drilling and coring strategy"** and Table **T3**
Downhole measurements program:	• Hole A: APCT-3 (SET if needed) formation temperature measurements • Hole D: wireline logging with triple combo, FMS-sonic, VSI, and Magnetic Properties tool strings • See **"Downhole measurements strategy"** and Table **T3**
Anticipated lithology:	Mud (possibly diatom rich), silt, fine sand, volcanic ash, ice-rafted debris

Site summaries (continued)

Proposed Site GOAL-16B

Priority:	Alternate
Position:	58°46.1750′N, 144°29.7917′W
Water depth (mbrf):	3701
Target drilling depth (mbsf):	986
Approved maximum penetration (mbsf):	1100
Survey coverage:	Inline GOA3201 (CDP 571), Xline GOA3202 (CDP 445) (navigation and bathymetric maps Figs. **AF12, AF13;** seismic profiles Figs. **AF14, AF15**)
Objective:	• Tectonic and climate history of upper Surveyor Fan and origin of Surveyor Fan sequence boundaries • Provenance of unroofed sediments
Drilling and coring program:	• Hole A: APC to ~200 mbsf with non-magnetic core barrels and core orientation • Hole B: APC to ~200 mbsf with non-magnetic core barrels • Hole C: APC to ~200 mbsf with non-magnetic core barrels • Hole D: APC/XCB to 986 mbsf • See **"Drilling and coring strategy"** and Table **T3**
Downhole measurements program:	• Hole A: APCT-3 (SET if needed) formation temperature measurements • Hole D: wireline logging with triple combo, FMS-sonic, VSI, and Magnetic Properties tool strings • See **"Downhole measurements strategy"** and Table **T3**
Anticipated lithology:	Mud (possibly diatom rich), silt, fine sand, volcanic ash, ice-rafted debris

Site summaries (continued)

Proposed Site GOA18-2A

Priority:	Primary
Position:	56.96°N 147.11°W
Water depth (mbrf):	4188
Target drilling depth (mbsf):	780 (sediment/basalt interface at 777 mbsf)
Approved maximum penetration (mbsf):	858 (pending EPSP review)
Survey coverage:	Inline MGL1109MCS01 (Shotpoint 1399), MGL1109MCS14 (Shotpoint 1790) (navigation and bathymetric maps Figs. **AF18, AF19;** seismic profiles Figs. **AF21, AF24**)
Objective:	• Tectonic and climate history from 10 Ma to recent • Provenance of unroofed sediments
Drilling and coring program:	• Hole A: APC to ~200 mbsf with non-magnetic core barrels and core orientation • Hole B: APC to ~200 mbsf with non-magnetic core barrels • Hole C: APC/XCB to 780 mbsf with non-magnetic core barrels • Hole D: APC/XCB to 425 mbsf with non-magnetic core barrels • See **"Drilling and coring strategy"** and Table **T2**
Downhole measurements program:	• Hole A: APCT-3 (SET if needed) formation temperature measurements • Hole C: wireline logging with triple combo, FMS-sonic, VSI, and Magnetic Properties tool strings • See **"Downhole measurements strategy"** and Table **T2**
Anticipated lithology:	Mud (possibly diatom rich), silt, fine sand, volcanic ash, ice-rafted debris, basalt

Site summaries (continued)

Proposed Site GOAL-18A

Priority:	Alternate
Position:	56°57.3852′N, 147°8.2545′W
Water depth (mbrf):	4229
Target drilling depth (mbsf):	780 (sediment/basalt interface at 777 mbsf)
Approved maximum penetration (mbsf):	856
Survey coverage:	Inline MGL1109MCS01 (Shotpoint 1423), Xline L-6-81 line 678-04/05 (JD157 06:37) (navigation and bathymetric maps Figs. **AF18, AF19;** seismic profiles Figs. **AF21, AF22**)
Objective:	• Tectonic and climate history from 10 Ma to recent • Provenance of unroofed sediments
Drilling and coring program:	• Hole A: APC to ~200 mbsf with non-magnetic core barrels and core orientation • Hole B: APC to ~200 mbsf with non-magnetic core barrels • Hole C: APC/XCB to 780 mbsf with non-magnetic core barrels • Hole D: APC/XCB to 500 mbsf with non-magnetic core barrels • See **"Drilling and coring strategy"** and Table **T2**
Downhole measurements program:	• Hole A: APCT-3 (SET if needed) formation temperature measurements • Hole C: wireline logging with triple combo, FMS-sonic, VSI, and Magnetic Properties tool strings • See **"Downhole measurements strategy"** and Table **T2**
Anticipated lithology:	Mud (possibly diatom rich), silt, fine sand, volcanic ash, ice-rafted debris, basalt

Site summaries (continued)

Proposed Site GOA18-1A

Priority:	Alternate
Position:	56°56.3571′N, 147°22.3703′W
Water depth (mbrf):	4273
Target drilling depth (mbsf):	758 (sediment/basalt interface at 755 mbsf)
Approved maximum penetration (mbsf):	834 (pending EPSP review)
Survey coverage:	Inline MGL1109MCS01 (Shotpoint 1720), Xline F-6-89 line 13 (CDP 5380) (navigation and bathymetric maps Figs. **AF18, AF20;** seismic profiles Figs. **AF21, AF23**)
Objective:	• Tectonic and climate history from 10 Ma to recent • Provenance of unroofed sediments
Drilling and coring program:	• Hole A: APC to ~200 mbsf with non-magnetic core barrels and core orientation • Hole B: APC to ~200 mbsf with non-magnetic core barrels • Hole C: APC/XCB to 758 mbsf with non-magnetic core barrels • Hole D: APC/XCB to 500 mbsf with non-magnetic core barrels • See **"Drilling and coring strategy"** and Table **T3**
Downhole measurements program:	• Hole A: APCT-3 (SET if needed) formation temperature measurements • Hole C: wireline logging with triple combo, FMS-sonic, VSI, and Magnetic Properties tool strings • See **"Downhole measurements strategy"** and Table **T3**
Anticipated lithology:	Mud (possibly diatom rich), silt, fine sand, volcanic ash, ice-rafted debris, basalt

Site summaries (continued)

Proposed Site KB-2A

Priority:	Primary
Position:	59°31.93′N, 144°8.03′W
Water depth (mbrf):	721
Target drilling depth (mbsf):	400
Approved maximum penetration (mbsf):	417
Survey coverage:	Inline GOA3101 (CDP 398) (navigation and bathymetric maps Figs. **AF25, AF28;** seismic profiles Figs. **AF26, AF27**)
Objective:	• Constrain the timing of multiple glacial events of the northern Cordilleran Ice Sheet, to test its relation to global ice sheet dynamics • Test role of North Pacific surface temperatures control of late Pleistocene glaciation at sub-century scale • Document dynamics of productivity and intermediate water circulation in the Northeast Pacific • Document paleomagnetic intensity and secular variation in NE Pacific to test hypothesis that lowermost mantle heterogeneities influence Earth's magnetic field
Drilling and coring program:	• Hole A: APC to ~200 mbsf with non-magnetic core barrels and core orientation • Hole B: APC to ~200 mbsf with non-magnetic core barrels • Hole C: APC to ~200 mbsf with non-magnetic core barrels • Hole D: APC/XCB to 400 mbsf • See **"Drilling and coring strategy"** and Table **T2**
Downhole measurements program:	• Hole D: wireline logging with triple combo, FMS-sonic, VSI, and Magnetic Properties tool strings • See **"Downhole measurements strategy"** and Table **T2**
Anticipated lithology:	Hemipelagic mud, glacimarine sediment with diamict

Figure AF1. Overview bathymetry and seismic reflection profiles with proposed primary Sites GOAL-15C and GOAL-17B and alternate Site GOA15-1A, on the outer continental shelf and upper continental slope on the Gulf of Alaska near the Bering Trough. Line annotations are CDPs. Squares = navigation map area for close-up seismic profiles in Figures **AF2, AF6,** and **AF9.** See inset for approximate location.

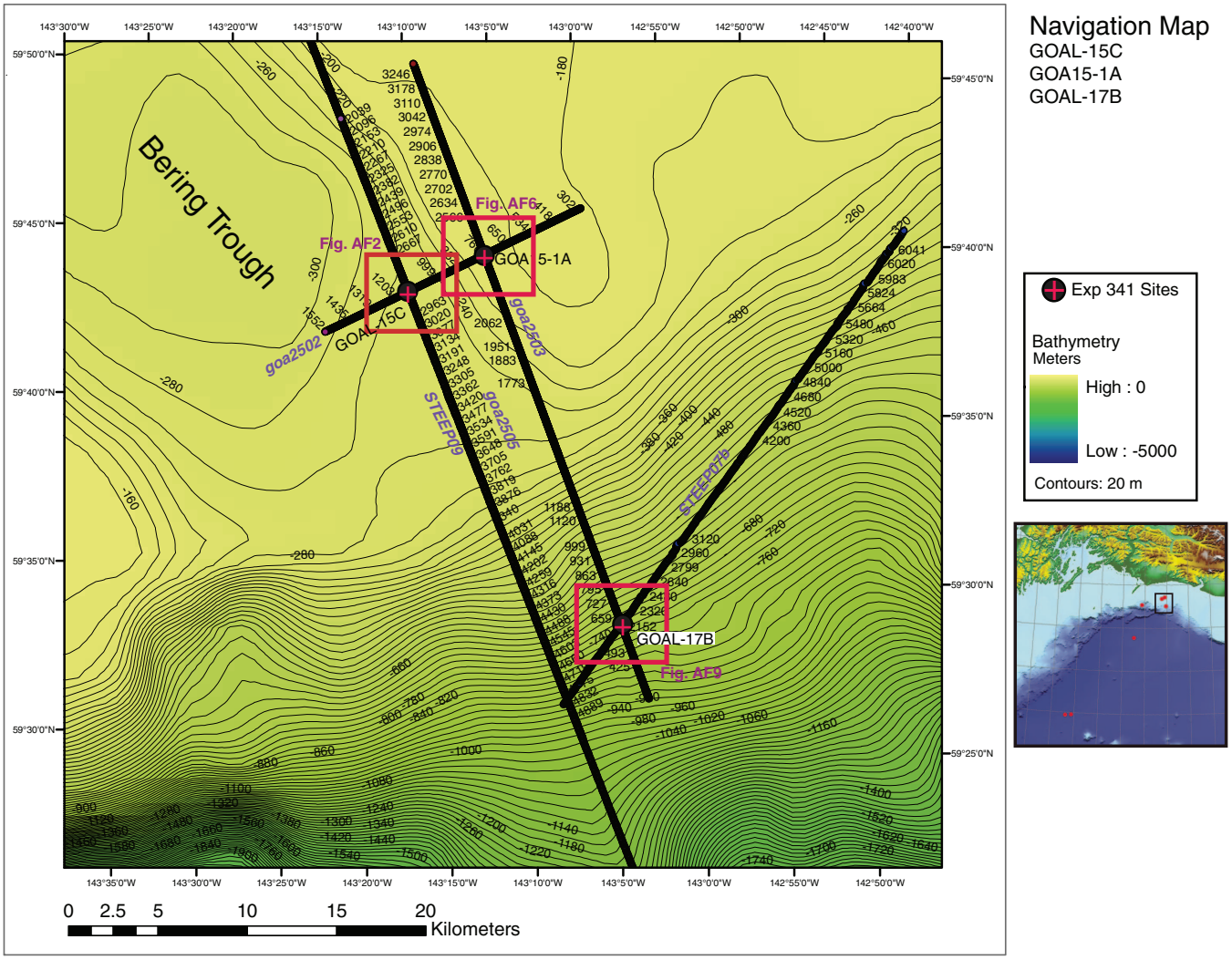

Figure AF2. Close-up navigation map of proposed primary Site GOAL-15C, showing seismic reflection profiles MGL08-014 STEEP09 (Fig. **AF3**), EW0408 GOA2505 (Fig. **AF4**), and EW0408 GOA2502 (Fig. **AF5**). GOAL-15C is located at crossing point of GOA2502 (CDP 1137) with GOA2505 (CDP 2845) and STEEP09 (CDP 14018).

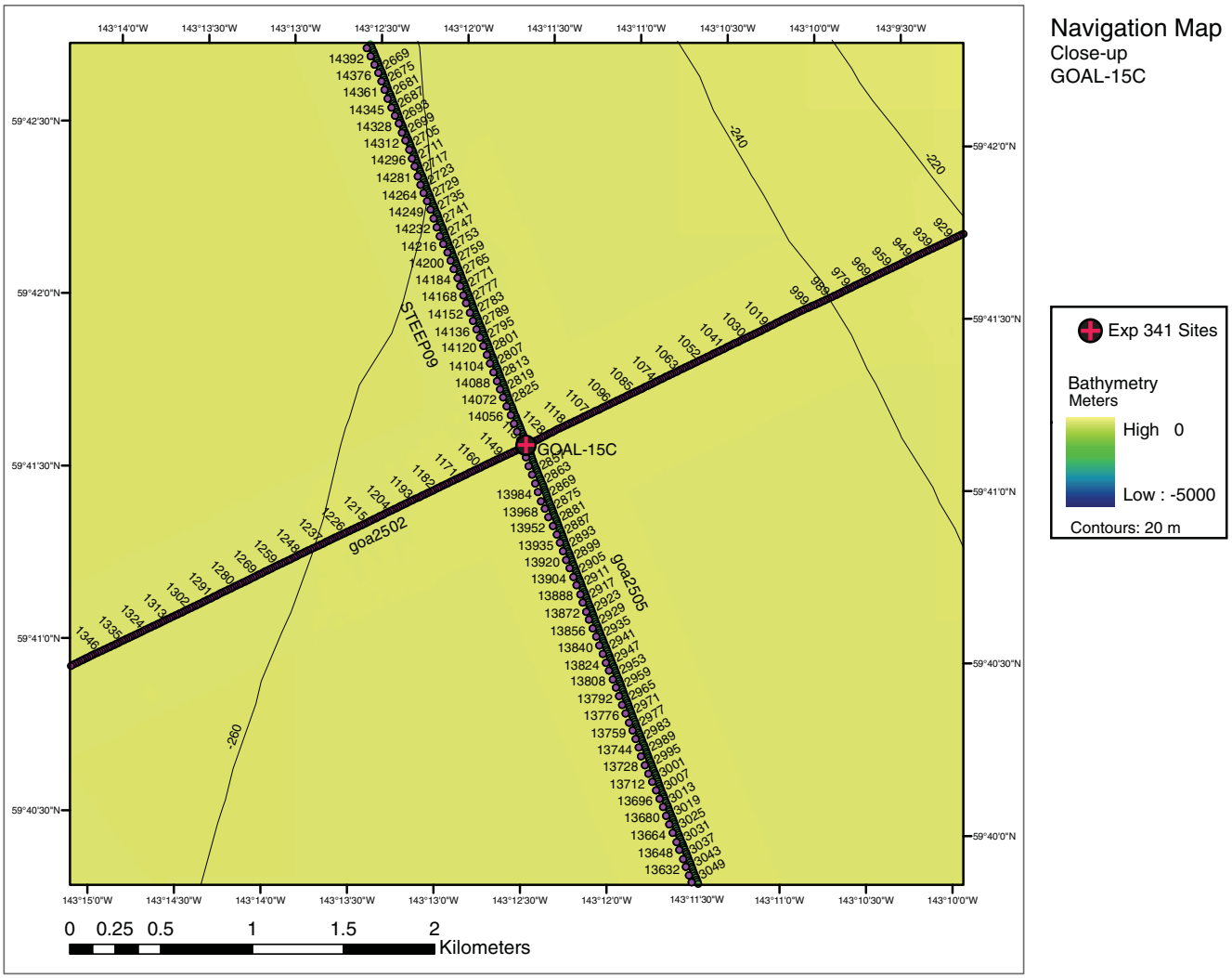

Figure AF3. Seismic profile of *Marcus G. Langseth* Cruise MGL08-014 MCS Line STEEP09 (NW–SE) with location of primary Site GOAL-15C (143°12.0552′W, 59°41.3394′N; CDP 14018; water depth = 250 m; target depth = 1112 mbsf).

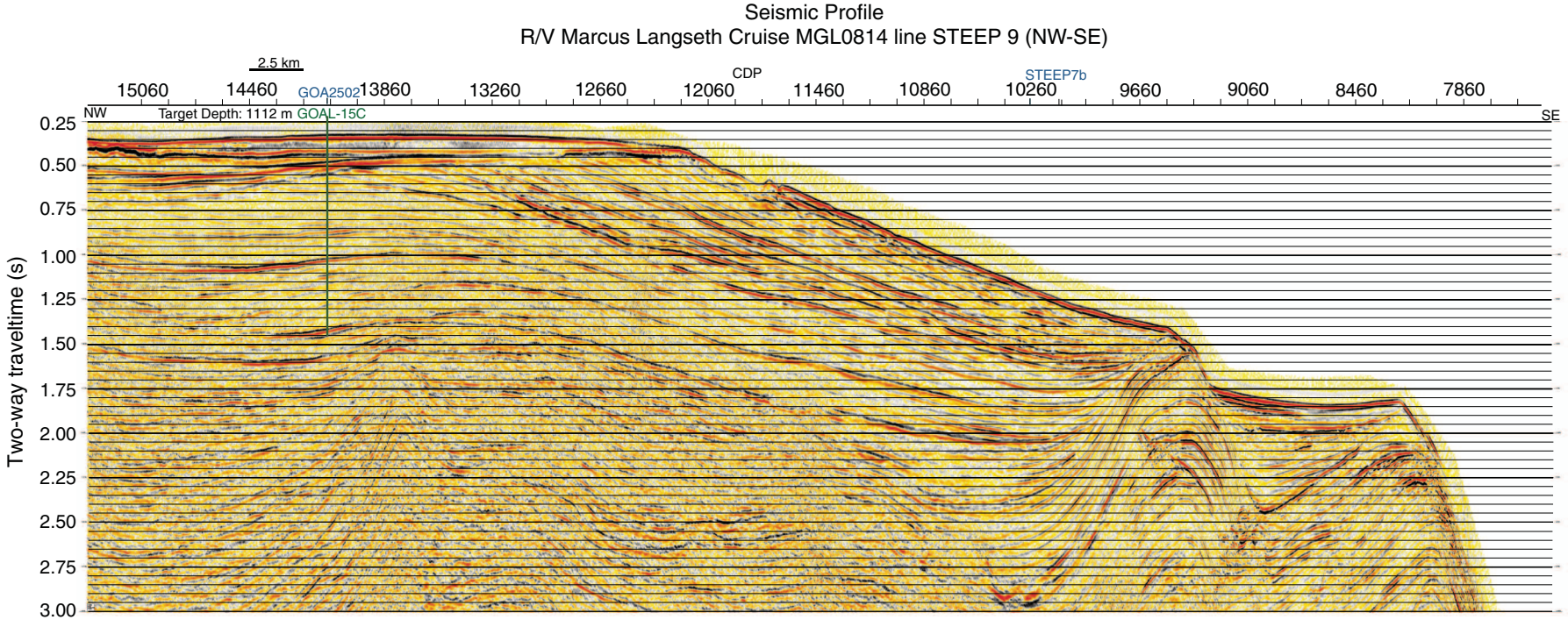

Figure AF4. Seismic profile of *Maurice Ewing* Cruise EW0408 MCS Line GOA2505 (NW–SE) with location of primary Site GOAL-15C (143°12.0552′W, 59°41.3394′N; CDP 2845; water depth = 250 m; target depth = 1112 mbsf).

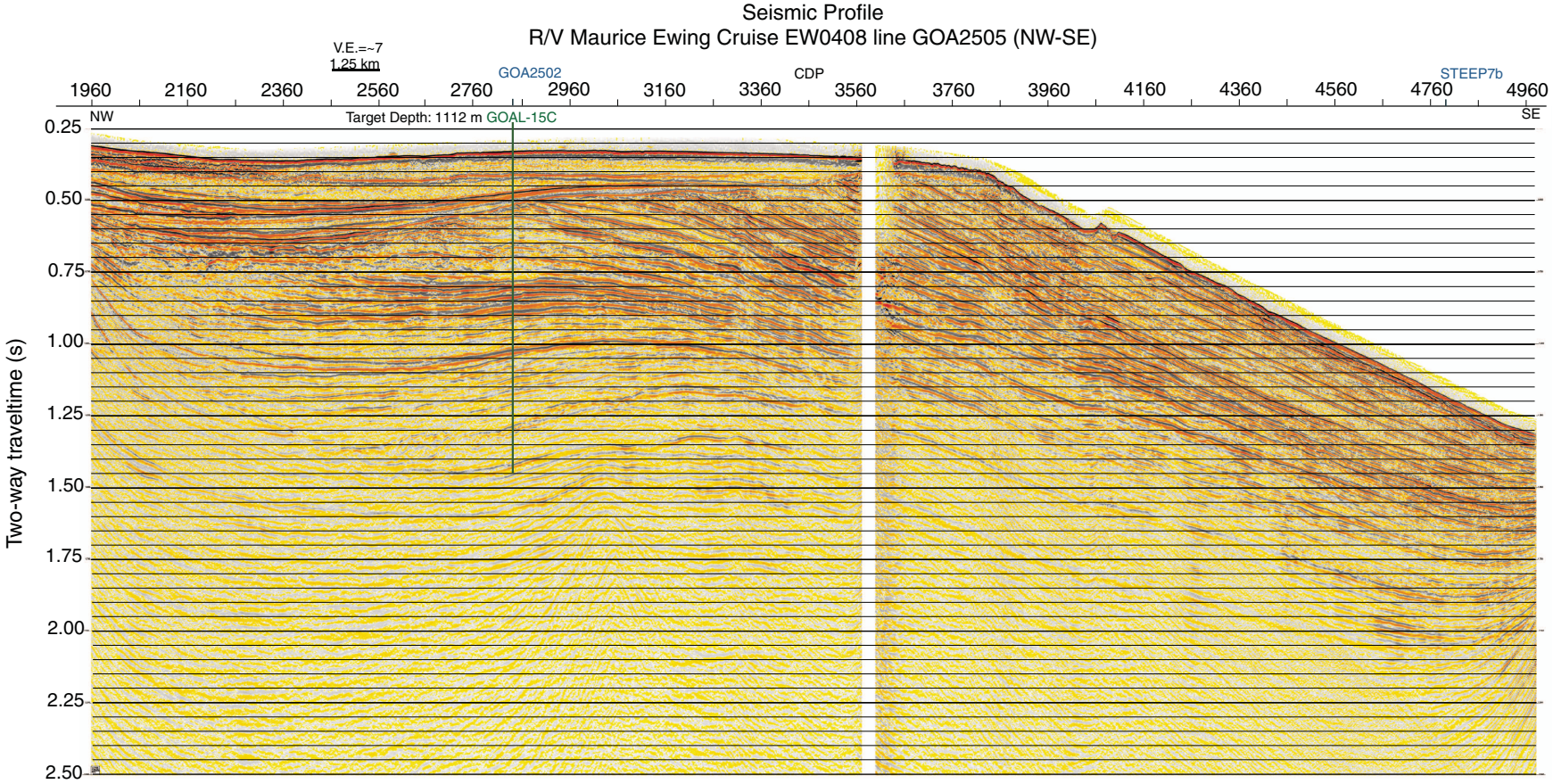

Figure AF5. Seismic profile of *Maurice Ewing* Cruise EW0408 MCS Line GOA2502 (SW–NE) with location of primary Site GOAL-15C (143°12.0552′W, 59°41.3394′N; CDP 1137; water depth = 250 m; target depth = 1112 mbsf) and alternate Site GOA15-1A (143°7.2012′W, 59°42.0600′N; CDP 758; water depth = 178 m; target depth = 1158 mbsf).

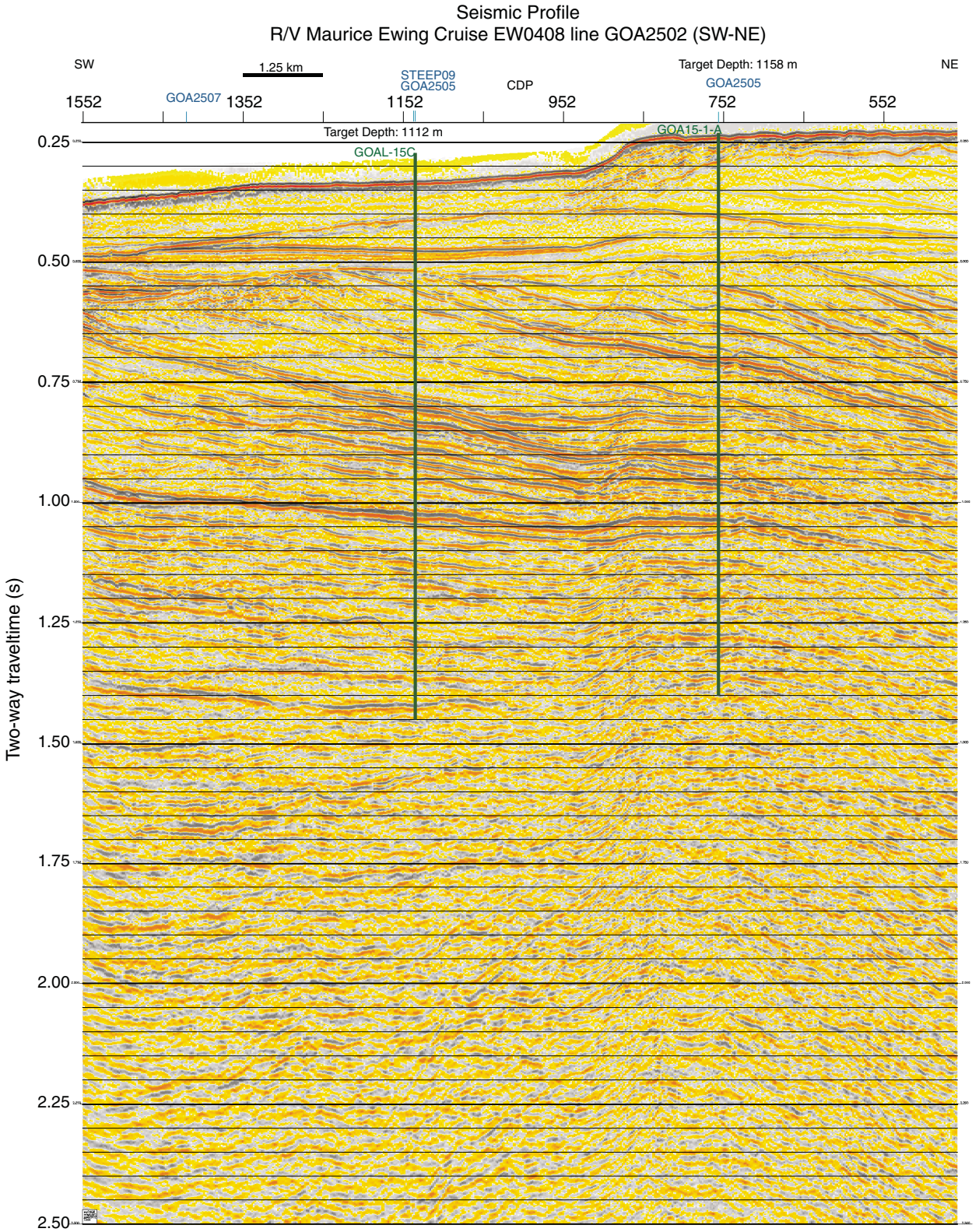

Figure AF6. Close-up navigation map of proposed alternate Site GOA15-1A, showing seismic reflection Profiles EW0408 GOA2502 (Fig. AF5) and EW0408 GOA2503 (Fig. AF7). GOA15-1A is located at the crossing point of GOA2502 (CDP 758) with GOA2503 (CDP 2336).

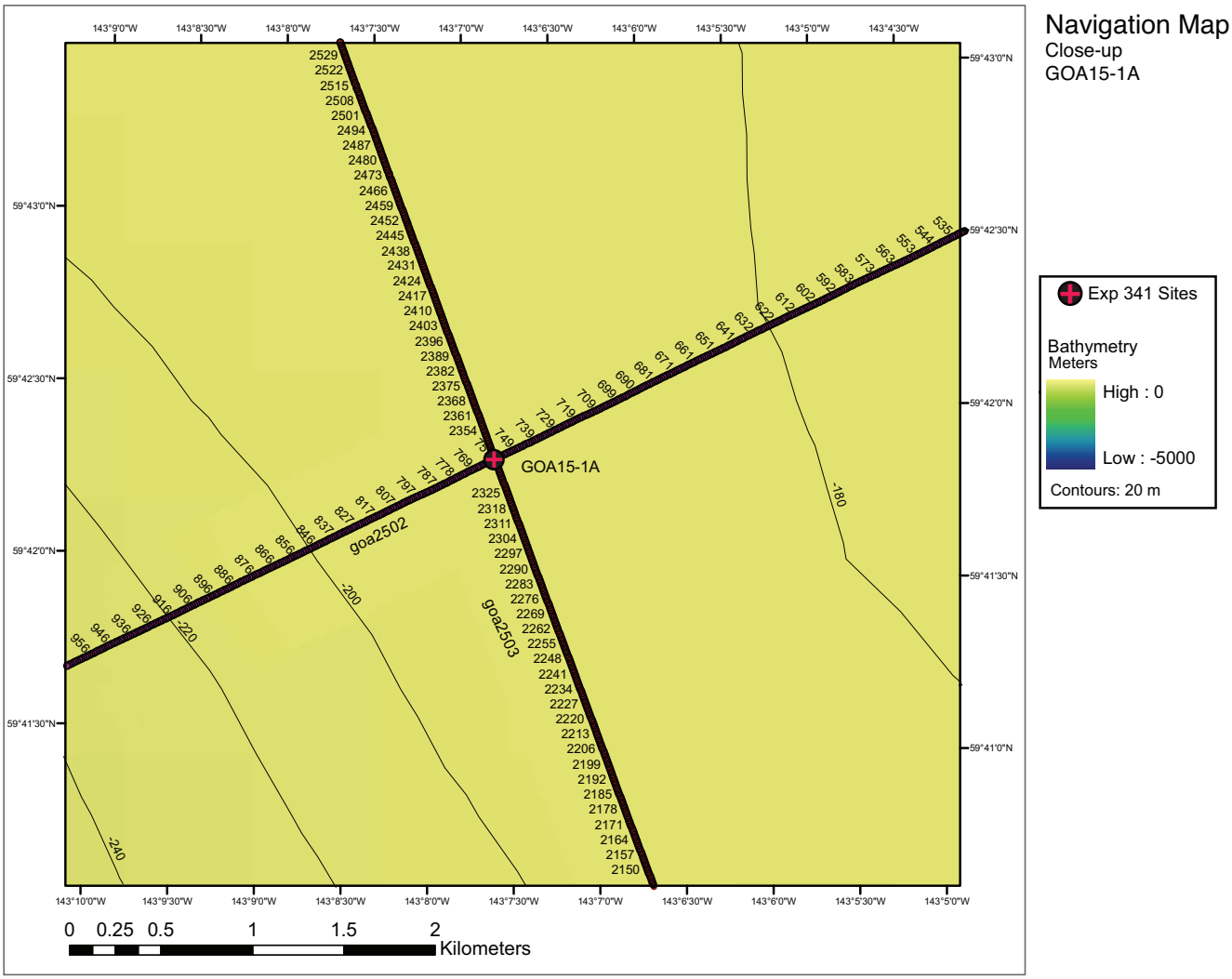

Figure AF7. Seismic profile of *Maurice Ewing* Cruise EW0408 MCS Line GOA2503 (NW–SE) with location of alternate Site GOA15-1A (143°7.2012′W, 59°42.0600′N; CDP 2336; water depth = 178 m; target depth = 1158 mbsf) and primary Site GOAL-17B (143°2.7378′W, 59°30.4398′N; CDP 576; water depth = 727 m; target depth = 1032 mbsf).

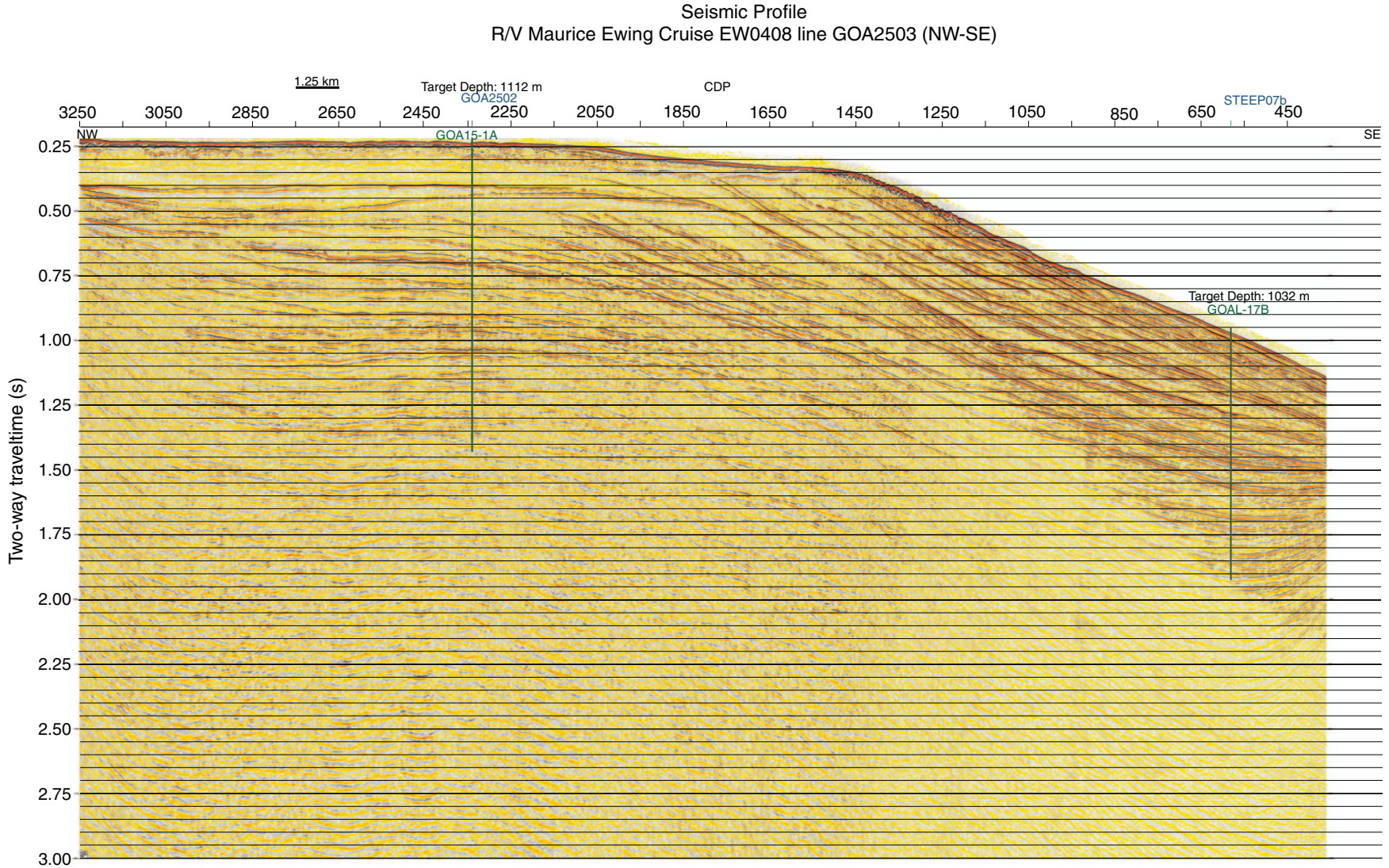

Figure AF8. Swath bathymetric map with track chart of *Maurice Ewing* Cruise EW0408 around Sites GOAL-15C and GOA15-1A.

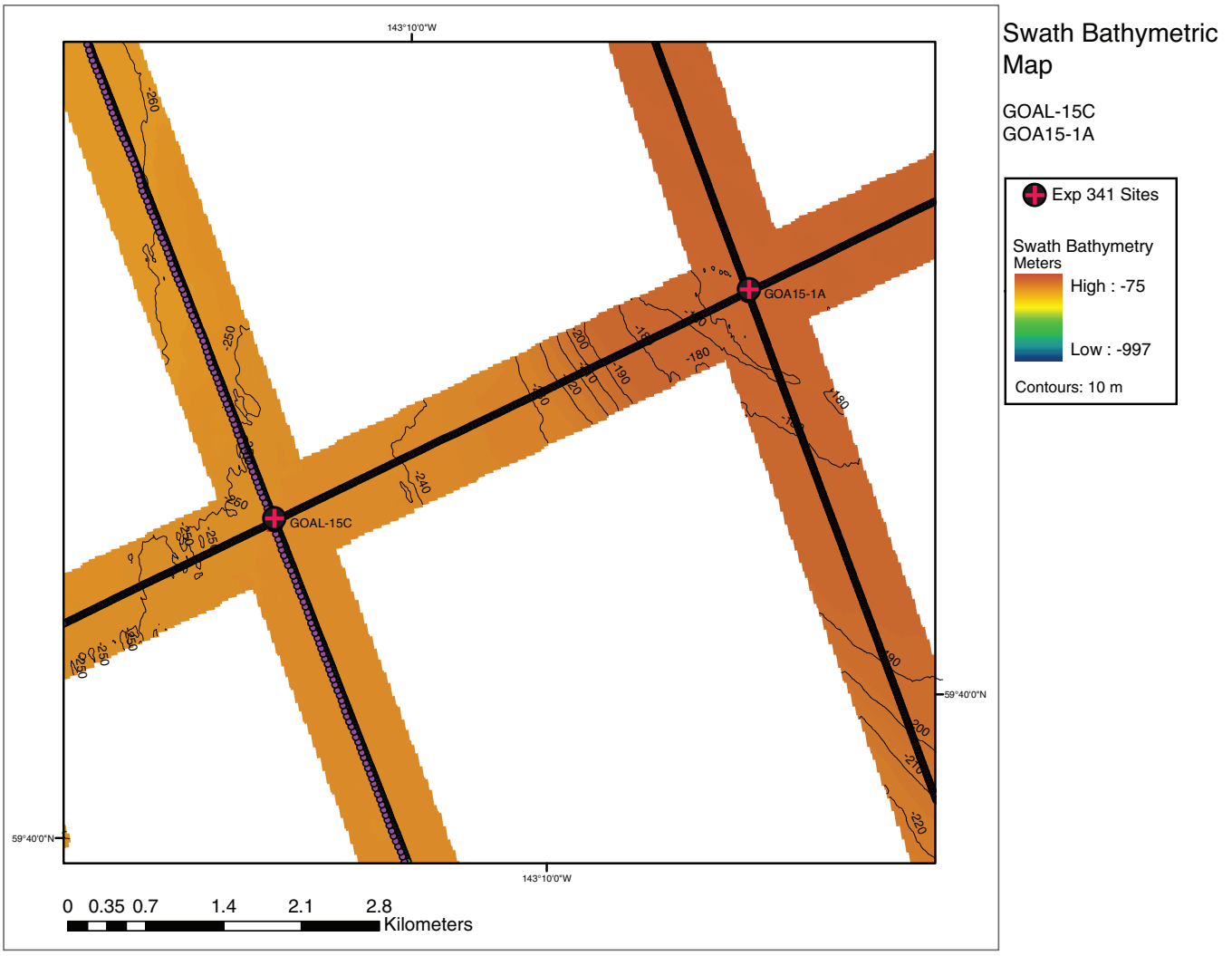

Figure AF9. Close-up navigation map of proposed primary Site GOAL-17B, showing seismic reflection Profiles EW0408 GOA2503 (Fig. AF7) and MGL08-014 MCS Line STEEP07b (Fig. AF10). GOAL-17B is located at the crossing point of GOA2503 (CDP 576) with STEEP07b (CDP 2165).

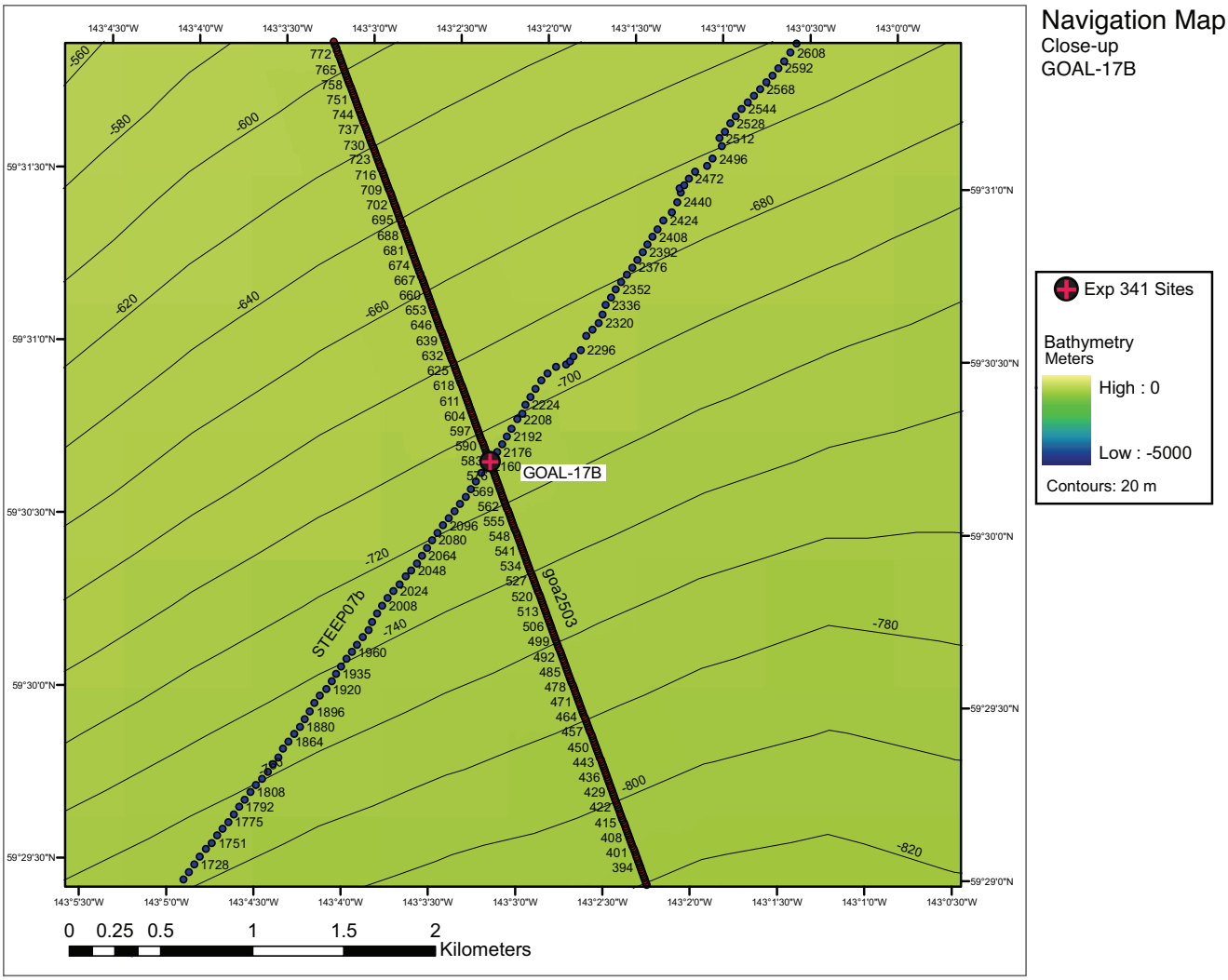

Figure AF10. Seismic profile of *Marcus G. Langseth* Cruise MGL08-014 MCS Line STEEP07b (SW–NE) with location of primary Site GOAL-17B (143°2.7378′W, 59°30.4398′N; CDP 576; water depth = 727 m; target depth = 1032 mbsf).

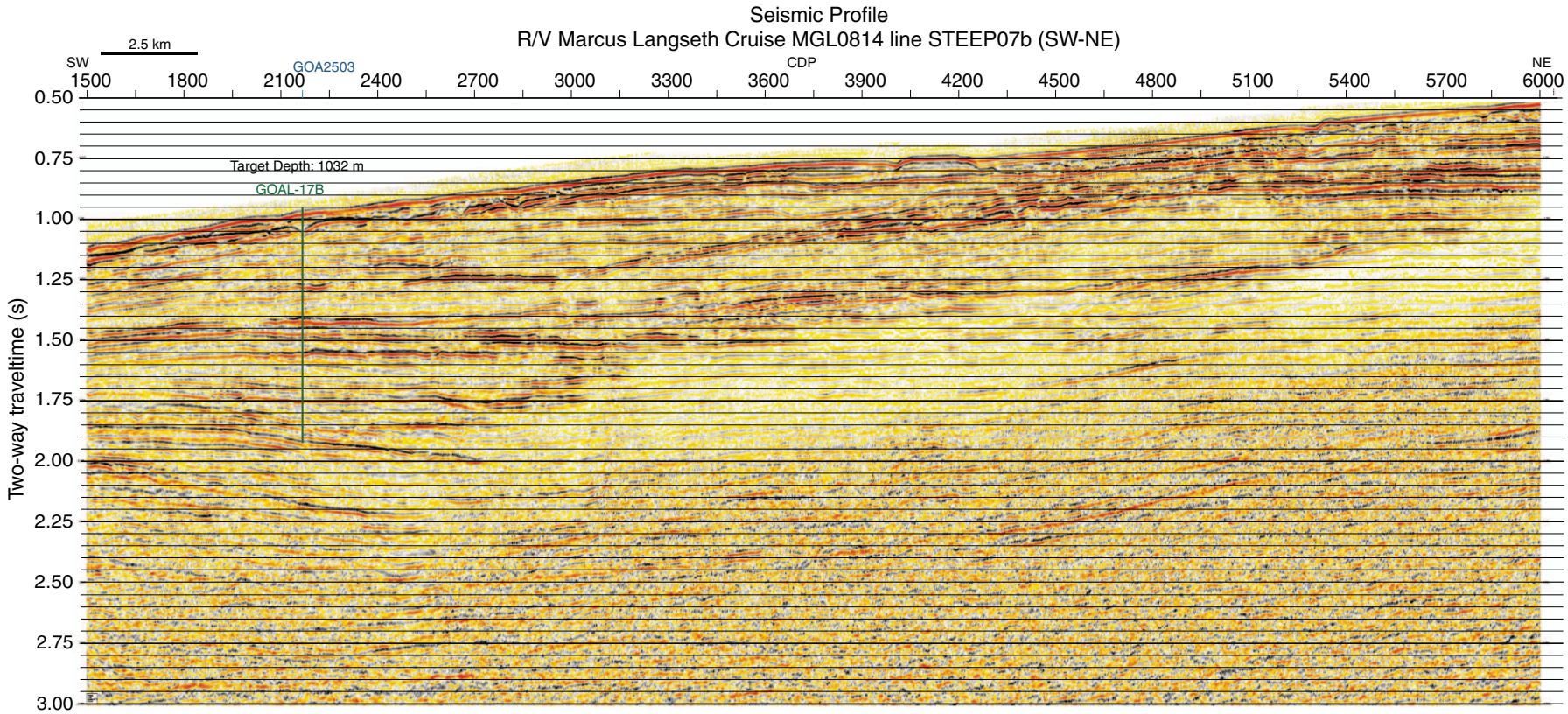

Figure AF11. Swath bathymetric map with track chart of *Maurice Ewing* Cruise EW0408 around Site GOAL-17B.

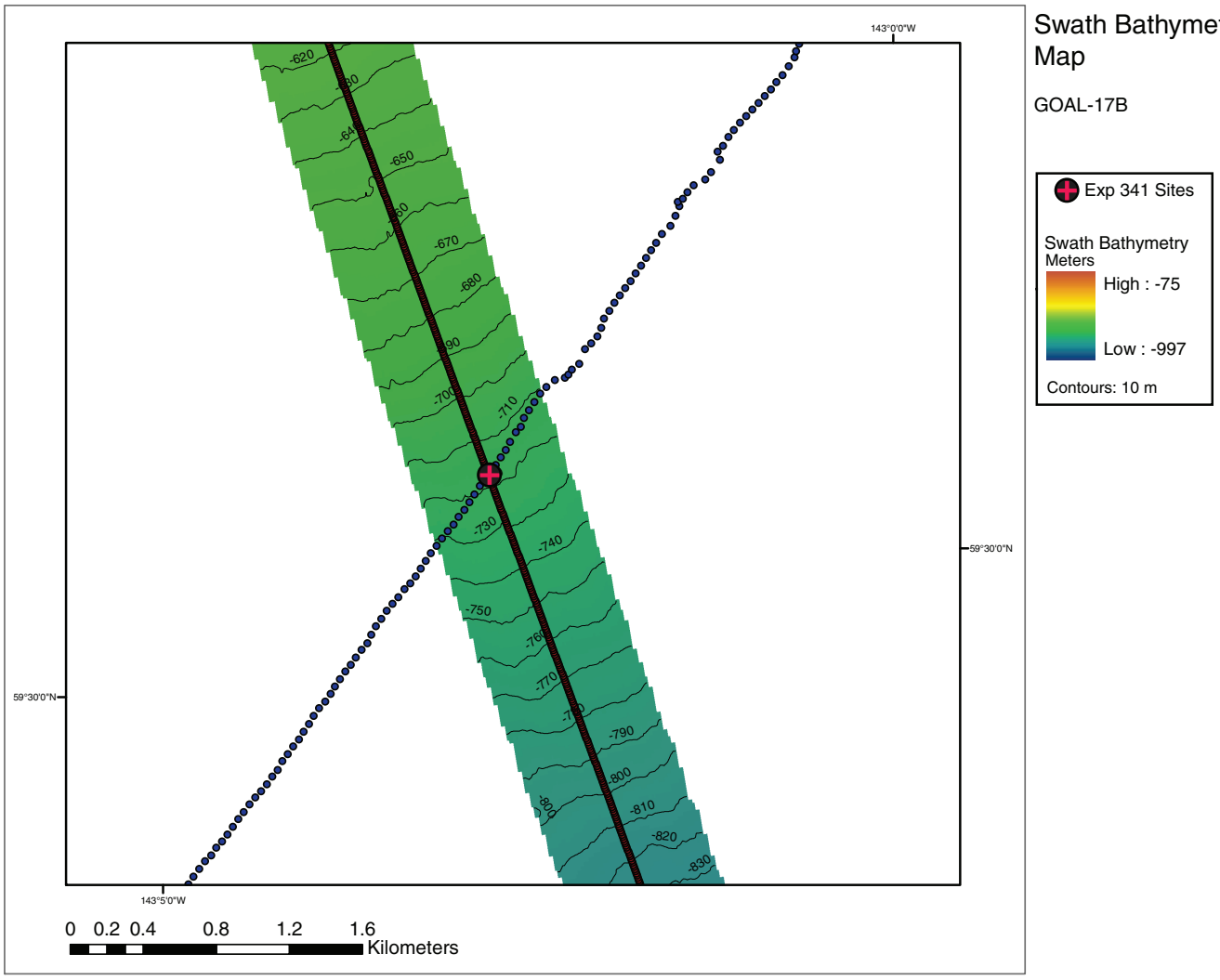

Figure AF12. Close-up navigation map of proposed primary Site GOA16-1A and alternate Sites GOAL-16B and GOA16-2A. Shown are seismic reflection Profiles EW0408 GOA3201 (Fig. **AF14**), GOA3202 (Fig. **AF15**), MGL08-014 MCS Line STEEP07 (Fig. **AF16**), and MGL08-014 MCS Line STEEP013 (Fig. **AF17**). GOA16-1A is located at the crossing point of GOA3202 (CDP 510) and STEEP07 (CDP 3592). GOAL-16B is located at the crossing point of GOA3201 (CDP 571) and GOA3202 (CDP 445). GOA16-2A is located at the crossing point of Line GOA3201 (CDP 535) and lines STEEP07 (CDP 3478) and STEEP13 (CDP 21728). See inset for approximate location.

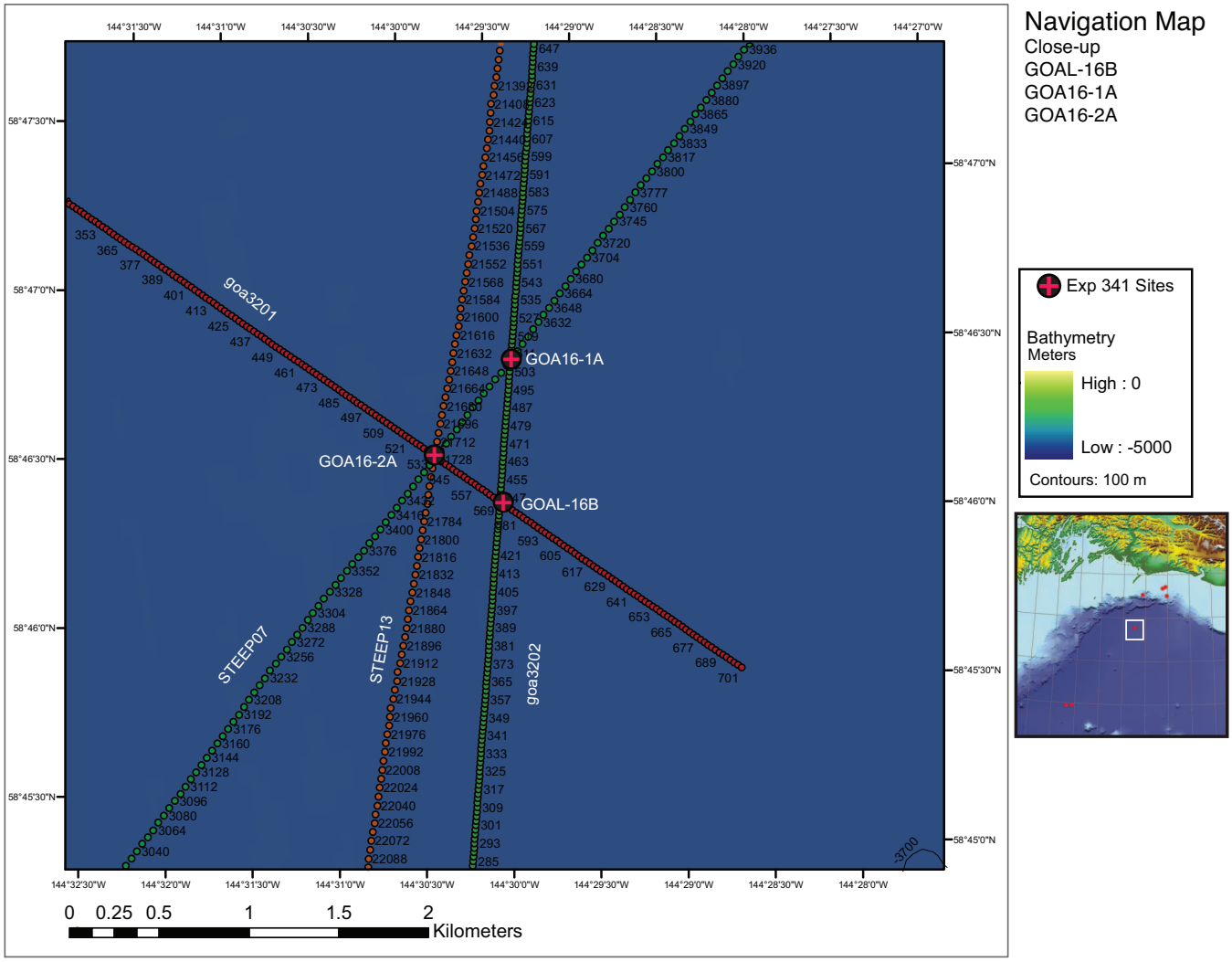

Figure AF13. Swath bathymetric map with track chart of *Maurice Ewing* Cruise EW0408 and *R/V Marcus G. Langseth* Cruise MGL08-014 around primary Site GOA16-1A and alternate Sites GOAL-16B and GOA16-2A on the proximal Surveyor Fan.

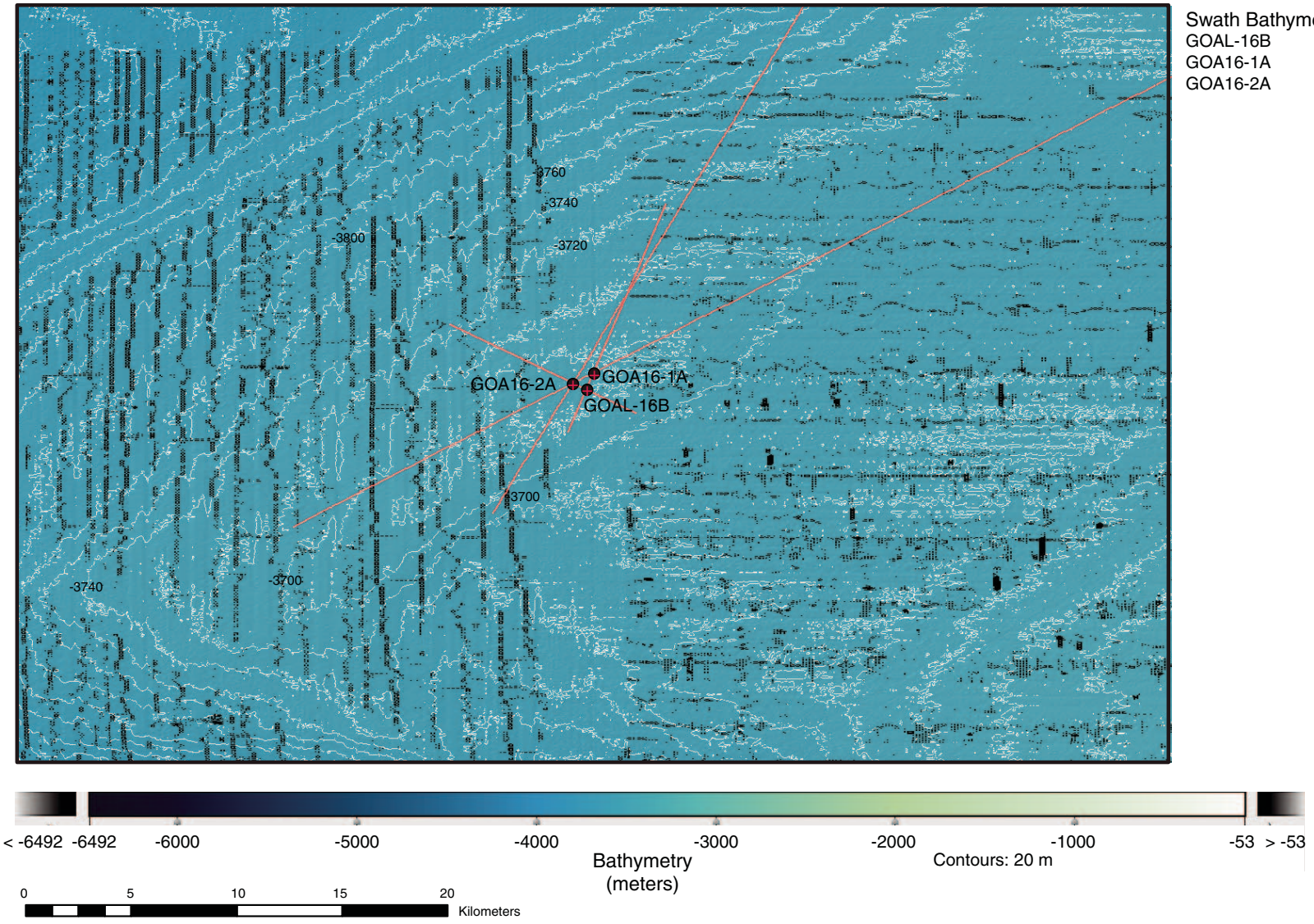

Figure AF14. Seismic profile of *Maurice Ewing* Cruise EW0408 MCS Line GOA3201 (NW–SE) with location of alternate Site GOAL-16B (144°29.7917′W, 58°46.1750′N; CDP 571; water depth = 3690 m; target depth = 986 mbsf) and alternate Site GOA16-2A (144°30.1200′W, 58°46.3476′N; CDP 535; water depth = 3690 m; target depth = 962 mbsf).

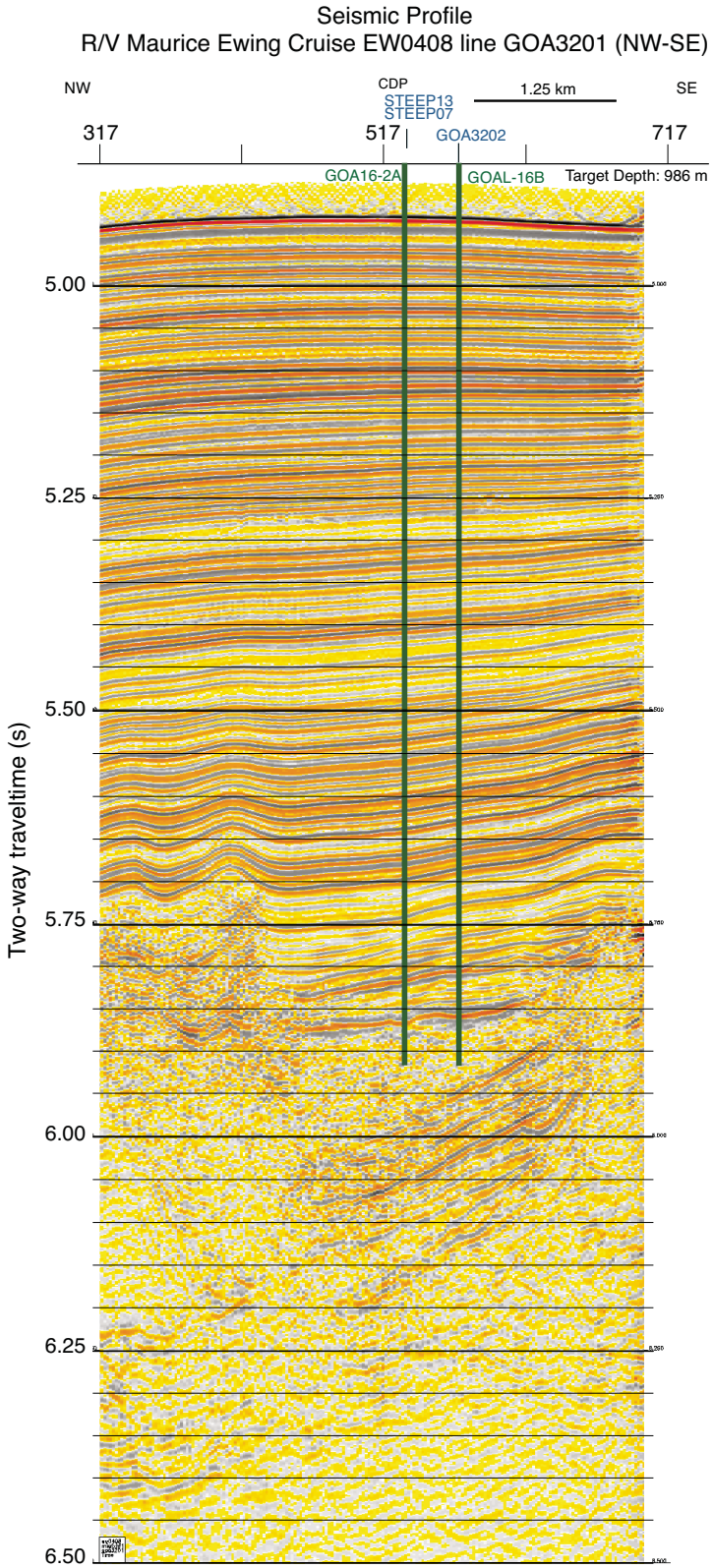

Figure AF15. Seismic profile of *Maurice Ewing* Cruise EW0408 MCS Line GOA3202 (SW–NE) with location of alternate Site GOAL-16B (144°29.7917′W, 58°46.1750′N; CDP 445; water depth = 3690 m; target depth = 986 mbsf) and primary Site GOA16-1A (144°29.5968′W, 58°46.6122′N; CDP 510; water depth = 3692 m; target depth = 978 mbsf).

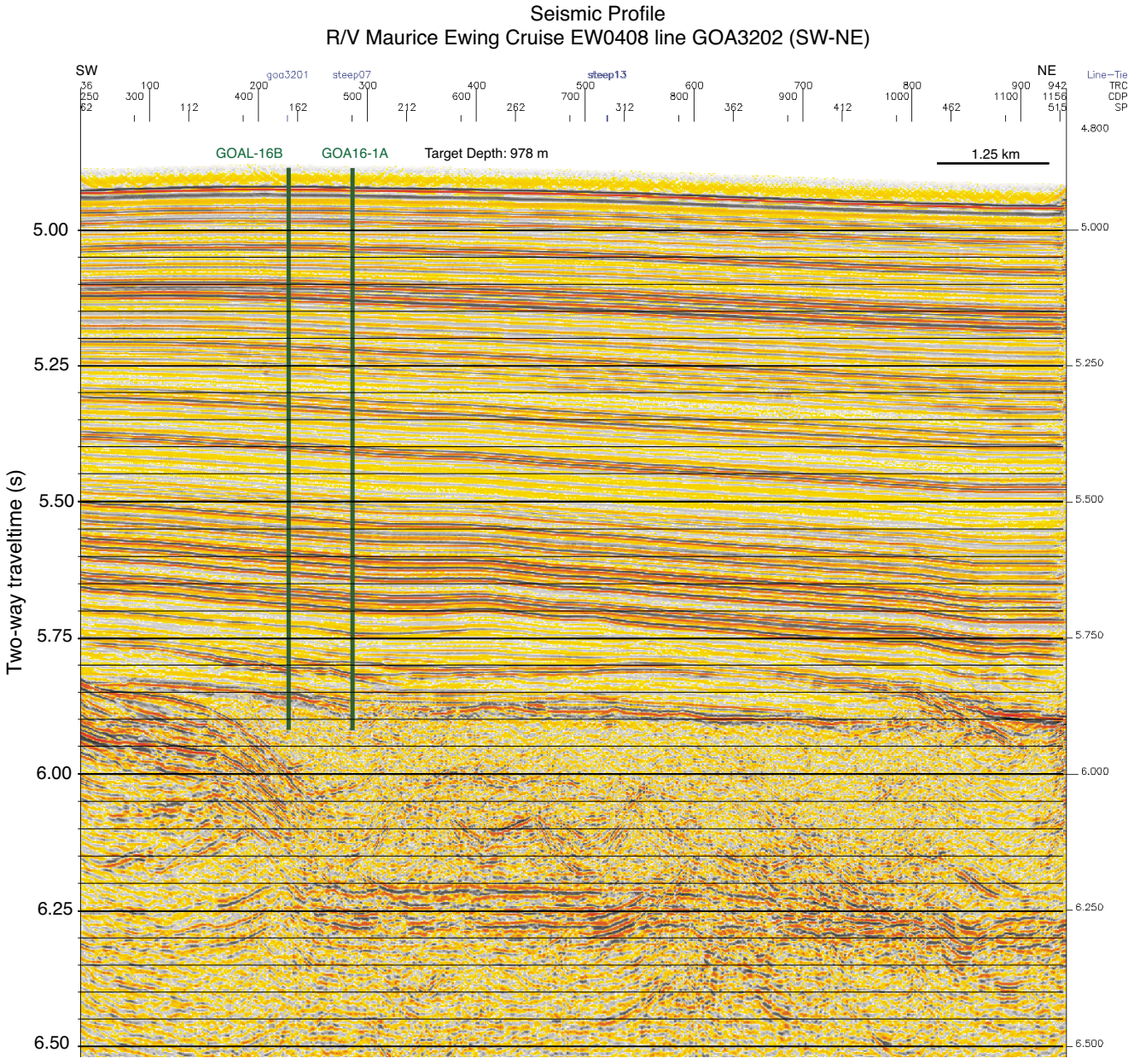

Figure AF16. Seismic profile of *Marcus G. Langseth* Cruise MGL08-014 MCS Line STEEP07 (SW–NE) with location of primary Site GOA16-1A (144°29.5968′W, 58°46.6122′N; CDP 3592; water depth = 3692 m; target depth = 978 mbsf) and alternate Site GOA16-2A (144°30.1200′W, 58°46.3476′N; CDP 3478; water depth = 3690 m; target depth = 962 mbsf).

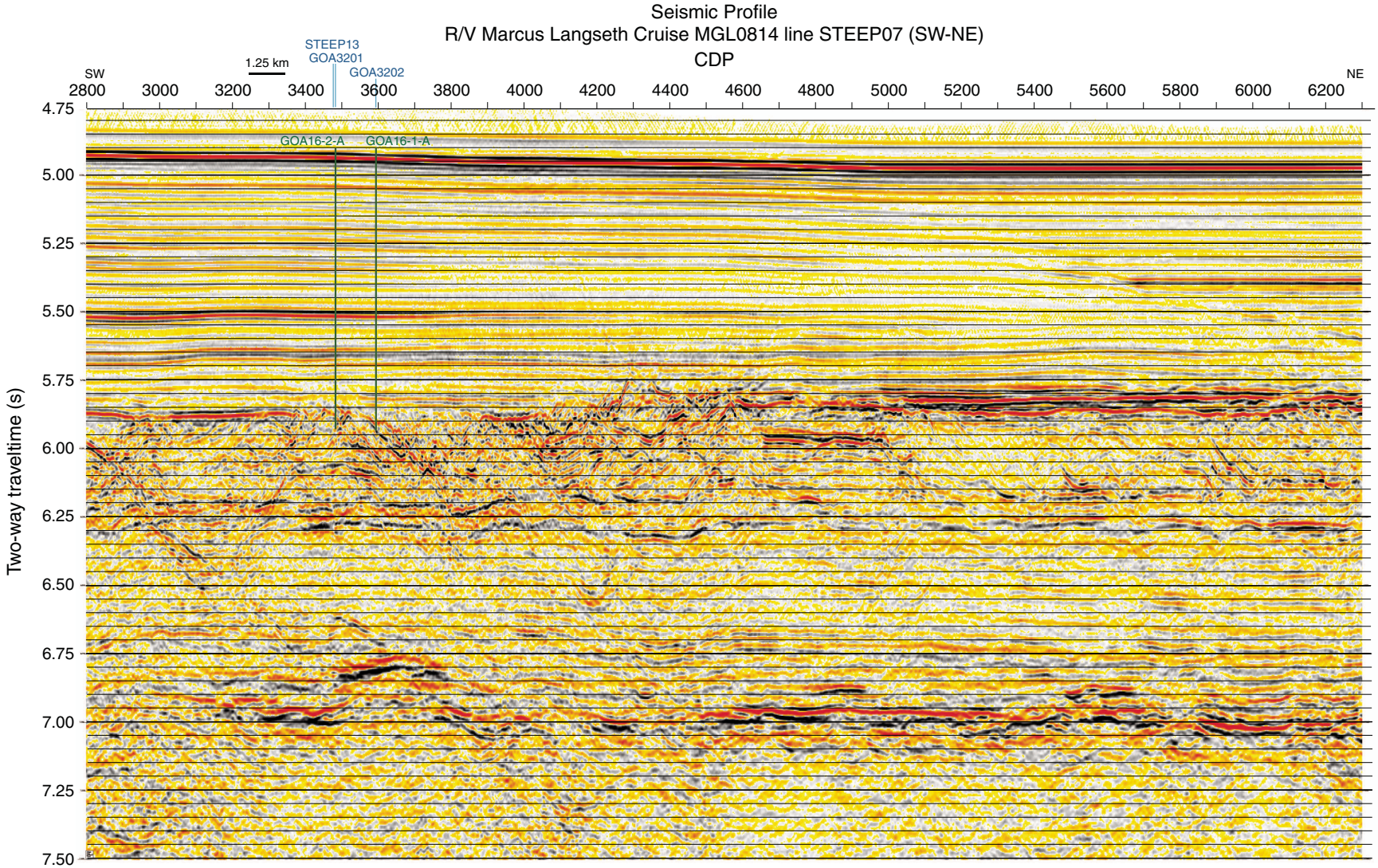

Figure AF17. Seismic profile of *Marcus G. Langseth* Cruise MGL08-014 MCS Line STEEP13 (SW–NE) with location of alternate Site GOA16-2A (144°30.1200′W, 58°46.3476′N; CDP 21728; water depth = 3690 m; target depth = 962 mbsf).

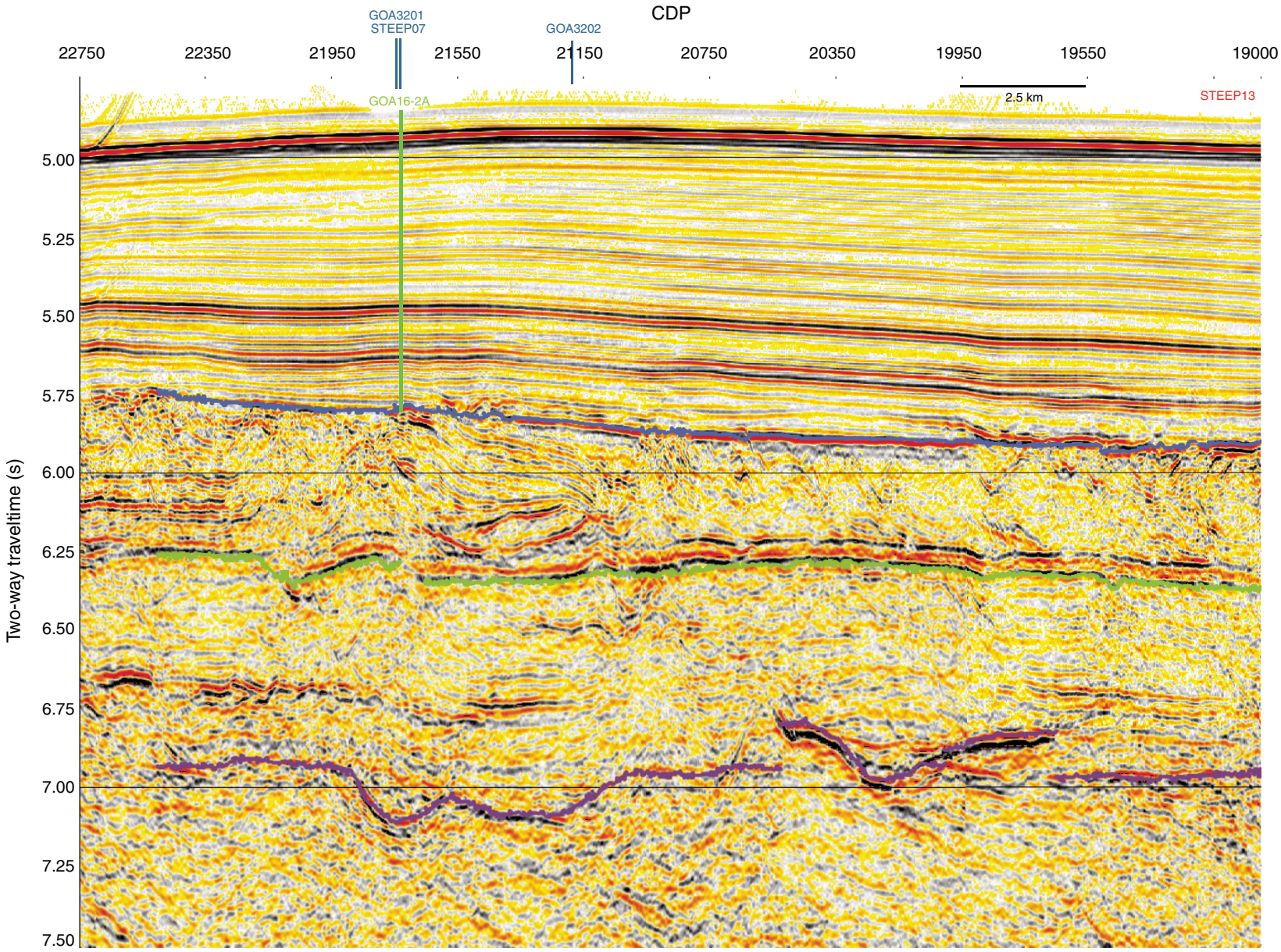

Figure AF18. Overview bathymetry and seismic reflection profiles with proposed primary Site GOA18-2A and alternate Sites GOA18-1A and GOAL-18A, on Surveyor Fan. Squares = navigation map area for close-up seismic profiles in Figures AF19 and AF20. See inset for approximate location.

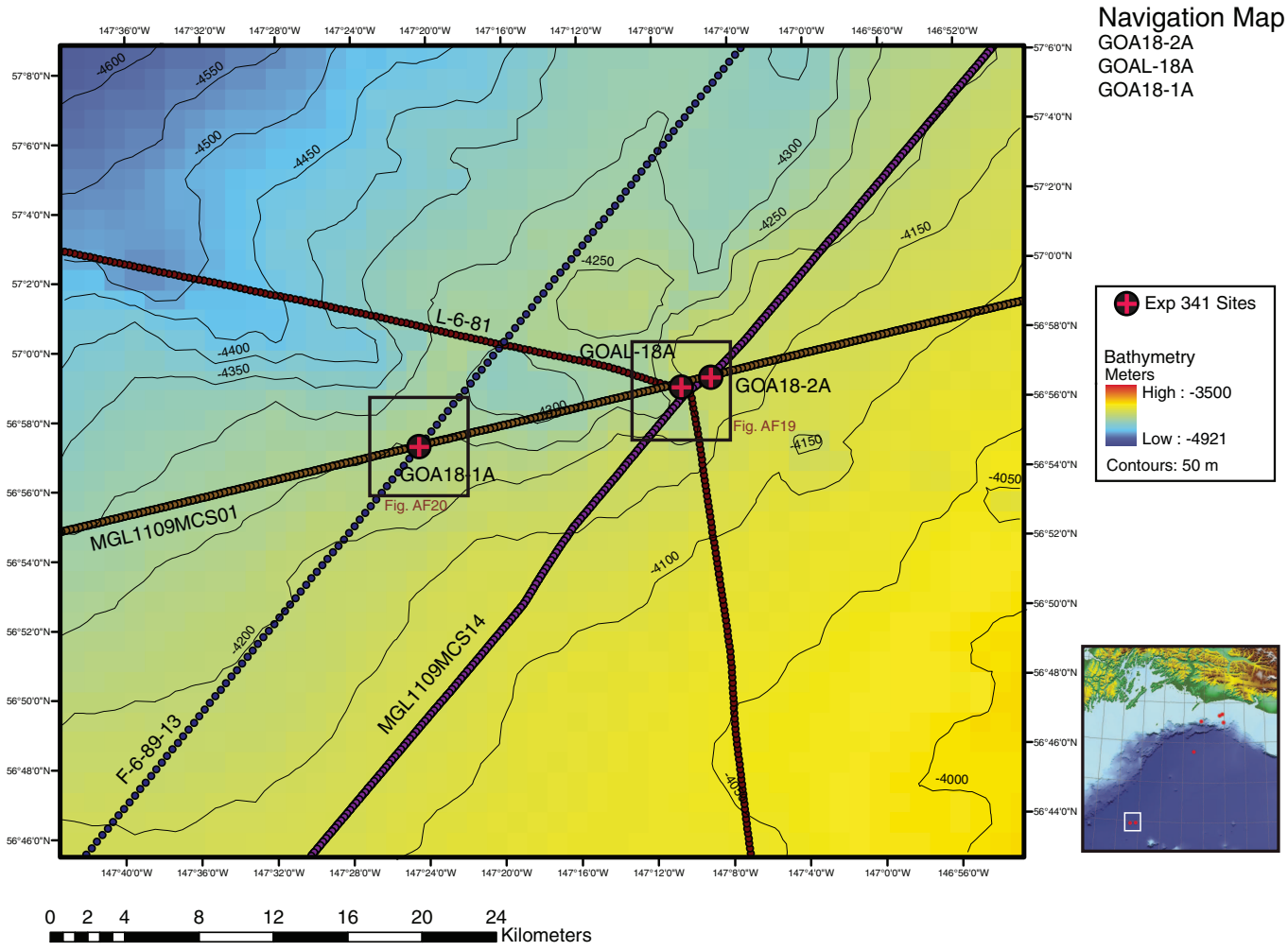

Figure AF19. Close-up navigation map of proposed primary Site GOA18-2A (56.96°N, 147.11°W; water depth = 4177 m; target depth = 780 mbsf) and alternate Site GOAL-18A, which is a redrill of DSDP Site 178, showing seismic reflection Profiles MGL1109MCS01 (Fig. AF21), L-6-81 Line 678-04/05 (Fig. AF22) and MGL1109MCS14 (Fig. AF24). GOAL-18A is located at the LORAN position of DSDP Site 178. Seismic Line L-6-81 attempted to cross Site 178, and with LORAN positioning precision of ~500 m may cross the drill site. GOAL-18A is closest to line MGL1109MCS01 (Shot point 1423).

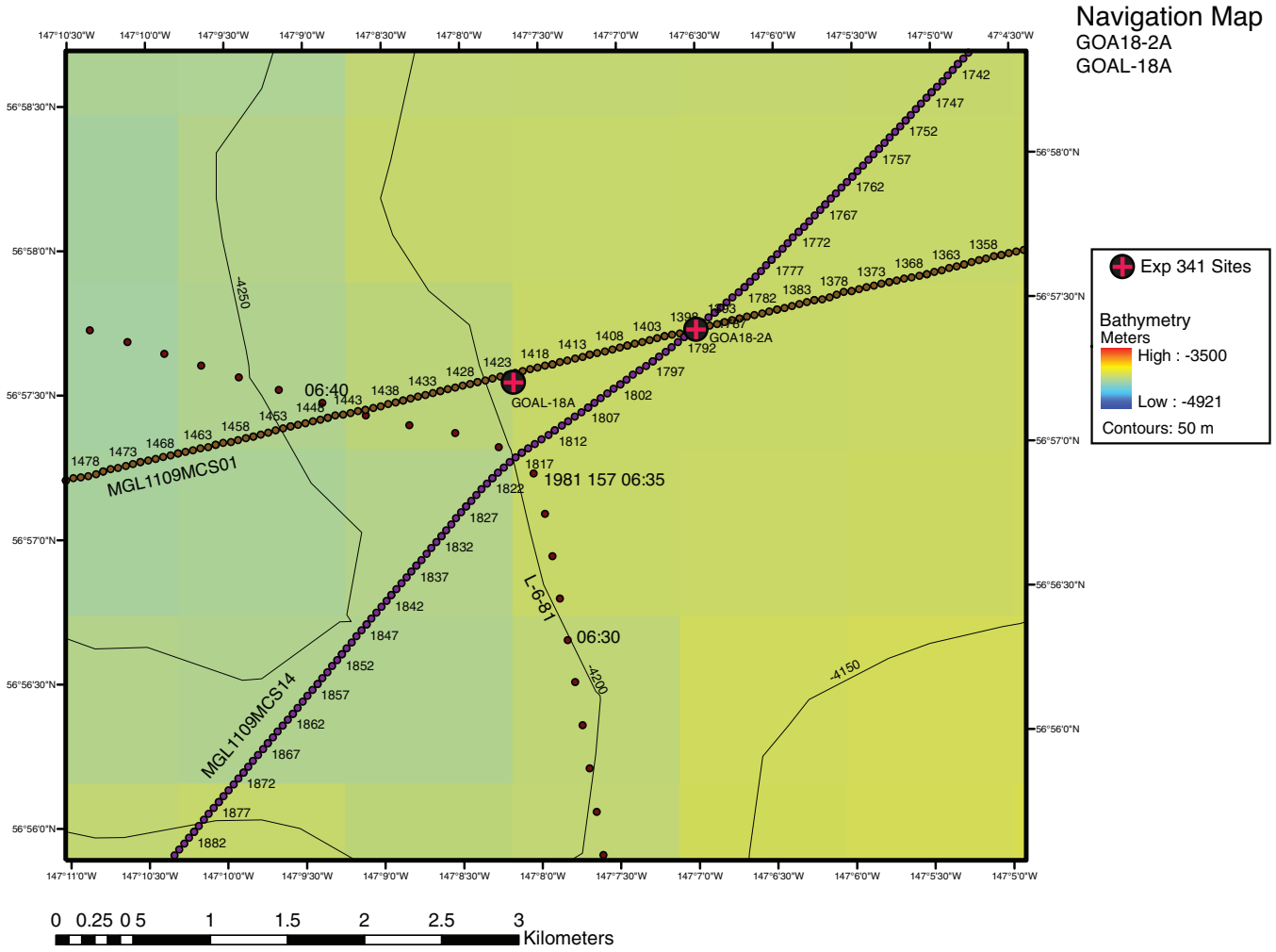

Figure AF20. Close-up navigation map of proposed alternate Site GOA18-1A, showing seismic reflection Profiles MGL1109MCS01 (Fig. AF21) and F-6-89 Line 13 (Fig. AF23). GOA18-1A is located at crossing point of MGL1109MCS01 (Shot 1723) and F-6-89 Line 13 (Shot/CDP 5380). This intersection is located at 56.94°N, 147.38°W in 4262 m water depth.

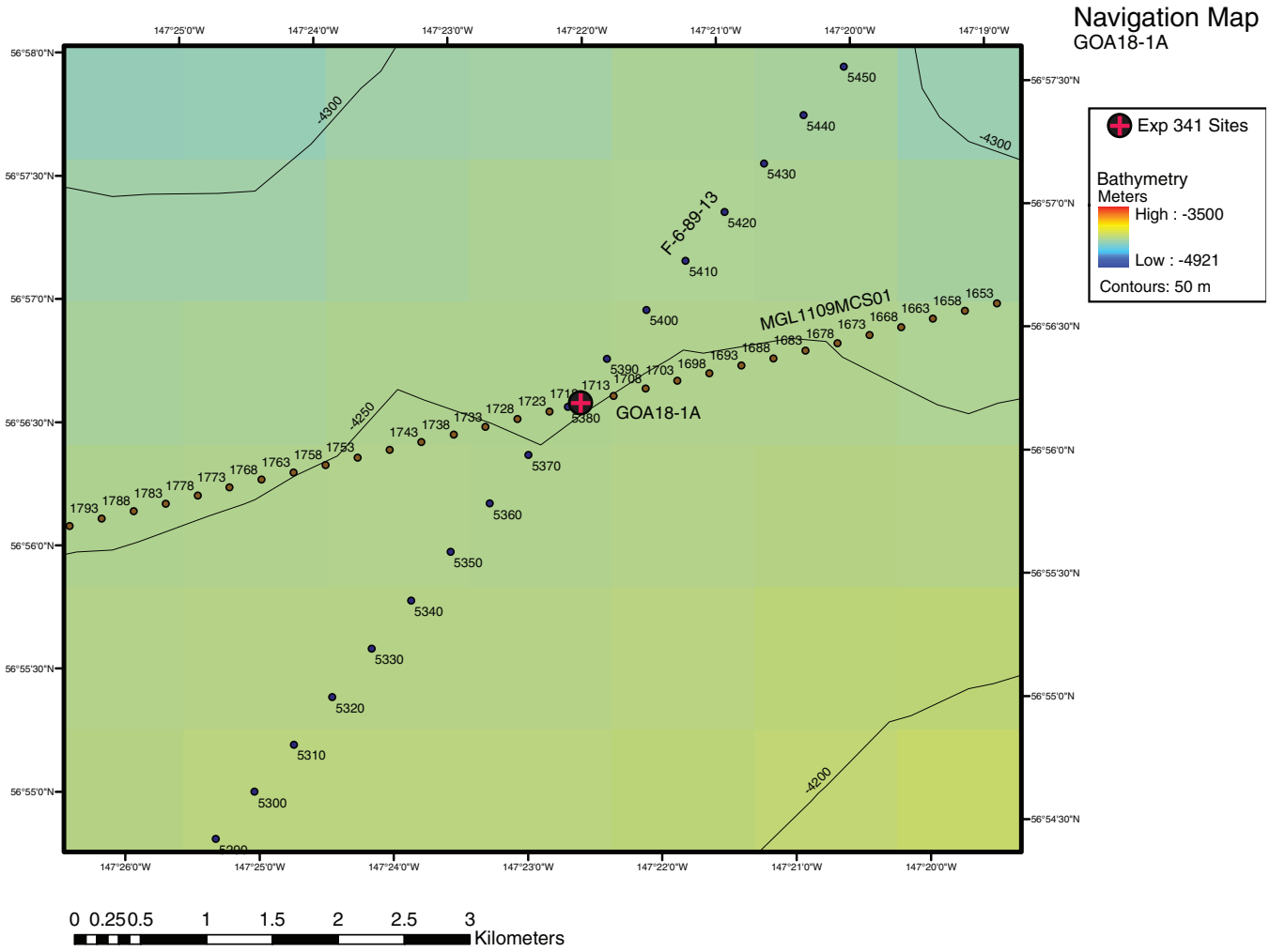

Figure AF21. Seismic profile of *Marcus G. Langseth* Cruise MGL11-09 MCS Line MCS01 (SW–NE) with location of primary Site GOA18-2A (56.96°N, 147.11°W; Shot 1399; water depth = 4177 m; target depth = 780 mbsf) and alternate Sites GOAL-18A (147°8.2545′W, 56°57.3852′N; Shot 1423; water depth = 4218 m; target depth = 780 mbsf) and GOA18-1A (56.94°N, 147.38°W; Shot 1723; water depth = 4262 m; target depth = 758 mbsf).

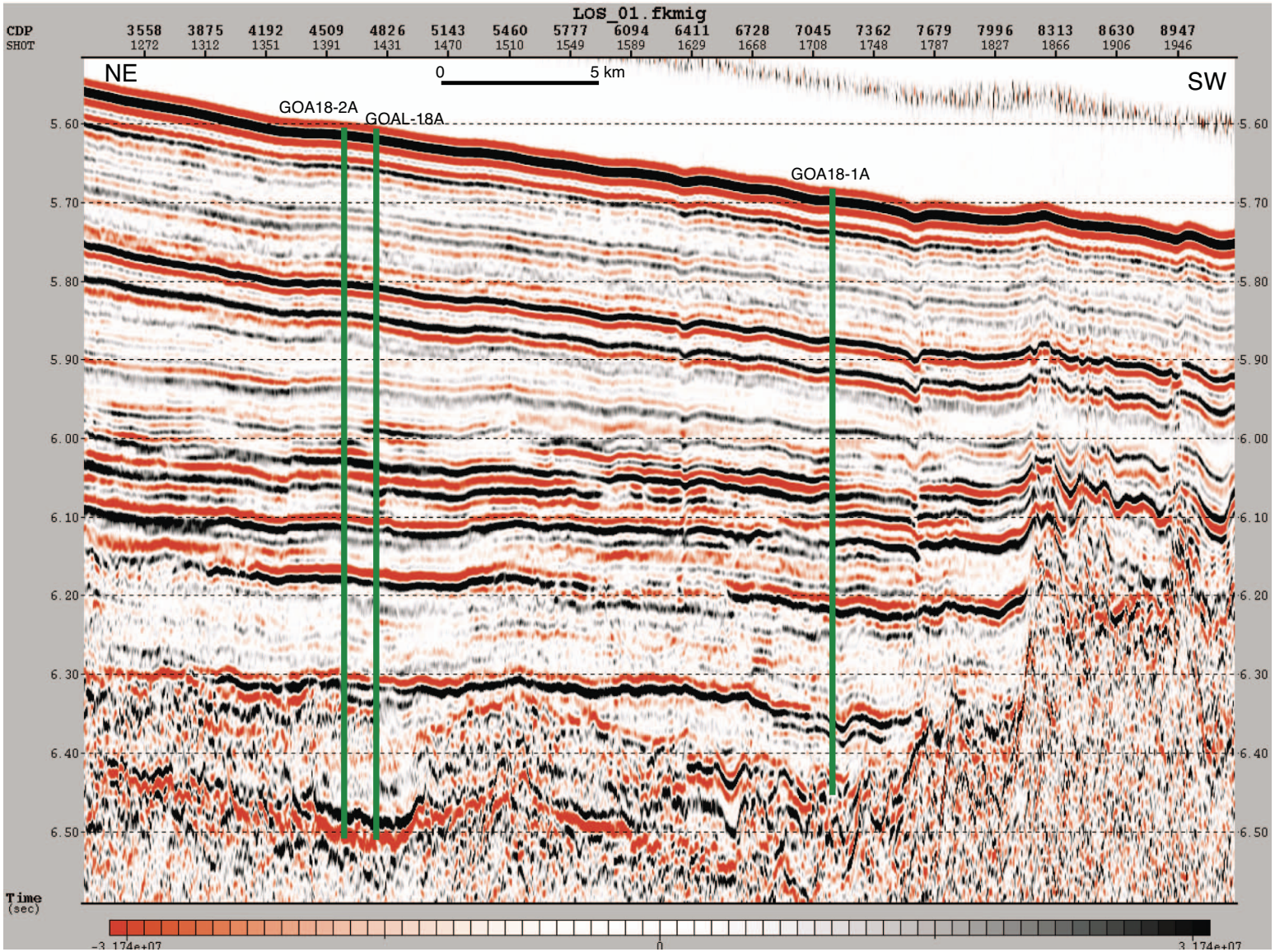

Figure AF22. Seismic profile of *S.P. Lee* Cruise L-6-81 Line 678-04/05 (NW–SE) with location of alternate Site GOAL-18A (147°8.2545′W, 56°57.3852′N; Shot ~JD157 06:37; water depth = 4218 m; target depth = 780 mbsf). Site is located on course change from Line 04 to Line 05 and paper record was advanced at course change, with no data gaps.

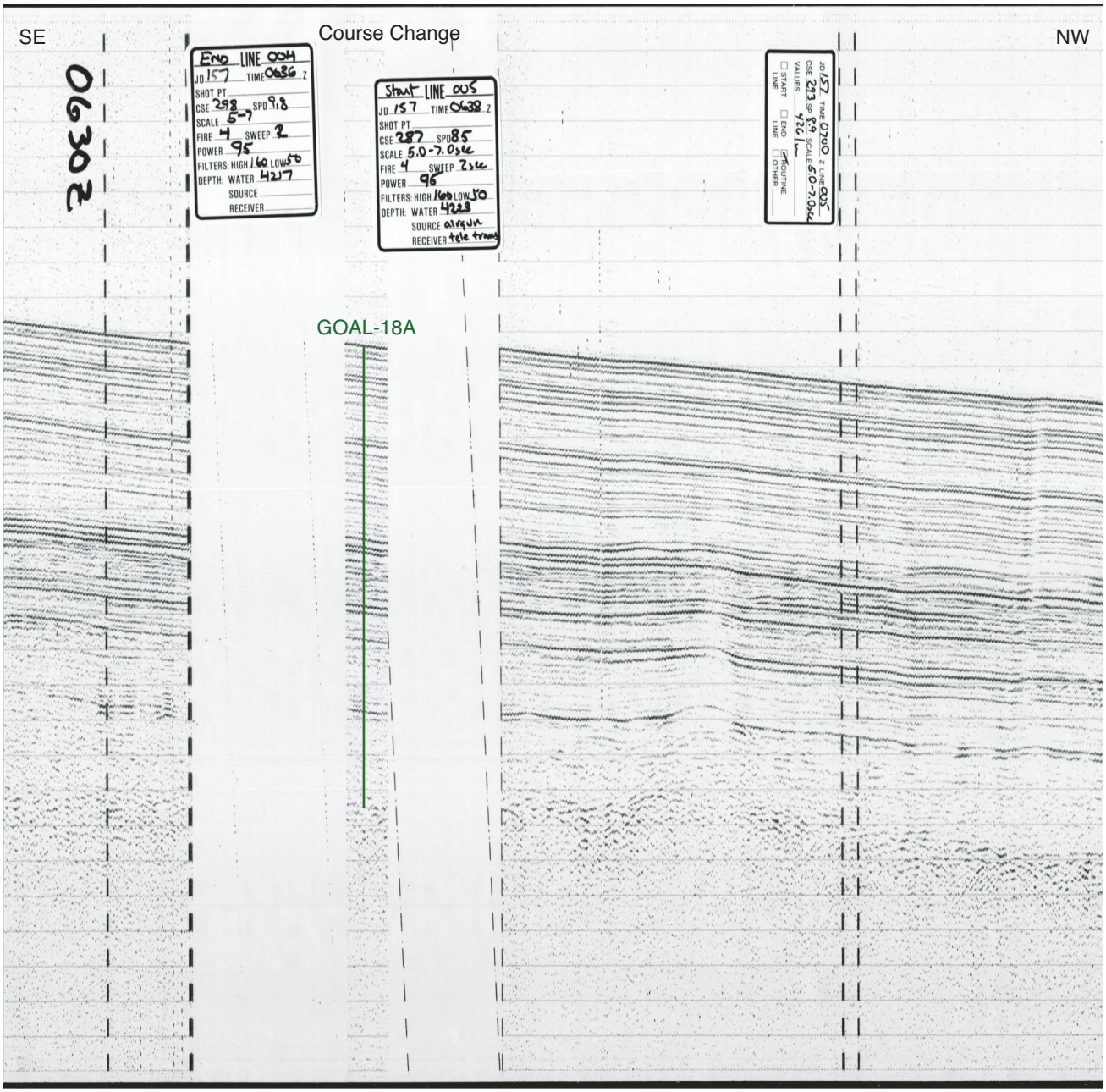

Figure AF23. Seismic profile of *Farnella* Cruise F-6-89 Line 13 (NE–SW) with location of alternate Site GOA18-1A (56.94°N, 147.38°W; CDP 5380; water depth = 4262 m; target depth = 758 mbsf).

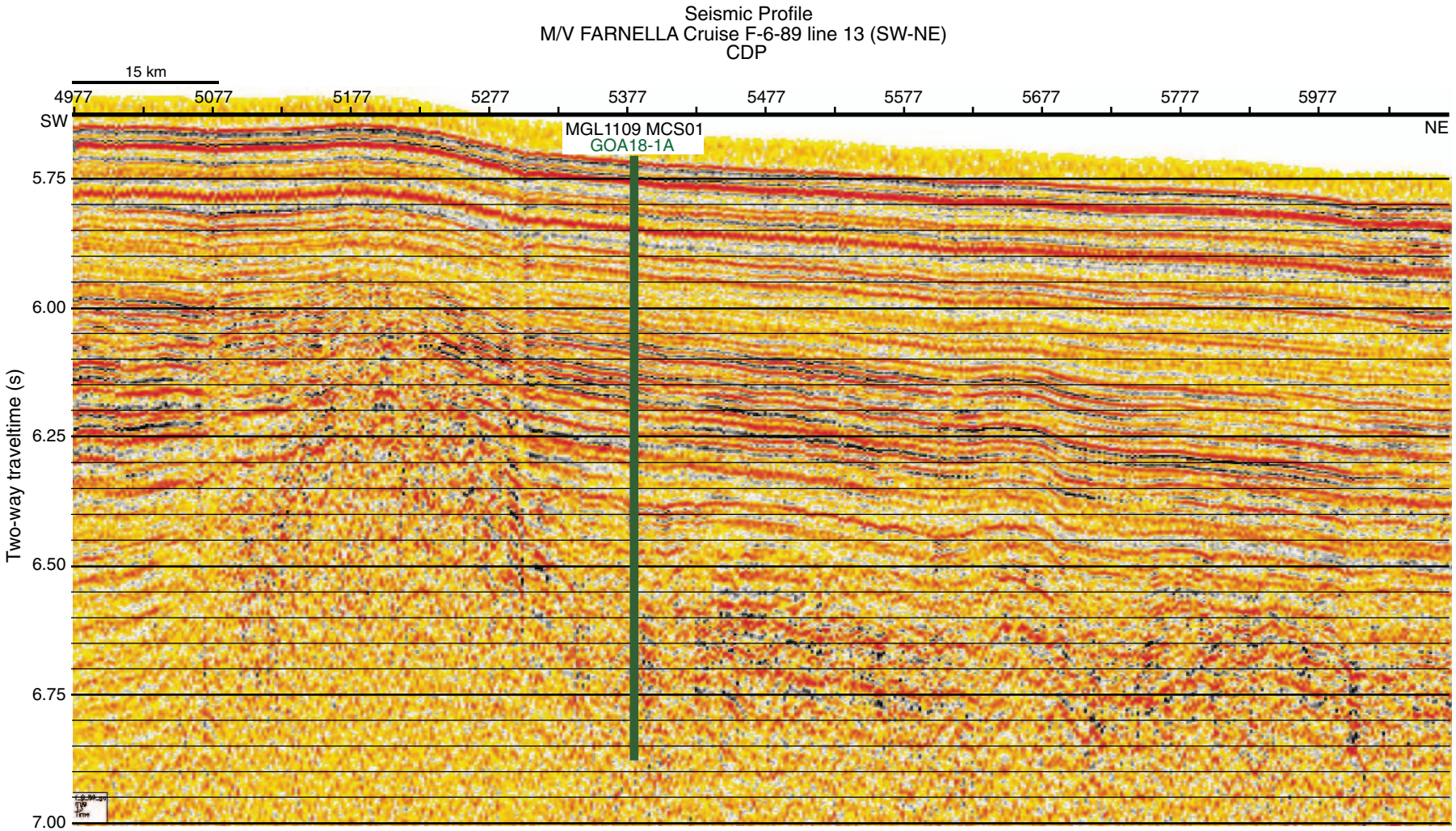

Figure AF24. Seismic profile of *Marcus G. Langseth* Cruise MGL11-09 MCS Line MCS14 (N–S) with location of primary Site GOA18-2A (56.96°N, 147.11°W; Shot 1790; water depth = 4177 m; target depth = 780 mbsf).

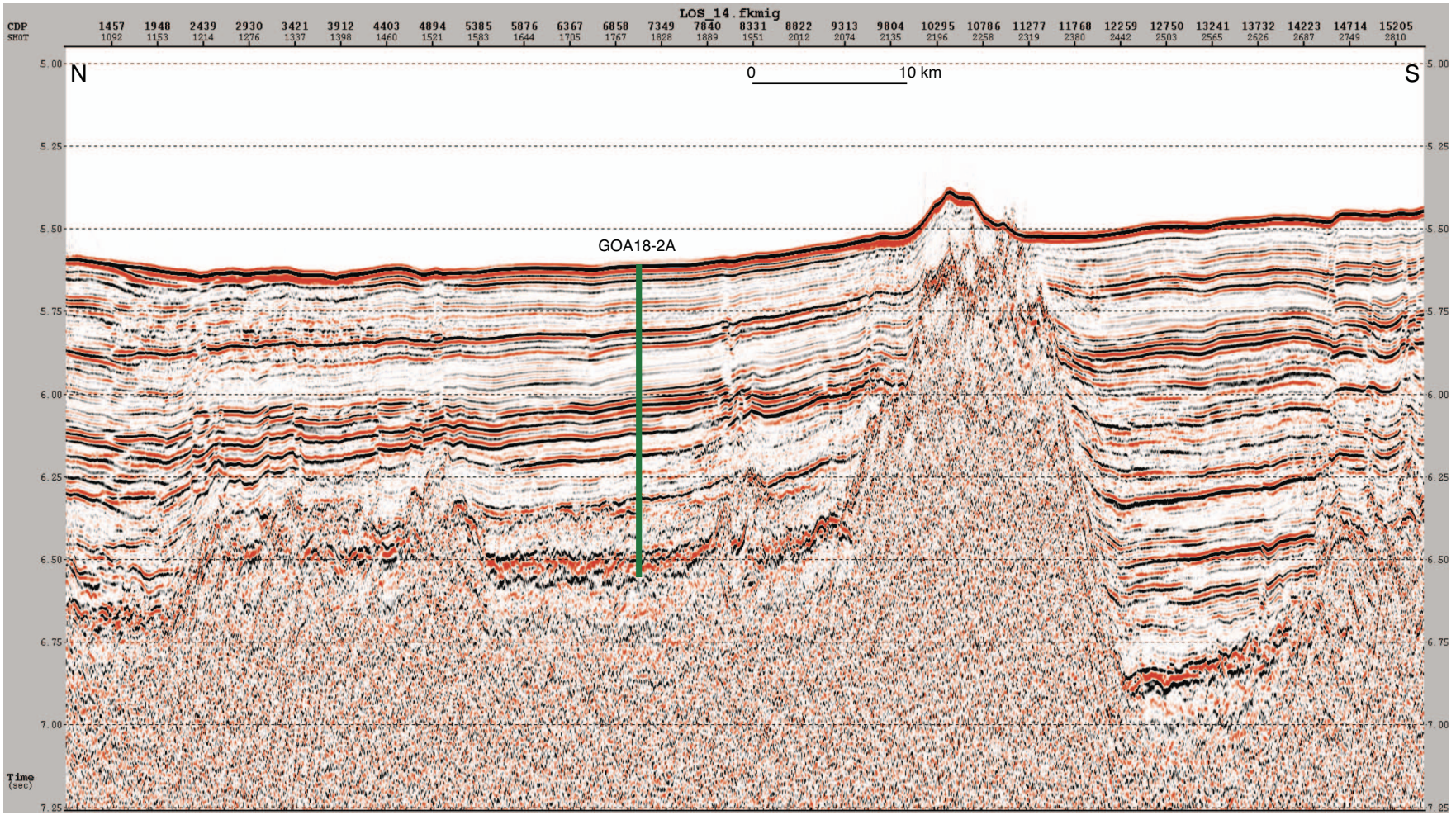

Figure AF25. Close-up navigation map of proposed primary Site KB-2A, showing seismic reflection Profiles EW0408 GOA3101 (Fig. AF26) and EW0408 GOA3102 (Fig. AF27). KB-2A is located at crossing point of GOA3101 (CDP 398) with GOA3102 (CDP 663).

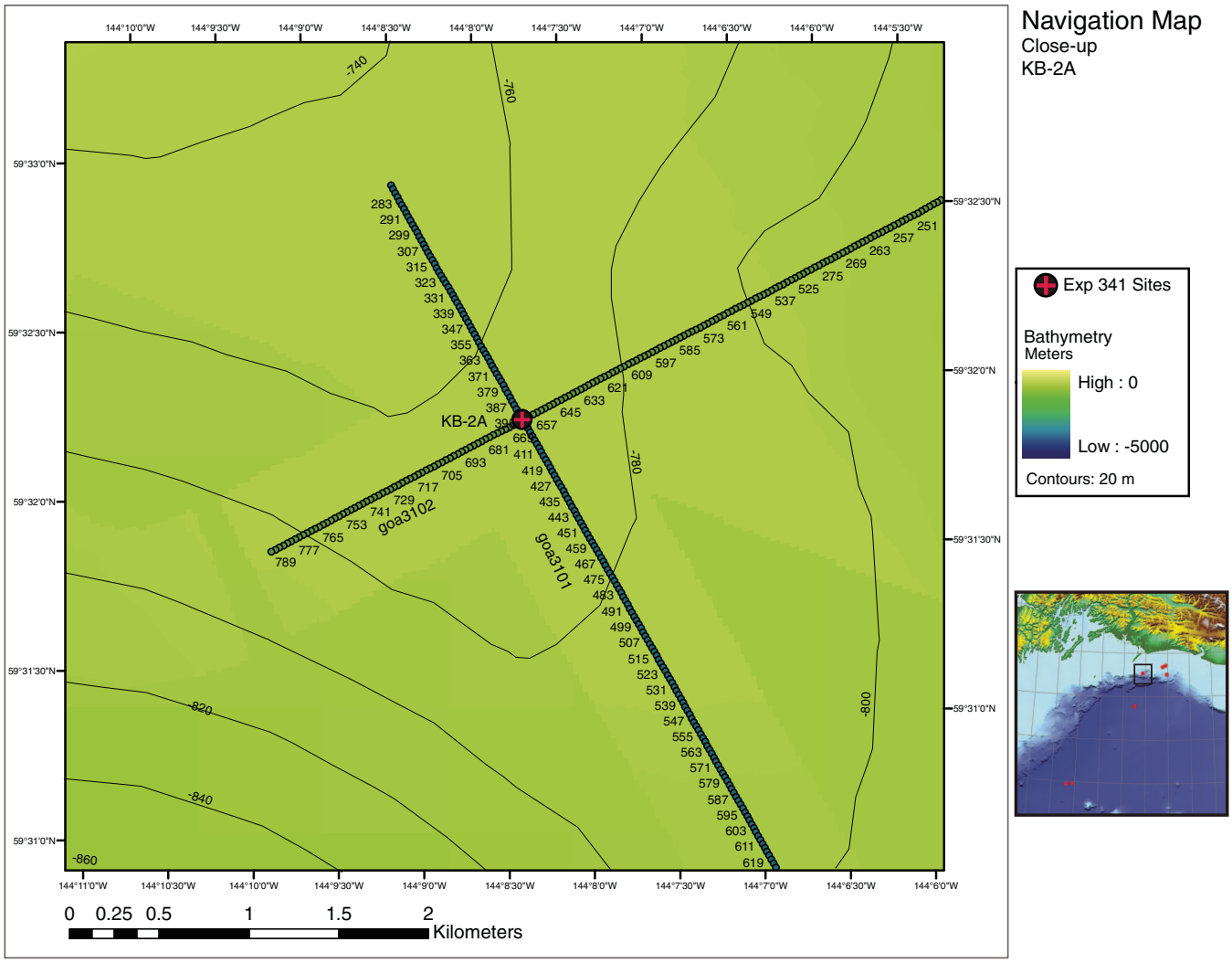

Figure AF26. Seismic profile of *Maurice Ewing* Cruise EW0408 MCS Line GOA3101 (NW–SE) with location of primary Site KB-2A (144°08.03′W, 59°31.93′N; CDP 398; water depth = 710 m; target depth = 400 mbsf).

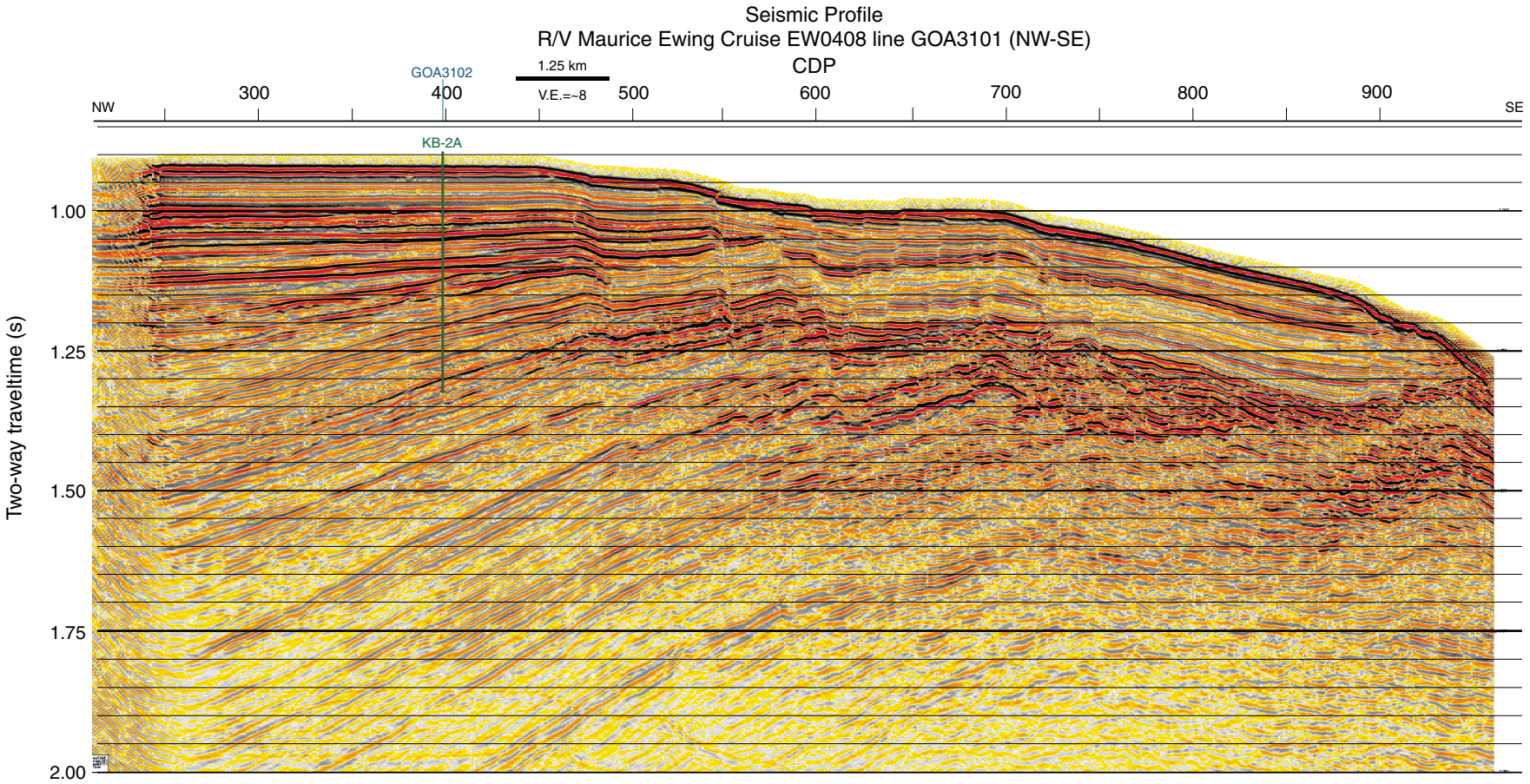

Figure AF27. Seismic profile of *Maurice Ewing* Cruise EW0408 MCS Line GOA3102 (SW–NE) with location of primary Site KB-2A (144°08.03′W, 59°31.93′N; CDP 663; water depth = 710 m; target depth = 400 mbsf).

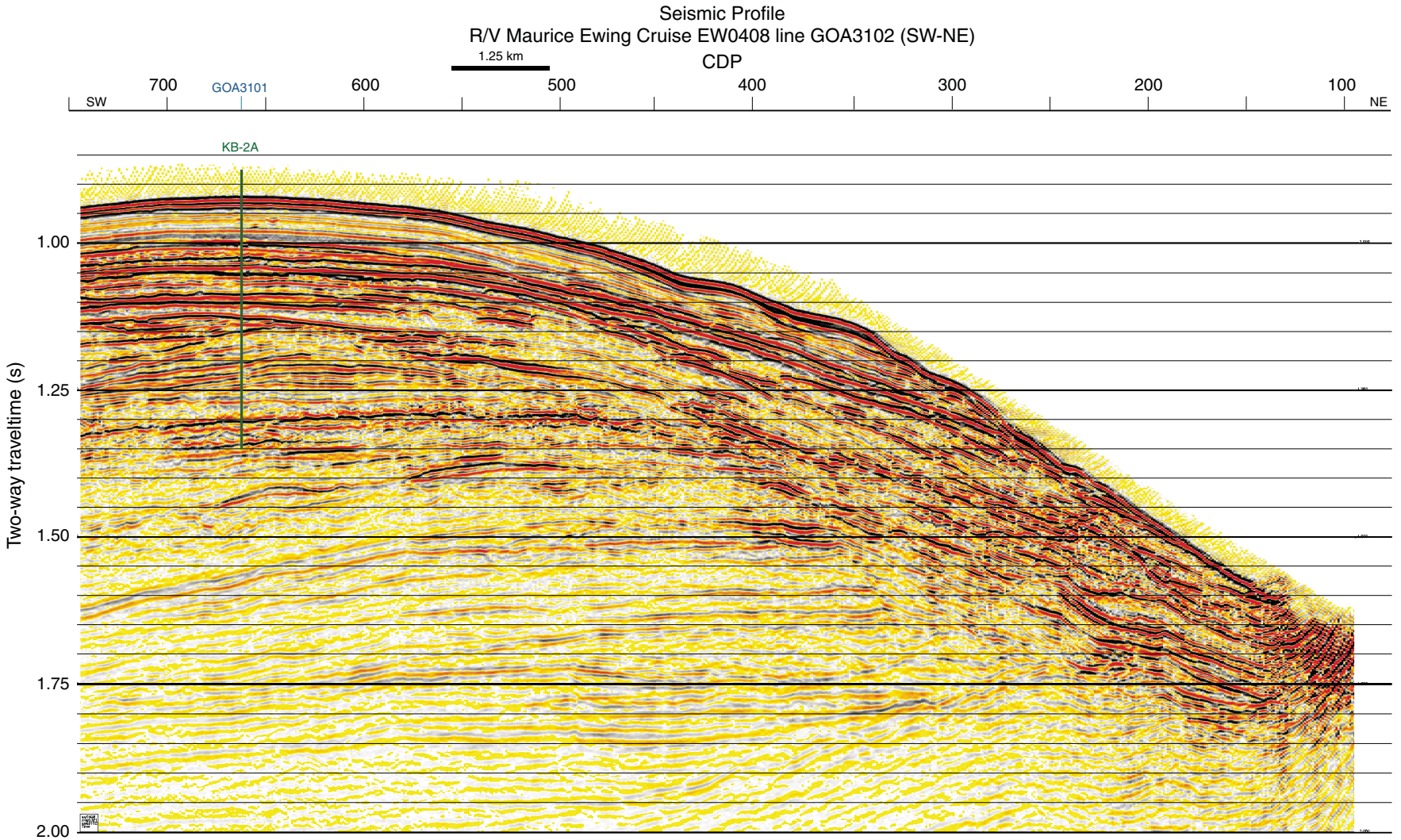

Figure AF28. Swath bathymetric map with track chart of *Maurice Ewing* Cruise EW0408 around Site KB-2A.

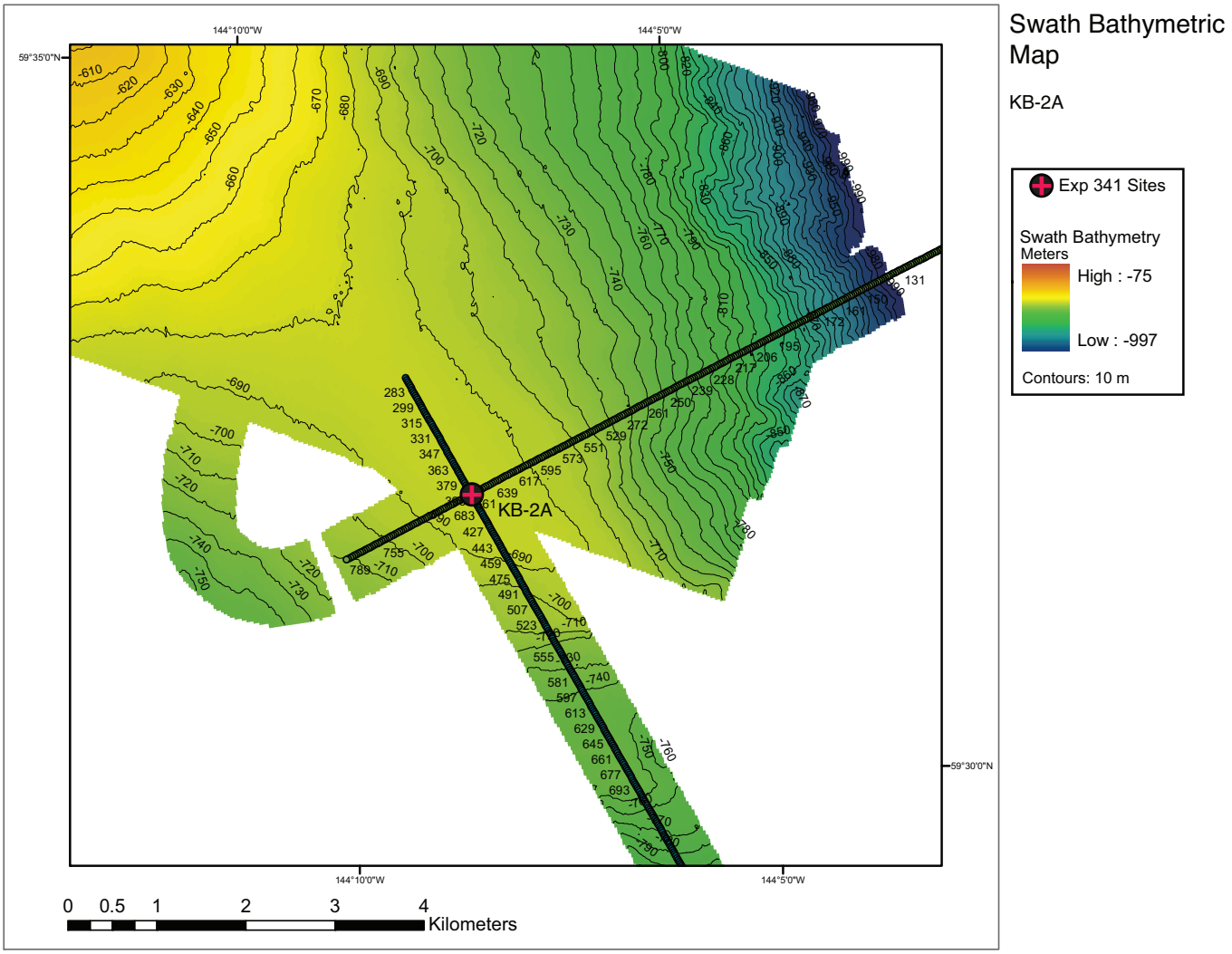

Expedition scientists and scientific participants

The current list of participants for Expedition 341 can be found at **iodp.tamu.edu/ science-ops/precruise/alaskamargin/participants.html.**